


1996

Water quality modeling as an inverse problem

Jian Shen

College of William and Mary - Virginia Institute of Marine Science

Follow this and additional works at: <https://scholarworks.wm.edu/etd>

 Part of the [Environmental Engineering Commons](#), [Hydrology Commons](#), and the [Oceanography Commons](#)

Recommended Citation

Shen, Jian, "Water quality modeling as an inverse problem" (1996). *Dissertations, Theses, and Masters Projects*. Paper 1539616852.

<https://dx.doi.org/doi:10.25773/v5-2jpp-fw57>

This Dissertation is brought to you for free and open access by the Theses, Dissertations, & Master Projects at W&M ScholarWorks. It has been accepted for inclusion in Dissertations, Theses, and Masters Projects by an authorized administrator of W&M ScholarWorks. For more information, please contact scholarworks@wm.edu.

INFORMATION TO USERS

This manuscript has been reproduced from the microfilm master. UMI films the text directly from the original or copy submitted. Thus, some thesis and dissertation copies are in typewriter face, while others may be from any type of computer printer.

The quality of this reproduction is dependent upon the quality of the copy submitted. Broken or indistinct print, colored or poor quality illustrations and photographs, print bleedthrough, substandard margins, and improper alignment can adversely affect reproduction.

In the unlikely event that the author did not send UMI a complete manuscript and there are missing pages, these will be noted. Also, if unauthorized copyright material had to be removed, a note will indicate the deletion.

Oversize materials (e.g., maps, drawings, charts) are reproduced by sectioning the original, beginning at the upper left-hand corner and continuing from left to right in equal sections with small overlaps. Each original is also photographed in one exposure and is included in reduced form at the back of the book.

Photographs included in the original manuscript have been reproduced xerographically in this copy. Higher quality 6" x 9" black and white photographic prints are available for any photographs or illustrations appearing in this copy for an additional charge. Contact UMI directly to order.

UMI

A Bell & Howell Information Company
300 North Zeeb Road, Ann Arbor MI 48106-1346 USA
313/761-4700 800/521-0600

WATER QUALITY MODELING AS AN INVERSE PROBLEM

A Dissertation

Presented to

The Faculty of the School of Marine Science

The College of William and Mary in Virginia

In Partial Fulfillment

Of the Requirements of the Degree of

Doctor of Philosophy

by

Jian Shen

1996

UMI Number: 9701097

UMI Microform 9701097
Copyright 1996, by UMI Company. All rights reserved.

**This microform edition is protected against unauthorized
copying under Title 17, United States Code.**

UMI
300 North Zeeb Road
Ann Arbor, MI 48103

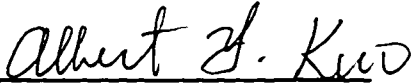
APPROVAL SHEET

This dissertation is submitted in partial fulfillment of
the requirements for the degree of

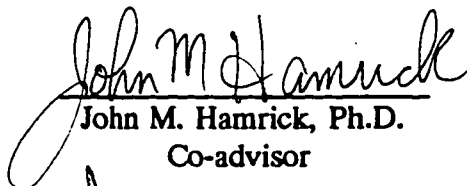
Doctor of Philosophy

Jian Shen

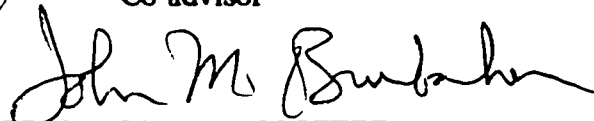
Approved, July 1996



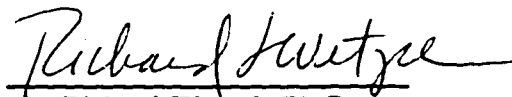
Albert Y. Kuo, Ph.D.
Committee Chairman/Advisor



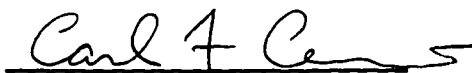
John M. Hamrick, Ph.D.
Co-advisor



John M. Brubaker, Ph.D



Richard Wetzel, Ph.D



Carl F. Cerco, Ph.D

US Army Engineers Waterways Experiment Station

TABLE OF CONTENTS

	Page
ACKNOWLEDGMENT.....	vi
LIST OF TABLES.....	vii
LIST OF FIGURES.....	ix
ABSTRACT.....	xi
INTRODUCTION.....	2
1.1 Problem Description.....	2
1.2 Background and Previous Works.....	4
1.3 Objectives.....	11
METHODOLOGY.....	12
2.1 Model Equation.....	12
2.2 Scaling Model Equation.....	13
2.3 Adjoint Model.....	15
2.4 Method of Solution.....	22
2.4.1 Solution procedure.....	22
2.4.2 Grid system and geometry.....	24
2.4.3 Finite difference treatment.....	24
2.4.4 Decoupling kinetic processes.....	25
2.5 Weights of the Cost Function.....	34

2.6	Preconditioning Method.....	39
	INVERSE MODEL EXPERIMENT.....	46
3.1	Experiments With Constant Boundary Conditions.....	46
3.1.1	Test Model Description.....	46
3.1.2	Test of preconditioning.....	48
3.1.3	Basic parameter estimation tests.....	50
3.1.4	Experiments with noisy data.....	53
3.1.5	Long period simulation with limited data sets.....	55
3.2	Experiments With Time Varying Boundary Conditions.....	70
3.2.1	Model boundary conditions and sample data.....	70
3.2.2	Basic parameter estimation tests.....	72
3.2.3	Experiments with noisy data.....	73
	THE UNCERTAINTY OF THE PARAMETER.....	79
4.1	Parameter Uncertainty.....	79
4.2	Parameter Correlation and Singular Value Decomposition.....	82
	MODEL CALIBRATION WITH FIELD DATA.....	90
5.1	Model Calibration.....	90
5.2	Model Verification.....	95
5.3	Calibration Summary.....	99
	SUMMARY, CONCLUSIONS, AND RECOMMENDATIONS.....	110
6.1	Summary.....	110
6.1.1	The inverse model formulation.....	111

6.1.2 The inverse model experiments.....	113
6.1.3 Inverse model application.....	115
6.2 Conclusions.....	115
6.3 Recommendations.....	118
APPENDIX A SOURCE AND SINK FUNCTIONS.....	120
APPENDIX B SCALED SOURCE AND SINK FUNCTIONS.....	125
APPENDIX C FINITE DIFFERENCE EQUATIONS OF ADJOINT MODEL.....	127
C-1 Finite Difference Scheme of The Adjoint Model.....	127
C-2 Finite Difference Equation of The Adjoint Model.....	132
LITERATURE CITED.....	134
VITA.....	140

ACKNOWLEDGMENTS

I am greatly indebted to my major professor, Dr. Albert Y. Kuo, for his guidance, support, and encouragement throughout the course of this study. This work would not be possible without his idea, encouragement, and in depth understanding of the eutrophication modeling. I am grateful to Dr. John M. Hamrick for his suggestions on numerical methods. I am grateful to Dr. Carl Cerco for his helpful suggestions on the eutrophication model calibration. I am thankful to Drs. Richard Wetzel, and John M. Brubaker for their reviewing of the manuscripts. I am thankful to Dr. Kyeong Park for his assistance in model coding and field data preparation.

My special thanks go to my parents, my wife Ming, and my daughter Ye-Ye for their love, support, and understanding throughout the course of my graduate studies.

LIST OF TABLES

TABLE	Page
TABLE 1. Parameter Values Used in The Inverse Model.....	56
TABLE 2. Values of Parameters for Eutrophication Model.....	57
TABLE 3. Parameter Scale Values and Empirical Coefficients for Run P3.....	58
TABLE 4. Condition Number of Test Runs.....	58
TABLE 5. Estimated and True Values of the Parameters..... for Run C1, Run C2, and Run C6	59
TABLE 6. Estimated and True Values of The Parameters for Run C3.....	60
TABLE 7. Estimated and True Values of The Parameters..... for Run C4 and Run C5	60
TABLE 8. Estimated and True Values of Parameters for Run T1 and Run T2..... (basic parameter estimation tests with time vary boundary conditions)	76
TABLE 9. Estimated and True Values of Parameters for Run T3..... (experiments with 10% random error data)	76
TABLE 10. Parameter Uncertainty of Run T1.....	87
TABLE 11. Parameter Uncertainty of New Parameters..... After Parameter Transformation (Run T1)	87
TABLE 12. Correlation Matrix of the Estimated Parameters..... (Run T1 in absolute values)	88
TABLE 13. The Coefficients of the First Four Vectors of V Matrix.....	89
TABLE 14. The Coefficients of the First Four Vectors of V Matrix of New Parameters (after transformation).....	89
TABLE 15. Estimated Parameter Values of Model Calibration.....	101

TABLE 16. Root-Mean-Square Errors Between the Observations and Model predictions	102
TABLE 17. Mean Errors Between the Observations and Model Predictions.....	102
TABLE 18. Relative Errors Between the Observations and Model Predictions.....	102
TABLE 19. Comparisons of Errors Between Different Calibrations.....	103

LIST OF FIGURES

Figure 2-1	A schematic diagram of interacting water quality state variables.....	29
Figure 2-2	Grid pattern, location and indexing of variable.....	30
Figure 2-3	The solution method for the forward model (a) and backward..... model (b), employing an alternate solution of physical transport and kinetic processes or error source update.	31
Figure 2-4	A comparison of calculated concentrations (surface maximum..... and bottom minimum) between updating kinetic processes every 8 minuets ($\Delta t = 480s$, $m = 1$) and every two hours ($15\Delta t$, $m = 15$).	32
Figure 3-1	The model transects in the tidal Rappahannock River.....	61
Figure 3-2	Distributions of initial concentrations at the surface..... and the bottom layers for experiments with constant boundary conditions.	62
Figure 3-3	Comparisons of the rate of convergence of different..... preconditioning methods.	63
Figure 3-4	Comparisons of daily surface maximum and bottom..... minimum concentrations of the state variables between the model results (Run C1) with initial guess parameter values and the true results over the 10th day.	64
Figure 3-5	The relative error of cost function as a function of the number of..... iterations for Run C1.	65
Figure 3-6	Comparisons of instantaneous surface and bottom concentrations..... of the state variables between the inverse model results (Run C4) and the true results together with sample data (with 10% error) at the 10th day.	66
Figure 3-7	Comparisons of instantaneous surface and bottom..... concentrations of the state variables between the inverse model	67

results (Run C5) and the true results together with sample data (with 20% error) at the 10th day.

Figure 3-8	Scatterplots of the inverse model results (Run C4) vs. true results and sample data (with 10% error).	68
Figure 3-9	Comparisons of daily surface maximum and bottom minimum concentrations of the state variables between the inverse model results (Run C6) and the true results over the 30th day.	69
Figure 3-10	Distributions of initial concentrations at the surface and the bottom layers for experiments with time varying boundary conditions and field data calibration.	77
Figure 3-11	Comparisons of instantaneous surface and bottom concentrations of the state variables between the inverse model results (Run T3) and the true results together with sample data (with 10% error) at the 30th day.	78
Figure 5-1.	The inverse model (IMC-1) calibration results on 7/5/90 (daily maximum and minimum at the surface and bottom).	104
Figure 5-2.	The original model (OMC) calibration results on 7/5/90 (daily maximum and minimum at the surface and bottom).	105
Figure 5-3	The inverse model (IMC-2) calibration results on 7/5/90 (daily maximum and minimum at the surface and bottom).	106
Figure 5-4	The inverse model (IMC-1) verification results on 8/7/90 (daily maximum and minimum at the surface and bottom)	107
Figure 5-5	The original model (OMC) verification results on 8/7/90 (daily maximum and minimum at the surface and bottom).	108
Figure 5-6	The inverse model (IMC-2) verification results on 8/7/90 (daily maximum and minimum at the surface and bottom).	109

ABSTRACT

An inverse mathematical estuarine eutrophication model with eight state variables has been developed. The model provides a framework to estimate unknown parameter values by assimilation of the concentration data of those state variables. The inverse model developed is a laterally integrated, two-dimensional, real-time model which consists of a hydrodynamic model, an eutrophication model (forward model) and an adjoint model (backward model). The hydrodynamic model simulates tide, current, salinity, and dispersion to supply the dynamic fields for the transport portion of both the eutrophication model and the adjoint model. The eutrophication model simulates eight water quality state variables which are phytoplankton, organic nitrogen, ammonium nitrogen, nitrite-nitrate nitrogen, organic phosphorus, inorganic (ortho) phosphorus, carbonaceous biochemical oxygen demand and dissolved oxygen. The adjoint model is used during the processes of the parameter estimation to provide gradients of the cost function, data misfit, with respect to the parameters to be estimated. To increase the computational efficiency and reduce the computer storage space, a decoupling scheme is implemented in the inverse model, in which the kinetic processes are decoupled from the physical transport for the purpose of numerical computation. An efficient preconditioning technique is introduced in the inverse model to speed up the rate of convergence.

The experiments conducted in this study provide the information of the feasibility of parameter estimation, uniqueness of the parameters, and the field data requirement for the model calibration. The model experiments with hypothetical data sets show that the unknown parameters can be accurately estimated for short period and long period model simulations under both constant and time-varying boundary conditions. The inverse model is convergent with different initial guess parameter values and under different environmental conditions.

The inverse model was successfully applied to aid calibration of the eutrophication model of the tidal Rappahannock River, Virginia. With the use of the inverse model, the eutrophication model can be calibrated efficiently and systematically. The results of both model calibrations and verifications show that the agreement between the model predictions and observations are very satisfactory.

The studies show that the inverse model is not only useful to aid model calibration but also useful in addressing the important questions of whether the estimated parameter values are unique and whether sample data are sufficient to calibrate a model. Therefore, the inverse model may also serve as a tool in helping design a field program to collect data for model calibration.

WATER QUALITY MODELING AS AN INVERSE PROBLEM

I. INTRODUCTION

1.1 Problem Description

In recent years, mathematical models have often been used to study and analyze eutrophication and other water quality problems in aquatic environments. Most eutrophication models incorporate many parameters which quantify biogeochemical processes in the water column and between water and bottom sediment. The reliability of a model is dependent on how well these parameters are estimated. However, estimation of these parameter values cannot always be obtained by controlled experiments or independent measurements in the field or laboratory. Moreover, some parameters incorporated in the model are lumped parameters in the sense that they represent a number of underlying processes for which separate modeling is undesirable or impractical, so that their numerical values have a well-defined physical meaning only for the system under study with the context of the model specified (van Straten 1983). In most cases, it is difficult to give precise parameter values in advance. Consequently, model calibration achieved by adjusting the parameter values in some way is inevitable.

Traditionally, model calibration or parameter estimation is based upon trial-and-error and graphical matching techniques. Parameter values are adjusted until calculated concentrations of state variables match field data in a "satisfactory" fashion. Such techniques are often laborious and sometimes subjective. It would be difficult in a

situation where parameters are cross-related to each other and parameters are spatially dependent. Also, questions as to whether or not the derived set of values is the optimum and as to how many sets of values are equally good are difficult to answer (Cooley 1977). There is no knowledge whether the parameters estimated are unique when a trial-and-error method is used. As a consequence, the response of model and system may differ for inputs different from those that have been used for calibration. These problems have stimulated considerable research of inverse modeling strategies to obtain the required parameter values more systematically.

Although many methods have been introduced to obtain model parameter values, the variational method has recently received wide attention and has been shown to be one of the most efficient techniques for parameter estimation. It has been used in estimating groundwater flow model parameters (Jacquard and Jain 1965; Carter et al. 1982; Sun and Yeh 1985; Carrera and Neumann 1986), estimating friction and wind forcing in ocean circulation model (Tziperman and Thacker 1989), estimating vertical eddy viscosities (Yu and O'Brien 1991; Panchang et al. 1992; Lardner and Das 1994), estimating phase speed for a Pacific Ocean model (Smedstad and O'Brien 1991), in numerical weather prediction (Lorenz 1986; Navon 1986), in petroleum reservoir simulation (Chavent et al. 1975), in the field of oceanography (Bennett and McIntosh 1982; Prevost and Salmon 1986). Although the literature on applying the variational method to solve inverse problems in the field of meteorology, oceanography and others is quite rich, the same is not true in the field of eutrophication modeling. The inverse eutrophication modeling is a typical coupled inverse problem, which is governed by a set of nonlinear partial differential equations. The basic concepts and

methods of parameter estimation for a coupled inverse problem are similar to those for the single state variable. However, there are several differences between them that make the inverse eutrophication modeling more complex and challenge. There are at least four important factors which contribute to this situation: (1) the number of nonlinear governing equations for eutrophication processes are large, and usually range from eight to more than twenty, as are the state variables. (see, for example, Cerco and Cole 1994; Kuo and Park 1995; Kuo et. al. 1991; EHL 1986). (2) the number of parameters is very large, with different scales and units and many of them are spatially dependent. (3) the available prototype observations are scattered in the spatial and temporal domains. The interval between two measurements can be weeks or months, i.e., long period model simulation is necessary. (4) the concentration of each state variable often depends on several parameters, i.e., there are cross effects among parameters. These nonlinearities and cross effects can be expected to degrade the common methods used in other fields. The feasibility of an inverse estimation of parameter values for an eutrophication system is still questionable. A basic issue needing study is whether the unknown parameter values of an eutrophication model can be estimated accurately, uniquely, efficiently.

1.2 Background and Previous Works

The inverse method or optimization method for parameter estimation in the numerical modeling concerns the optimal determination of parameter values by observing the difference between the model results and the state variables measured in the spatial and temporal domains. Many techniques have been introduced to estimate

parameter values during the last two decades. Possible approaches include a variety of optimization methods and statistical methods as well as stochastic methods (Yeh 1986; Beck 1987). Articles and reports covering research on estimation parameters include those by Jacquard and Jain (1965), Neuman (1973), Carter et al. (1974), Chavent (1975), Cooley (1977), van Straten (1983), Yeh (1983, 1986, 1990), Das and Lardner (1991), Smedstad and Brien (1991), Yu and O' Brien (1991), Lardner and Das (1994), Carrera and Neuman (1986), Panchang et al. (1992) and Lal (1995). The parameters estimated are friction coefficient, transmissivity, storage coefficient, roughness, and eddy diffusivity. The early contributions to parameter estimation in water quality modeling were mostly with models of two state variables, dissolved oxygen (DO) and biochemical oxygen demand (BOD). Articles include those by Lee and Hwang (1971), Koivo and Phillips (1971; 1976), Shastry et al. (1973), Beck and Young (1976), Rinaldi et al. (1976; 1979). Many models considered were steady state models or time varying models with spatially uniform distribution of state variables. Beck (1974), Di Toro and van Straten (1979), Jørgensen et al. (1981), Mejer and Jørgensen (1983), and van Straten (1983) studied uncertainty of parameter estimation problems for more complicated eutrophication systems. Many of these applications have focussed, with varying degrees of complexity (from one to 17 state variables), on the development of models for phytoplankton dynamics in lake ecosystems. Di Toro and van Straten (1979) and van Straten (1983) have addressed one of the largest scale problems of parameter estimation. They have used a 12-state variable model with 20 parameters to be estimated. To date, no detailed studies have been conducted on the feasibility of estimating biochemical parameters for a real time estuarine eutrophication model

which simulates both temporal and spatial distributions of algal population and its associated nutrients as well as dissolved oxygen. Questions as to if there is an efficient method for the inverse modeling of estuarine eutrophication model and as to if the solution is unique are still open.

The available methods for parameter estimation fall into two categories, i.e., either "direct" or "indirect" based on Neuman's (1973) classification. The "direct approach" treats the model parameters as dependent variables in a formal inverse boundary value problem. The "indirect approach" is based upon an output error criterion where an existing estimation of parameter value is iteratively improved until the model output is sufficiently close in a sense to that of the measured data.

If "direct approach" is used in eutrophication modeling, one needs full knowledge of variations and derivatives of the state variables over the entire flow region and time domain. With the aid of boundary conditions and flow data, the direct solution for the unknown parameter values may be possible if a set of algebraic equations of unknown parameters can be derived. Direct methods have been applied in several areas of water resources (see, for example, Sagaret et al. 1975; Nutbrown 1975; and Yeh et al. 1983). However, direct methods ignore most of the statistical aspects of the estimation problems and involve large errors due to differentiation of measured data and interpolation of missing data in the spatial and temporal domains. Because of its dependence on linearization and by its somewhat artificial nature of the cost function, direct methods are probably most useful when the model of interest is linear and computation simplicity is a dominant consideration (McLaughlin 1978).

The basic idea of "indirect method" is that the output of a numerical model must

agree with the measurements, allowing for observational errors. The procedure generally adopted in the indirect approach is to adjust parameter values so as to minimize a cost function which measures the misfit between computed results and measured data. The main advantage of this approach is that the formulation of the inverse problem is applicable to the situation where the number of observations is limited and it does not require differentiation of measured data (Yeh 1986).

Various optimization algorithms have been used to perform the minimization. Solution of the problem generally proceeds through one of three approaches. The first group of methods is based on various modifications to the steepest descent method. The second group of methods is based on various modifications of the Gauss-Newton method. The third group of methods is the conjugate gradient method. All these methods are iterative methods which produce better parameter values to minimize the cost function with each iteration. When using these algorithms, the gradients of the state variables or cost function with respect to the parameters are needed for the optimization algorithms used in computing the parameter values that gives the best fit. There are several ways to calculate these gradients, sometime referred to as "sensitivity coefficients". The general methods are the influence coefficient method, the sensitivity equation method, and the variational method (Yeh 1986). The influence coefficient method uses the concept of parameter perturbation. The method requires perturbation of each parameter one at a time. The increment of a parameter used in the perturbation is usually determined on a trial-and-error basis. If there is one governing equation with L unknown parameters, the governing equation has to be solved $(1+L)$ times for each iteration. The sensitivity equation method obtains sensitivity coefficients

by solving a sensitivity equation, a partial differential equation similar to the governing equation. However, the number of sensitivity equations to be solved are on the order of the number of unknown parameters (same as the influence coefficient method). For a system with spatial varying parameters, the number of equations to be calculated will increase very dramatically. This method is not an efficient way if the number of unknown parameters is more than the number of governing equations, such as the eutrophication model. For the variational method, the best fit of the model output is determined by a system of equations consisting of the model equations and their corresponding adjoint equations forced by the model data misfit. The adjoint equations provide the gradient of the cost function (total misfit) with respect to each parameter. The number of adjoint equations to be solved is the same as that of the governing equations. Because the gradient of the cost function with respect to each parameter can be directly computed from the solutions of the adjoint equations, one does not need to calculate the sensitivity matrix. The computation time can be reduced dramatically. Since the adjoint equations have similar forms as the governing equations, a similar computation scheme can be easily developed. Therefore, the variational method provides a powerful technique for computing such gradients, and it is especially useful when the number of parameters to be estimated is large.

In recent years the variational method or the variational data assimilation has been widely used in numerical weather prediction (Lorenz 1986; Navon 1986; Le Dimet et al. 1986), in petroleum reservoir simulation (Chavent et al. 1975), in the field of oceanography (Bennett and McIntosh 1982; Prevost and Salmon 1986), in estimating eddy viscosity of tidal flow model (Yu and O'Brien 1991; Lardner and Day 1994),

and in groundwater hydrology modeling (Yeh and Sun 1990). The variational method was first used for solving the inverse problem of parameter estimation in groundwater modeling by Jacquard and Jain (1965) and then by Carter et al. (1982), and recently by Sun and Yeh (1985) and Yeh and Sun (1990). The parameters they estimated are transmissivity, storage coefficient, and leakage coefficient. The first application of the variation method to estimate eddy viscosity was by Yu and O' Brien (1991), who estimated the eddy viscosity and surface drag coefficient in an ideal horizontal uniform model of the ocean from measured velocities of a wind-driven flow. Recently, Lardner and Das (1994) applied this approach to estimate viscosity in a quasi three dimensional numerical tidal and storm surge model. Yu and Lardner's approach is different from Yeh's approach. Yu and Lardner introduced Lagrange multipliers and processed the variational analysis on the Lagrange function. A point that should be stressed is that the use of Lagrange multipliers greatly simplifies the derivation of the adjoint equations, especially deriving the adjoint equations from the finite difference equations of the governing equations. Their studies suggest that the variational method is an efficient technique to be introduced to estimate parameters in a large system with large number of parameters to be estimated.

One difficulty in parameter estimation is that parameter estimation and, in general, inverse modeling techniques are often ill-posed problems. The ill-posedness is generally characterized by the nonuniqueness and instability of the parameters in the identification process. It has been found by several authors, e.g. Chavent (1974, 1983), Yeh (1986), Smedstad and O'Brien (1991), Carrera and Neuman 1986, and Das and Lardner (1991), that if one is estimating parameters which are distributed in the space-

time domain, the study is fraught with instability and non-uniqueness. The uniqueness problem has great practical importance, as addressed by Chavent (1974), because in the case of non-uniqueness, the estimated parameters will differ according to the initial estimation of the parameters, and there will be no reason for estimated parameters to be close to the "true" parameters. Chavent studied the uniqueness problem for two situations: (1) the case of constant parameters and (2) the case of distributed parameters, i.e, parameters that are spatially dependent. It is shown in Chavent's study that in the case of constant parameters, the inverse problem is unique because there are generally more measurements than unknowns. However, in the case of distributed parameters, the inverse problem is often non-unique due to a shortage of measurements. The uniqueness problem in parameter estimation is intimately related to identifiability (Carrera and Neuman 1986). The basic issue is how many measurements and what kind of data sets, which are practically feasible, are needed in order to reach the uniqueness. To overcome these problems special techniques have to be introduced in the algorithms for each particular inverse problem (Richardson and Panchang 1992; Lardner and Das 1994). The suggested methods include choosing different criteria to measure data misfit (Yeh and Sun 1984; Chavent 1983; van Straten 1983) and adding penalty terms into cost function (Lardner and Das 1994; Richardson and Panchang 1992; Carrera and Neuman 1986). Since identifiability is closely related to the model to be investigated, there is no general method to be adopted so far. More research is warranted in this area.

1.3 Objectives

The purpose of this study is to investigate the feasibility of the inverse approach of eutrophication modeling in estuarine system and to improve the understanding of the possibility of inverse parameter estimation through theoretical and numerical investigations of a typical eutrophication model. The basic objectives are: (1) to investigate inverse numerical modeling of estuarine eutrophication problems theoretically, (2) to develop an inverse eutrophication model with the capability of estimating unknown parameter values of the system, (3) to develop an efficient algorithm for estimation of model parameter values, (4) to investigate the feasibility and uniqueness of parameter estimation for a particular system through numerical experiments, and (5) to apply the inverse model to calibrate a real estuarine eutrophication model.

II. METHODOLOGY

In this chapter, an inverse eutrophication model is developed by using the variational method. The inverse eutrophication model is built on the top of a vertical two-dimensional eutrophication model developed by Park and Kuo (1996). The basic idea of the inverse approach is that the model parameter values are varied until a defined cost function, which measures the misfit between the model output and observation data, is minimized while the model dynamics and kinetics are treated as strong constraints. The best fit is determined by a system of equations consisting of the model equations and their corresponding adjoint model equations forced by the model data misfit. The adjoint equations provide intermediate results to calculate the gradients of the cost function with respect to the unknown parameters. The gradients are used with an appropriate iterative descent method to search out the optimal estimations of the model parameter values.

2.1 Model Equation

The eutrophication model used in this study is a laterally integrated two-dimensional model developed by Park and Kuo (1993a). Eight water quality state variables are modeled, which are phytoplankton, organic nitrogen, ammonium

nitrogen, nitrite-nitrate nitrogen, organic phosphorus, inorganic (ortho) phosphorus, carbonaceous biochemical oxygen demand and dissolved oxygen (Fig. 2-1). The mass-balance equation of a water quality state variable can be written as

$$\frac{\partial(C_i B)}{\partial t} + \frac{\partial(C_i B u)}{\partial x} + \frac{\partial(C_i B v)}{\partial z} = \frac{\partial}{\partial x} K_x B \frac{\partial C_i}{\partial x} + \frac{\partial}{\partial z} K_z B \frac{\partial C_i}{\partial z} + B S_i(C, \beta) \quad (2-1)$$

where t = time; u, v = the horizontal and vertical velocities, respectively; C_i = laterally averaged concentration of the i th state variable ($i = 1, 2, \dots, 8$); S_i = functions describing the time rate of internal increase (or decrease) of mass by biochemical reaction and external addition (or withdrawal) of the i th state variable; $\beta = (\beta_1, \beta_2, \dots, \beta_m)^T$ is the parameter to be estimated; m = the number of unknown parameters; K_x & K_z = dispersion coefficients in the x and z directions, respectively; B = river width. The concentration corresponding to each state variable is denoted as $C = (C_1, C_2, \dots, C_8)^T = (\text{Chl}, \text{N1}, \text{N2}, \text{N3}, \text{P1}, \text{P2}, \text{CBOD}, \text{DO})^T$, where Chl = chlorophyll 'a' ($\mu\text{g l}^{-1}$); N1 = organic nitrogen (mg l^{-1}); N2 = ammonium nitrogen (mg l^{-1}); N3 = nitrite-nitrate nitrogen (mg l^{-1}); P1 = organic phosphorus (mg l^{-1}); P2 = inorganic phosphorus (mg l^{-1}); CBOD = carbonaceous biochemical oxygen demand (mg l^{-1}); DO = dissolved oxygen (mg l^{-1}). The model formulation of source and sink functions are fully described in Park and Kuo (1993a) and listed in Appendix A.

2.2 Scaling Model Equations

In Eq. 2-1, the state variables have different units and magnitudes. They have to

be scaled so that each state variable has similar "weight" during optimization processes. The system chosen to scale the state variables are as follows:

$$\begin{aligned} Chl' &= \frac{Chl}{Chl^0} , & NI' &= \frac{NI}{NI^0} , & N2' &= \frac{N2}{N2^0} , & N3' &= \frac{N3}{N3^0} , \\ P1' &= \frac{P1}{P1^0} , & P2' &= \frac{P2}{P2^0} , & CBOD' &= \frac{CBOD}{CBOD^0} , & DO' &= \frac{DO}{DO^0} , \end{aligned}$$

where superscript "0" denotes maximum concentrations of the state variables.

Introducing some scale factors defined as follows:

$$\begin{aligned} \gamma_{CN1} &= \frac{Chl^0}{NI^0} , & \gamma_{CN2} &= \frac{Chl^0}{N2^0} , & \gamma_{CN3} &= \frac{Chl^0}{N3^0} , & \gamma_{CP1} &= \frac{Chl^0}{P1^0} , & \gamma_{CP2} &= \frac{Chl^0}{P2^0} \\ \gamma_{CBO} &= \frac{Chl^0}{CBOD^0} , & \gamma_{CDO} &= \frac{Chl^0}{DO^0} , & \gamma_{N12} &= \frac{NI^0}{N2^0} , & \gamma_{N23} &= \frac{N2^0}{N3^0} , & \gamma_{P12} &= \frac{P1^0}{P2^0} \\ \gamma_{N3DO} &= \frac{N3^0}{DO^0} , & \gamma_{CBDO} &= \frac{CBOD^0}{DO^0} , & \gamma_{N2DO} &= \frac{N2^0}{DO^0} \end{aligned}$$

Substituting dimensionless variables and scale factors into Eq. 2-1, the original mass balance equations can be written as

$$F_i(C', \beta) = FT(C'_i) + FS_i(C', \beta) = 0 \quad i=1,2,\dots,8 \quad (2-2)$$

where

$$FT(C'_i) = \frac{\partial(C'_i B)}{\partial t} + \frac{\partial(C'_i Bu)}{\partial x} + \frac{\partial(C'_i Bv)}{\partial z} - \frac{\partial}{\partial x} K_x B \frac{\partial C'_i}{\partial x} - \frac{\partial}{\partial z} K_z B \frac{\partial C'_i}{\partial z} \quad (2-2a)$$

is the transport function, and

$$FS(C', \beta) = -BS'(C', \beta) \quad (2-2b)$$

is the scaled source and sink function. The scaled source and sink functions (S_i') are listed in Appendix B.

2.3 Adjoint Model

Eq. 2-2 provides a set of differential equations for eight water quality state variables over a domain M with spatial domain Ω , boundary Γ , and temporal domain $[0, T_N]$; T_N is a time later than the last date when prototype observations are available. In the equations, the velocity fields, $u(t, x, z)$ and $v(t, x, z)$, dispersion coefficients $K_x(t, x, z)$ and $K_z(t, x, z)$, are assumed to be known values which are obtained from the hydrodynamic model.

Denoting $F = (F_1, F_2, \dots, F_8)^T$, the mass-balance equation (Eq. 2-2) can be written symbolically as

$$F(C', \beta) = 0 \quad (2-3)$$

Let $\hat{C}' = (\hat{C}'_1, \hat{C}'_2, \hat{C}'_3, \hat{C}'_4, \hat{C}'_5, \hat{C}'_6, \hat{C}'_7, \hat{C}'_8)^T$ be the available prototype observed data of

concentrations of the state variables over domain M , where \hat{C}'_i 's are also scaled

concentrations. A weighted least-squares criterion is chosen to measure the data misfit. the cost function is then defined as

$$J(C'; \beta') = \int_{T_0}^{T_N} \int_{\Omega} \frac{1}{2} \sum_{i=1}^8 w_i(t, x, z) (C_i' - \hat{C}'_i)^2 B d\Omega dt \quad (2-4)$$

where $w_i(t, x, z)$ = weight with respect to the i th state variables; and $d\Omega = dx dz$. The goal is to seek a set of optimum parameter values β such that the difference between the model results C' and the observation data \hat{C}' , or J , is minimized.

A systematic approach for solving the problem is based on a generalization of the classical Lagrange multiplier technique used in finite-dimensional spaces. Let

$\Lambda = (\lambda_1, \lambda_2, \dots, \lambda_8) = (\lambda_{CH}, \lambda_{N1}, \lambda_{N2}, \lambda_{N3}, \lambda_{P1}, \lambda_{P2}, \lambda_{CBOD}, \lambda_{DO})$ be scalars called Lagrange

multipliers. The Lagrangian of the constraint problem is the scalar function of C' , β and Λ defined by

$$L(C', \beta, \Lambda) = J(C', \beta) + \sum_{i=1}^8 \int_{T_r} \int_{\Omega} \lambda_i F_i(C', \beta) d\Omega dt \quad (2-5)$$

The first-order variation of δL resulting from perturbations δC , $\delta \lambda$ and $\delta \beta$ is equal to (Le Dimet and Talagrand 1986):

$$\delta L = \sum_{i=1}^8 \int_{T_r} \int_{\Omega} w_i (C'_i - \hat{C}'_i) B \delta C'_i d\Omega dt + \sum_{i=1}^8 \int_{T_r} \int_{\Omega} [\lambda_i \delta F_i(C', \beta) + F_i(C', \beta) \delta \lambda_i] d\Omega dt \quad (2-6)$$

Integrating by parts of Eq. 2-6 gives

$$\begin{aligned} \delta L = & \sum_{i=1}^8 \int_{T_r} \int_{\Omega} [w_i (C'_i - \hat{C}'_i) B + \hat{F}_i(C', \Lambda, \beta)] \delta C'_i d\Omega dt + \sum_{i=1}^8 \int_{T_r} \int_{\Omega} F_i(C', \beta) \delta \lambda_i d\Omega dt \\ & + \sum_{k=1}^m \int_{T_r} \int_{\Omega} \left(\sum_{i=1}^8 \lambda_i \frac{\partial F_i}{\partial \beta_k} \right) \delta \beta_k d\Omega dt \end{aligned}$$

$$+\sum_{i=1}^8 \left\{ \int_{\Omega} B\lambda_i|_{t_0}^{T_n} \delta C_i' d\Omega + \int_{T_n} \int_{\Omega} Bu\lambda_i|_{\Gamma_i} \delta C_i' dzdt \right\} + \int_{T_n} \int_{\Omega} Bv\lambda_i|_{\Gamma_i} \delta C_i' dxdt \quad (2-7)$$

where $\hat{F}_i(C', \Lambda, \beta)$ and $\partial FS_i / \partial \beta_k$ are the functions to be determined later. Ω_x ,

Ω_z are the spatial domains with respect to the horizontal (x) and vertical (z) directions, respectively. Γ_x and Γ_z are boundaries with respect to x and z directions, respectively.

For given C' , Λ and β , L will be stationary if and only if δL is zero for any perturbations $\delta C'_i$, $\delta \lambda_i$ and $\delta \beta_k$. This will be the case if and only if the following conditions are simultaneously satisfied.

$$F_i(C', \beta) = 0 \quad \text{on } M \quad i = 1, 2, \dots, 8 \quad (2-8)$$

$$w_i(C'_i - \hat{C}'_i) B + \hat{F}_i(C', \Lambda, \beta) = 0 \quad \text{on } M \quad i = 1, 2, \dots, 8 \quad (2-9)$$

$$\sum_{i=1}^8 \lambda_i \frac{\partial FS_i}{\partial \beta_k} = 0 \quad \text{on } M \quad k = 1, 2, \dots, m \quad (2-10)$$

$$\int_{\Omega} B\lambda_i|_{t_0}^{T_n} \delta C_i' dA = 0 \quad (2-11)$$

$$\int_0^{T_n} \int_{\Omega} Bu\lambda_i|_{\Gamma_i} \delta C_i' dzdt = 0 \quad (2-12)$$

$$\int_0^{T_n} \int_{\Omega} Bv\lambda_i|_{\Gamma_i} \delta C_i' dxdt = 0 \quad (2-13)$$

Eqs. 2-8 to 2-10, together with initial and boundary conditions Eqs. 2-11 to 2-13, are Euler-Lagrangian equations of the original mass balance equations. It can be seen that Eq. 2-8 recovers the original Eq. 2-2. Eq. 2-9 is the adjoint model of the original model. The terms on the left-hand-side of Eq. 2-10 (see Eq. 2-16) is the gradient of J

with respect to the parameter β_k at location (x, z) and time t . This gradient is used in the conventional algorithm to minimize the cost function by the conjugate gradient method or the steepest descent method (Gill and Murray 1982). It will vanish when the cost function (Eq. 2-4) reaches its minimum. All the initial conditions and boundary conditions can be satisfied if assuming $\lambda = 0$ at boundary Γ , and at times $t = 0$ and $t = T_N$.

The adjoint model (Eq. 2-9) that is obtained from integration by parts of Eq. 2-6 is listed below:

$$w_i(C'_i - \hat{C}'_i)B + \hat{F}_i(C', \Lambda, \beta) = 0 \quad (2-14)$$

where

$$\hat{F}_i(C', \lambda, \beta) = -\hat{F}T(\lambda_i) + B \hat{F}S_i(C', \Lambda, \beta) \quad (2-14a)$$

$$\hat{F}T(\lambda_i) = B \frac{\partial \lambda_i}{\partial t} + B_u \frac{\partial \lambda_i}{\partial x} + B_v \frac{\partial \lambda_i}{\partial z} + \frac{\partial}{\partial x} K_x B \frac{\partial \lambda_i}{\partial x} + \frac{\partial}{\partial z} K_z B \frac{\partial \lambda_i}{\partial z}$$

$$\hat{F}S_1 = -(G - R - P)\lambda_{chl} + K_{chl} \frac{\partial \lambda_{chl}}{\partial z} - a_n(R + a_r P) [\gamma_{CN1} F_n \lambda_{N1} + \gamma_{CN2} (1 - F_n) \lambda_{N2}]$$

$$+ a_n G [\gamma_{CN2} PR \lambda_{N2} + \gamma_{CN3} (1 - PR) \lambda_{N3}]$$

$$- a_p(R + a_r P) [\gamma_{CP1} F_p \lambda_{P1} + \gamma_{CP2} (1 - F_p) \lambda_{P2}]$$

$$+ \gamma_{CP2} a_p G \lambda_{P2} - a_c a_{co} [\gamma_{CBO} (a_r P) \lambda_{CBOD} + \gamma_{CDO} (PQ \cdot G - \frac{R}{RQ}) \lambda_{DO}] \quad (2-14b)$$

$$\hat{F}S_2 = \frac{K_{n12} K_{h12}}{(K_{h12} + NI)^2} (\lambda_{N1} - \gamma_{N12} \lambda_{N2}) + K_{n11} \frac{\partial \lambda_{N1}}{\partial z} \quad (2-14c)$$

$$\begin{aligned}
F\hat{S}_3 = & \frac{K_{n23}K_{h23}}{(K_{h23}+N2)^2} \frac{DO}{K_{nit}+DO} (\lambda_{N2} - \gamma_{N23}\lambda_{N3} + \gamma_{N2DO}a_{nit}\lambda_{DO}) \\
& + Chl' \cdot K_{gr} \theta_1^{T-20} I_L \frac{\partial N}{\partial N2} N2^0 (\gamma_{CP2} a_p \lambda_{P2} + \gamma_{CN3} a_n \lambda_{N3} - \gamma_{CDO} a_c a_{co} PQ \cdot \lambda_{DO} - \lambda_{Chl}) \\
& + a_n Chl' \cdot K_{gr} \theta_1^{T-20} I_L \frac{\partial(N \cdot PR)}{\partial N2} N2^0 (\gamma_{CN2} \lambda_{N2} - \gamma_{CN3} \lambda_{N3}) \quad (2-14d)
\end{aligned}$$

$$\begin{aligned}
F\hat{S}_4 = & K_{n33} \frac{K_{h33} \lambda_{N3}}{K_{h33} + DO} + a_n Chl' \cdot K_{gr} \theta_1^{T-20} I_L \frac{\partial(N \cdot PR)}{\partial N3} N3^0 (\gamma_{CN2} \lambda_{N2} - \gamma_{CN3} \lambda_{N3}) \\
& + Chl' \cdot K_{gr} \theta_1^{T-20} I_L \frac{\partial N}{\partial N3} N3^0 (\gamma_{CN3} a_n \lambda_{N3} + \gamma_{CP2} a_p \lambda_{P2} \\
& - \gamma_{CDO} a_c a_{co} PQ \cdot \lambda_{DO} - \lambda_{Chl}) \quad (2-14e)
\end{aligned}$$

$$F\hat{S}_5 = \frac{K_{p12}K_{hp12}}{(K_{hp12}+P1)^2} (\lambda_{P1} - \gamma_{P12}\lambda_{P2}) + K_{p11} \frac{\partial \lambda_{P1}}{\partial z} \quad (2-14f)$$

$$\begin{aligned}
F\hat{S}_6 = & K_{p22} \frac{\partial \lambda_{P2}}{\partial z} + Chl' \cdot K_{gr} \theta_1^{T-20} I_L \frac{\partial N}{\partial P2} P2^0 (\gamma_{CP2} a_p \lambda_{P2} \\
& + \gamma_{CN3} a_n \lambda_{N3} - \gamma_{CDO} a_c a_{co} PQ \cdot \lambda_{DO} - \lambda_{Chl}) \\
& + a_n Chl' \cdot K_{gr} \theta_1^{T-20} I_L \frac{\partial N \cdot PR}{\partial P2} P2^0 (\gamma_{CN2} \lambda_{N2} - \gamma_{CN3} \lambda_{N3}) \quad (2-14g)
\end{aligned}$$

$$F\hat{S}_7 = K_c \lambda_{CBOD} + \gamma_{CBDO} K_c \lambda_{DO} + K_{BOD} \frac{\partial \lambda_{CBOD}}{\partial z} \quad (2-14h)$$

$$\begin{aligned}
F\hat{S}_8 = & \gamma_{N2DO}^{-1} \frac{K_{n23}N2}{K_{h23}+N2} \frac{K_{nit}}{(K_{nit}+DO)^2} (\gamma_{N2DO} a_{nit} \lambda_{DO} + \lambda_{N2} - \gamma_{N23} \lambda_{N3}) \\
& + (1 - \gamma_1) K_r \lambda_{DO} - \gamma_{DON3} K_{n33} \frac{K_{h33}N3}{(K_{h33}+DO)^2} \lambda_{N3} \\
& + \frac{SOD}{B} \frac{K_{DO}}{(K_{DO}+DO)^2} \frac{\partial B}{\partial z} (\lambda_{DO} + \gamma_{CBDO}^{-1} \lambda_{CBOD}) \quad (2-14i)
\end{aligned}$$

$$\frac{\partial N}{\partial N2} = \frac{\partial N}{\partial N3} = \begin{cases} \frac{K_{mn}}{(K_{mn} + N2 + N3)^2} & \text{if } L_{N2,3} < L_{P2} \\ 0 & \text{otherwise} \end{cases} \quad (2-14j)$$

$$\frac{\partial N}{\partial P2} = \begin{cases} \frac{K_{mp}}{(K_{mp} + P2)^2} & \text{if } L_{P2} < L_{N2,3} \\ 0 & \text{otherwise} \end{cases} \quad (2-14k)$$

and $L_{N2,3}$ and L_{P2} are defined in Appendix A.

For the first order approach, the gradient of $N \cdot PR$ with respect to $N2$ and $N3$ can be neglected since both nutrient limitation N and ammonium preference PR approach constants if nutrients are abundant or both are small values if nutrients are scarce.

The terms on the left-hand-side of Eq. 2-10 is the gradient of the cost function with respect to the parameter β_k which can be obtained as follows.

Note that Eq. 2-6 can be written as

$$\begin{aligned} \delta L = & \delta J + \sum_{i=1}^8 \int_{T_n} \int_{\Omega} [\hat{F}_i(C', \Lambda, \beta)] \delta C_i' d\Omega dt + \sum_{i=1}^8 \int_{T_n} \int_{\Omega} F_i(C', \beta) \delta \lambda_i d\Omega dt \\ & + \sum_{k=1}^m \int_{T_n} \int_{\Omega} \left(\sum_{i=1}^8 \lambda_i \frac{\partial F S_i}{\partial \beta_k} \right) \delta \beta_k d\Omega dt + BIT \end{aligned} \quad (2-15)$$

where BIT is the initial and boundary conditions, i.e., Eqs. 2-11 - 2-13. Note that the condition $\delta L / \delta \beta = 0$ should be satisfied at the stationary point, which gives

$$\frac{\delta J}{\delta \beta_k} = - \int_{T_n} \int_{\Omega} \left(\sum_{i=1}^8 \lambda_i \frac{\partial F S_i}{\partial \beta_k} \right) \delta \beta_k d\Omega dt$$

(2-16)

In the present inverse model, thirteen parameters are chosen, as an example, to be estimated. They are :

- K_{gr} = optimum phytoplankton growth rate at 20 °C (day⁻¹);
 R_{20} = phytoplankton respiration rate at 20 °C (day⁻¹);
 P_{20} = phytoplankton mortality rate at 20 °C (day⁻¹);
 $K_{n12}(20)$ = ammonification rate of N1 to N2 (mg l⁻¹ day⁻¹);
 $K_{n23}(20)$ = nitrification rate of N2 to N3 (mg l⁻¹ day⁻¹);
 $K_{n33}(20)$ = denitrification rate at 20 °C (day⁻¹);
 $K_{p12}(20)$ = organic phosphorus mineralization rate at 20 °C (mg l⁻¹ day⁻¹);
 K_{Chl} = settling rate of phytoplankton (cm day⁻¹);
 K_{n11} = settling rate of N1 (cm day⁻¹);
 K_{p11} = settling rate of P1 (cm day⁻¹);
 K_{p22} = settling rate of P2 (cm day⁻¹);
 $K_c(20)$ = first-order decay rate of CBOD at 20 °C (day⁻¹); and
 K_{bod} = settling rate of CBOD (cm day⁻¹).

These parameters are related to the environment to be modeled and represent some underlying processes which are simplified in the model. The gradients of the cost function with respect to these parameters are listed below:

$$\delta J_{K_r} = \int_{T_r} \int_{\Omega} \left\{ \lambda_{Chl} - \gamma_{CN2} a_n PR \lambda_{N2} - \gamma_{CN3} a_n (1-PR) \lambda_{N3} - \gamma_{CP2} a_p \lambda_{P2} + \gamma_{CDO} a_c a_{co} PQ \lambda_{DO} \right\} B \cdot Chl' \cdot \theta_1^{T-20} I_L \cdot N d\Omega dt \quad (2-17)$$

$$\delta J_{R_n} = \int_{T_r} \int_{\Omega} \left\{ -\lambda_{Chl} + \gamma_{CN1} a_n F_n \lambda_{N1} + \gamma_{CN2} a_n (1-F_n) \lambda_{N2} + \gamma_{CP1} a_p F_p \lambda_{P1} + \gamma_{CP2} a_p (1-F_p) \lambda_{P2} - \gamma_{CDO} a_c a_{co} \frac{1}{RQ} \lambda_{DO} \right\} B \cdot Chl' \cdot \theta_2^{T-20} d\Omega dt \quad (2-18)$$

$$\delta J_{P_n} = \int_{T_r} \int_{\Omega} \left\{ -\lambda_{Chl} + a_r [\gamma_{CN1} a_n F_n \lambda_{N1} + \gamma_{CN2} a_n (1-F_n) \lambda_{N2} + \gamma_{CP1} a_p F_p \lambda_{P1} + \gamma_{CP2} a_p (1-F_p) \lambda_{P2} + \gamma_{CBO} a_c a_{co} \lambda_{CBOD}] \right\} B \cdot Chl' \cdot \theta_3^{T-20} d\Omega dt \quad (2-19)$$

$$\delta J_{K_{ni}} = \int_{T_n} \int_{\Omega} (\gamma_{N12} \lambda_{N2} - \lambda_{N1}) \theta_4^{T-20} \frac{NI'}{K_{h12} + NI} B \, d\Omega dt \quad (2-20)$$

$$\delta J_{K_{ni}} = \int_{T_n} \int_{\Omega} (\gamma_{N23} \lambda_{N3} - \lambda_{N2} - \gamma_{N2DO} a_{na} \lambda_{DO}) \theta_5^{T-20} \cdot \frac{N2'}{K_{h23} + N2} \frac{DO \cdot B}{K_{ni} + DO} \, d\Omega dt \quad (2-21)$$

$$\delta J_{K_{ni}} = \int_{T_n} \int_{\Omega} -\lambda_{N3} \frac{K_{h33} N3'}{K_{h33} + DO} \theta_6^{T-20} B \, d\Omega dt \quad (2-22)$$

$$\delta J_{K_{pi}} = \int_{T_n} \int_{\Omega} (\gamma_{P12} \lambda_{P2} - \lambda_{P1}) \frac{P1'}{K_{hp12} + P1} \theta_7^{T-20} B \, d\Omega dt \quad (2-23)$$

$$\delta J_{K_{chl}} = \int_{T_n} \int_{\Omega} \lambda_{chl} \frac{\partial chl'}{\partial z} B \, d\Omega dt \quad (2-24)$$

$$\delta J_{K_{ni}} = \int_{T_n} \int_{\Omega} \lambda_{NI} \frac{\partial NI'}{\partial z} B \, d\Omega dt \quad (2-25)$$

$$\delta J_{K_{pi}} = \int_{T_n} \int_{\Omega} \lambda_{P1} \frac{\partial P1'}{\partial z} B \, d\Omega dt \quad (2-26)$$

$$\delta J_{K_{pi}} = \int_{T_n} \int_{\Omega} \lambda_{P2} \frac{\partial P2'}{\partial z} B \, d\Omega dt \quad (2-27)$$

$$\delta J_{K_c} = \int_{T_n} \int_{\Omega} -(\lambda_{CBOD} + \gamma_{CBDO} \lambda_{DO}) \theta_8^{T-20} B \, d\Omega dt \quad (2-28)$$

$$\delta J_{K_{cb}} = \int_{T_n} \int_{\Omega} \lambda_{CBOD} \frac{\partial (CBDO')}{\partial z} B \, d\Omega dt \quad (2-29)$$

where $\delta J_{\beta} = (\delta J_{K_r}, \delta J_{R_{2n}}, \delta J_{P_{2n}}, \dots, \delta J_{K_{cb}})^T$ are the gradients of the cost function with respect to the parameters.

2.4 Method of Solution

2.4.1 Solution procedure

The solution scheme to solve the model equation (Eq. 2-1), forward model, is

detailed in Park and Kuo (1993a). The adjoint model equations have a similar form as the forward model equations, except for two important features. The dispersion terms have the opposite sign to those in the forward model equations. The source terms include the data misfit as an additional source, i.e., $w_i B(C_i - \hat{C}_i)$. Because of negative dispersion, the adjoint model is stable only if integrated backward, i.e. from time T_N to 0. A similar scheme as the forward model can be developed to integrate the adjoint model backward (see section 2.4.3). The procedural steps of using the inverse model to estimate parameters can be summarized as:

(1) Begin with a set of best initial guess values for the unknown parameters

$$\beta_1, \beta_2, \dots, \beta_{13}.$$

(2) Integrate the model equations (Eq. 2-1) forward in time to calculate the concentration of each state variable and use the output at times when field data are available to calculate the data misfit $w_i(C_i - \hat{C}_i)$ and the value of the cost function.

(3) Integrate the adjoint equations (Eq. 2-14) backward in time to calculate the values of λ 's.

(4) Calculate gradient ∇J_β (Eqs. 2-17 - 2-29) corresponding to each parameter β_1 to β_{13} .

(5) With the gradient information, apply the conjugate gradient algorithm (Navon 1987; Polak and Ribiere 1969) to obtain the new parameter (update parameter value).

(6) Verify that the minimization process is done. The convergence criterion is satisfied if $|\nabla J_\beta| / |\nabla J_\beta^0| < \epsilon$, where ∇J_β^0 is the value at the initial iteration, or verify that

the relative total error of the cost function $|J/J^0| < \epsilon_1$, where J^0 is the value of the cost function at time zero.

(7) Return to step (2) if the optimal solution is not found.

2.4.2 Grid system and geometry

The forward model equations and the adjoint model equations are solved using finite difference method with an uniform grid of spatial staggered variables. The geometry of the grid used in the model and the location of variables within the grid are shown in Fig. 2-2. The grid system has surface elevation (η) defined at the middle of each segment, while C , λ , and B are at the center of the grid cell. The variables, v , A_z , and K_z , are defined at the bottom face of the grid cell, while the grid containing u , A_x , and K_x is staggered by half the segment length as these that are defined at the grid cell walls.

2.4.3 Finite difference treatment

A two-time level finite difference scheme is used to solve the system. The finite difference scheme of the forward model is detailed in Park and Kuo (1993a). The finite difference scheme of the adjoint model is described in this section. Although the adjoint model (Eq. 2-14) is very similar to the forward model (Eq. 2-2), the finite difference scheme of the adjoint model is different from that of the forward model since the conservative control volume formulation is used to integrate the forward model. An alternate way to obtain the finite difference scheme of the adjoint model, which corresponds exactly to the scheme used in the forward model, is to derive it

directly from the finite difference equations of the forward model.

For the two-time level finite difference formulation, the finite difference form of the forward model at cell (i, k) and time level " $n+1$ " for the j th state variable ($j = 1, \dots, 8$) can be generally written as:

$$D_{ik}^{jn+1} = D(C_{ik}^{jn+1}, C_{ik}^{jn}, C_{i-1,k}^{jn+1}, C_{i+1,k}^{jn+1}, C_{i-1,k}^{jn}, C_{i+1,k}^{jn}, C_{i,k-1}^{jn+1}, C_{i,k+1}^{jn+1}, C_{i,k-1}^{jn}, C_{i,k+1}^{jn}) = 0 \quad (2-30)$$

where C_{ik}^{jn+1} is the scaled concentration of the j th state variable at cell (i, k) and

time-level $n+1$. The discrete form of the Lagrangian of the constraint problem

(Eq. 2-5) can be written as

$$L = \sum_n \sum_j \sum_i \sum_k \left(w_{ik} (C_{ik}^{jn+1} - \hat{C}_{ik}^{jn+1})^2 B_{ik} + \lambda_{ik}^{jn} \cdot D_{ik}^{jn+1} \right) \Delta x \Delta z \Delta t \quad (2-31)$$

where \hat{C}_{ik}^{jn+1} , λ_{ik}^{jn} are the scaled field observations and Lagrangian multipliers,

respectively. The finite difference equations of the adjoint model can be obtained by

taking the derivative of Eq. 2-31 with respect to C_{ik}^{jn} . The detailed derivations and

the finite difference equations of the adjoint model are presented in Appendix C.

2.4.4. Decoupling kinetic processes

The governing mass-balance equation (Eq. 2-1) and the adjoint model equation (Eq. 2-14) consist of physical transport, advective and dispersion, and kinetic processes

(or error source of misfit). Since the time step used for calculating physical transport processes is on the order of few minutes, the kinetic processes should be updated on the same time interval if they are solved simultaneously. Because the concentrations of the state variables at each time step will be used when integrating the adjoint model backward, the concentrations of all the state variables have to be stored at each time step at every cell. For long period model simulation, both computation speed and storage space should be considered. In the present model, the kinetic terms are decoupled from the physical transport processes when solving Eqs. 2-1 and 2-14. Decoupling of the physical transport and kinetic processes has been used in some models (Park et al. 1995; Kuo and Neilson 1988; Ambrose et al. 1988). The solution scheme involves a two-step computation, in which mass of state variables are physically transported first and then followed by the update of kinetic processes. The mass-balance equation for physical transport only, which takes the same form for each state variable, can be written as

$$\frac{\partial(CB)}{\partial t} + \frac{\partial(CBu)}{\partial x} + \frac{\partial(CBv)}{\partial z} = \frac{\partial}{\partial x} K_x B \frac{\partial C}{\partial x} + \frac{\partial}{\partial z} K_z B \frac{\partial C}{\partial z} \quad (2-32)$$

The equation for kinetic processes only, which will be referred to as the kinetic equation, is

$$\frac{\partial(CB)}{\partial t} = BS_c \quad (2-33)$$

In the same way, the error source and sink functions of the adjoint model can be

decoupled from its physical transport. The physical transport processes and error functions for the adjoint model can be written as

$$B \frac{\partial \lambda}{\partial t} + Bu \frac{\partial \lambda}{\partial x} + Bv \frac{\partial \lambda}{\partial z} = - \frac{\partial}{\partial x} K_x B \frac{\partial \lambda}{\partial x} - \frac{\partial}{\partial z} K_z B \frac{\partial \lambda}{\partial z} \quad (2-34)$$

and

$$\frac{\partial \lambda}{\partial t} = F \hat{S}(C', \Lambda, \beta) + w(C' - \hat{C}') \quad (2-35)$$

A two-step computation of the decoupling method is used in the present inverse model to solve Eqs. 2-32 to 2-35. Since the time scale of kinetic processes is on the order of hours, which is much slower than the time scale of physical transport, it is possible to update kinetic processes hourly instead of updating them every few minutes. That is, the kinetic equations can be updated following several time steps of physical transports. Fig. 2-3a illustrates the solution procedures over the time period from t_n to t_{n+m} , where subscripts represent time level and $m \geq 1$.

The first step, S1, solves kinetic processes alone (Eq. 2-33) over $m/2 \cdot \Delta t$ from t_n to $t_{n+1/2m}$ explicitly and gives an intermediate concentration, $C_{-P}^{n+1/2m}$, where subscript -P designates one lacking the physical transport over $m/2 \cdot \Delta t$. Next, S2, the intermediate concentration field $C_{-P}^{n+1/2m}$ or C_{+K}^n ($C_{+K}^n = C_{-P}^{n+1/2m}$), where the subscript +K designates one with a surplus kinetic update over $m/2 \cdot \Delta t$, are physically transported m time steps over $m\Delta t$ from t_n to t_{n+m} by the transport equation (Eq. 2-32). The intermediate results are denoted as C_{-K}^{n+m} , where subscript -K designates the

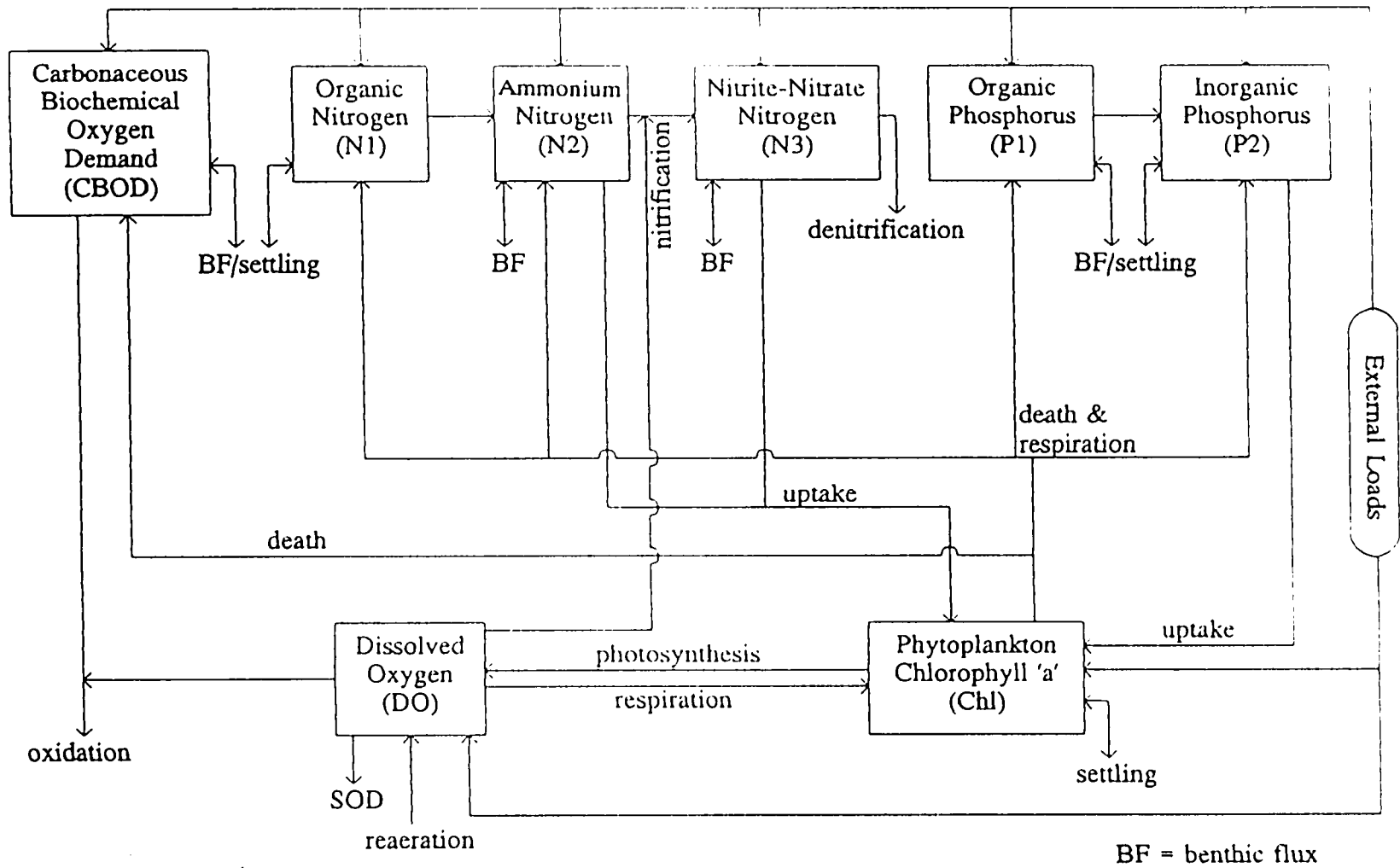
intermediate concentration that lacks a kinetic update over $1/2m \cdot \Delta t$. Finally, S3, the intermediate concentration C_{-K}^{n+m} or $C_{+P}^{n+1/2m}$ ($C_{+P}^{n+1/2m} = C_{-K}^{n+m}$), where the subscript +P designates one with a surplus physical transport over $m/2\Delta t$, are updated kinetic processes again by solving Eq. 2-33 explicitly to give the final results of concentration C^{n+m} . The same procedure will repeat every m time steps.

When solving the adjoint model, the same method is used to integrate Eqs. 2-34 and 2-35 backward. The procedures are illustrated in Fig. 2-3b. Because the errors of misfit functions (Eq. 2-35) are calculated twice for every m time steps of physical transport, one only needs to save concentrations of the state variables at the time steps corresponding to those at which errors of misfit are needed during the integrating processes of the forward model, i.e., only need to save concentrations $C_{-P}^{n+1/2m}$ and C^{n+m} at time $n+1/2m$ and $n+m$, respectively, for every m time steps. The values of λ^n and λ^{n+m} are used to calculate gradients of the cost function with respect to each parameter.

Fig. 2-4 shows an example of the comparisons of the forward model results of the concentrations of eight state variables (surface maximum and bottom minimum) between updating kinetic processes every 8 minutes ($\Delta t = 480s$, $m = 1$) and every two hours ($15\Delta t$, $m = 15$). It can be seen that results are very satisfactory even updating kinetic processes every two hours. Using a two-step computation of the decoupling method, both computation time and storage space can be reduced significantly.

Figure 2-1. A schematic diagram of interacting water quality state variables.

Rectangular boxes represent eight state variables being simulated and the arrows represent the biogeochemical processes included in the model.



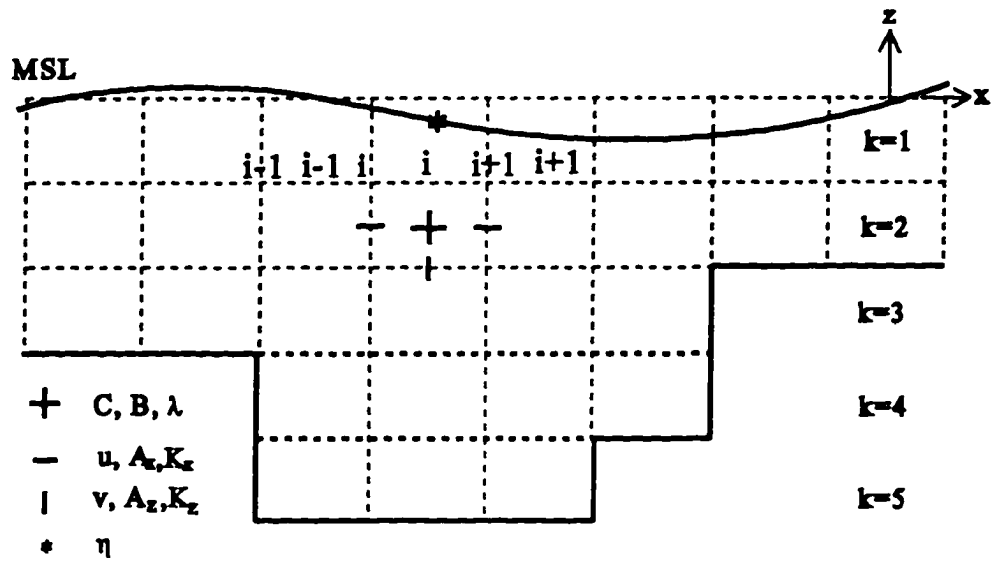
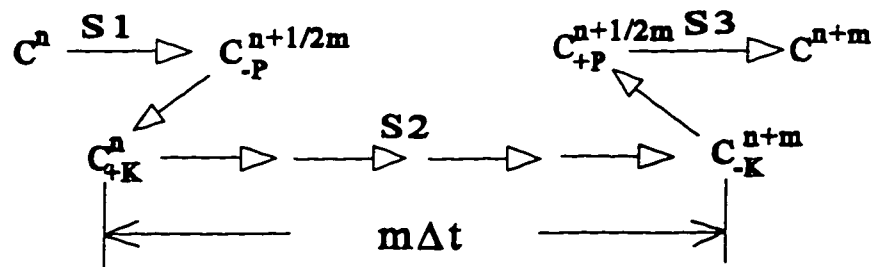
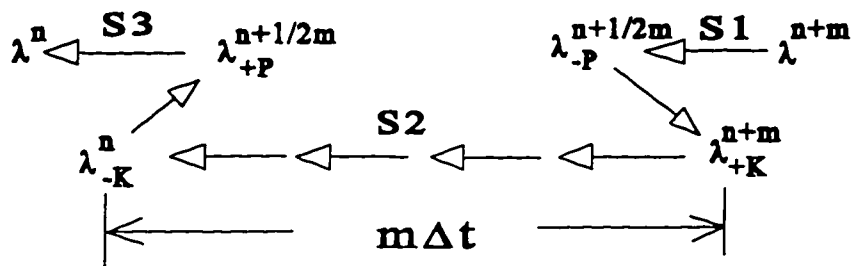


Figure 2-2. Grid pattern, location and indexing of variable



(a)



(b)

Figure. 2-3. The solution method for the forward model (a) and backward mode (b), employing an alternate solution of physical transport and kinetic processes or error source update. (The subscripts K and P indicate kinetic processes and physical transport respectively. The subscript + indicates surplus either kinetic processes or physical transport, while the subscript - indicates lacking either kinetic processes or physical transport.)

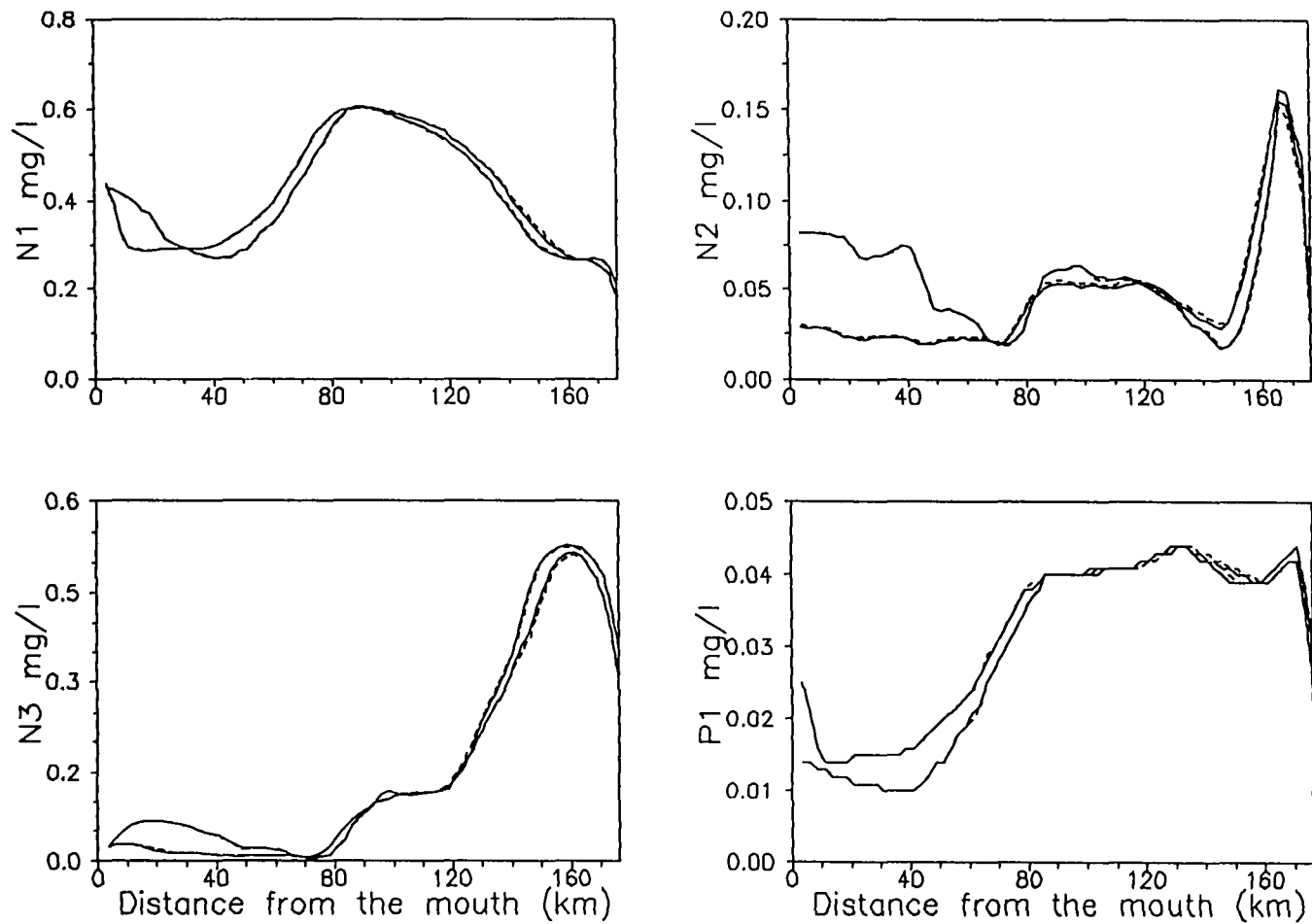


Figure 2-4. A comparison of calculated concentrations (surface maximum and bottom minimum) between updating kinetic processes every 8 minutes ($\Delta t=480s$, $m=1$) and every two hours ($15\Delta t$, $m=15$). Solid lines are the results of $m=1$ and dashed lines are the results of $m=15$.

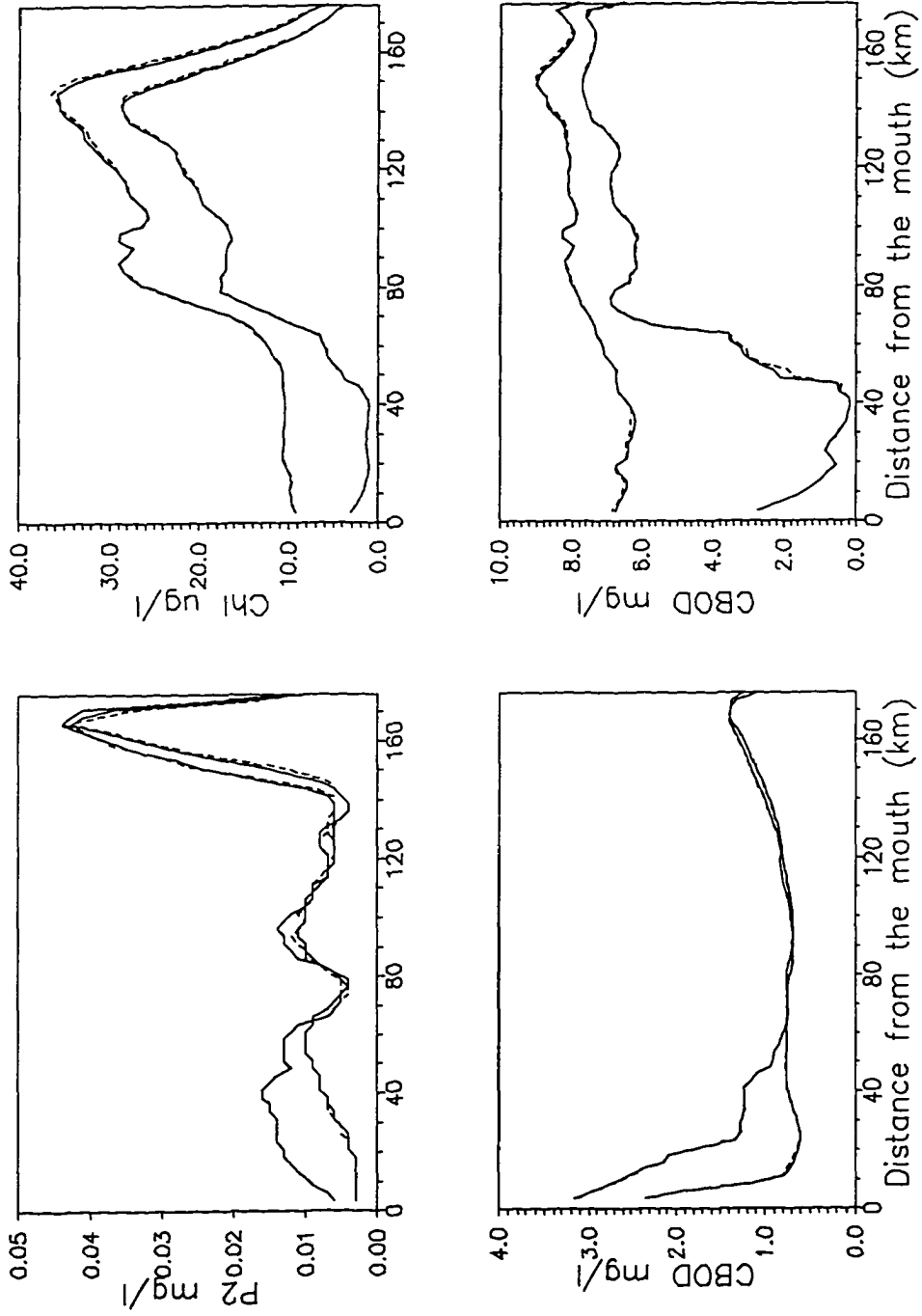


Figure 2-4. (Continued)

2.5 Weights of the Cost Function

Because random errors and sampling errors associated with the field data are different with respect to each state variable, the contribution of each state variable to the cost function should be carefully scaled so that each state variable has a proper weight. Moreover, the errors due to the model structure should be considered when applying a model to a real environment. To reduce errors due to the observations and model structure, the weighted least-squares criterion is used as the cost function. The weights in the cost function reflect confidence in the quality of the observed data and the model predictions. A proper weight increases the model accuracy. However, choosing a good weight for a given problem is considered to be an art. For practical applications, choosing weights often relies on engineering judgement and sometimes on a trial-and-error basis. van Straten (1983) and Carrera and Neuman (1986) proposed a method to choose the weights based on the likelihood theory. Their results give a probabilistic justification for the use of weighted least-squares criterion. To understand the limitation of the method, their results are discussed here. Some different symbols and subscripts are used for simplicity in the following derivations in which an upper case letter denotes a vector or a matrix and a lower case letter denotes a value at an individual point.

Following van Straten (1983) and Carrera and Neuman (1986), let C_{ij} be the column vector of the model results of the scaled concentrations of the state variables at instant time t_j and location (x_p, z_i) . Thus

$$C_{ij}(\beta) = \{c_{1ij}(\beta), \dots, c_{kij}(\beta), \dots, c_{Lij}(\beta)\}^T$$

for $j = 1, 2, \dots, n$; $i = 1, 2, \dots, p$; $k = 1, 2, \dots, L$

where β = the parameter vector with dimension m ; n = the number of observations;
and p = the number of sampling locations; L = the number of state variables; c_{kij} = the scaled concentrations of the k th state variables at location (x_i, z_i) and time t_j . Let \hat{C}_{ij} be the column vector of the observed scaled concentrations of the state variables at time instant t_j and location (x_i, z_i) . Thus

$$\hat{C}_{ij} = \{ \hat{c}_{1ij} \dots, \hat{c}_{kij} \dots, \hat{c}_{Lij} \}^T$$

where \hat{c}_{kij} = the observed concentration of the k th state variables at location (x_i, z_i) and instant time t_j . The cost function (Eq. 2-4) is then written as

$$J(C; \beta) = \sum_{k=1}^L \sum_{i=1}^p \sum_{j=1}^n \frac{1}{2} w_{kij} (\hat{c}_{kij} - c_{kij})^2 \quad (2-36)$$

where w_{kij} = the weight for the k th state variable at time instant t_j and location (x_i, z_i) .

Assuming w_{kij} are constant with respect to time and space, Eq. 2-36 can be written as

$$J(C, \beta) = \sum_{k=1}^L \hat{W}_k \sum_{i=1}^p \sum_{j=1}^n \frac{1}{2} (\hat{c}_{kij} - c_{kij})^2 \quad (2-37)$$

where the \hat{W}_k 's are global weights. Eq. 2-37 is the commonly used weighted least-

squares estimator. Since C_{ij} is a model for \hat{C}_{ij} , \hat{C}_{ij} can be expressed as

$$\hat{C}_{ij} = C_{ij}(\beta) + V_{ij} \quad (2-38)$$

where V_{ij} denotes the sum of all errors at time t_j and location (x_i, z_i) , which includes random errors, sampling errors, and model structure errors. Assuming V_{ij} is normally distributed with variance-covariance matrix R_{ij} , the multivariate probability density function of \hat{C}_{ij} with respect to the parameter β can be written as

$$l(\hat{C}_{ij}; \beta) = \frac{1}{(2\pi)^{L/2} (\det R_{ij})^{L/2}} \exp[-(1/2)(\hat{C}_{ij} - C_{ij}(\beta))^T R_{ij}^{-1} (\hat{C}_{ij} - C_{ij}(\beta))] \quad (2-39)$$

If the distributions V_{ij} are independent with respect to time and space, the likelihood function can be written as

$$L(\beta) = \prod_{i=1}^p \prod_{j=1}^n l(\hat{C}_{ij}; \beta) \quad (2-40)$$

The log-likelihood function can be written as

$$\begin{aligned} -\ln L(\beta) &= (pnL/2) \ln(2\pi) + \frac{1}{2} \sum_{i=1}^p \sum_{j=1}^n \ln(\det R_{ij}) \\ &+ \frac{1}{2} \sum_{i=1}^p \sum_{j=1}^n [(\hat{C}_{ij} - C_{ij}(\beta))^T R_{ij}^{-1} (\hat{C}_{ij} - C_{ij}(\beta))] \end{aligned} \quad (2-41)$$

In Eq. 2-40, both the elements of R_{ij} and the parameter β are unknown. Some assumptions are necessary to further simplify the equation. Following DiToro and van Straten (1979), it can be assumed that R_{ij} does not depend on the parameter estimates

β and no correlations exist among the error disturbances of the state variables. Under these assumptions, R_{ij} is a diagonal matrix which can be written as:

$$R_{ij} = \begin{bmatrix} \sigma_{1ij}^2 & 0 & 0 \\ \cdot & \cdot & \cdot \\ 0 & \sigma_{kij}^2 & 0 \\ \cdot & \cdot & \cdot \\ 0 & 0 & \sigma_{Lij}^2 \end{bmatrix} \quad (2-42)$$

Substituting Eq. 2-42 into Eq. 2-41 gives

$$\begin{aligned} -\ln L(\beta) &= (pnL/2)\ln(2\pi) + \frac{1}{2} \sum_{k=1}^L \sum_{i=1}^p \sum_{j=1}^n \ln(\sigma_{kij}^2) \\ &+ \frac{1}{2} \sum_{k=1}^L \sum_{i=1}^p \sum_{j=1}^n \frac{1}{\sigma_{kij}^2} (\hat{c}_{kij} - c_{kij}(\beta))^2 \end{aligned} \quad (2-43)$$

Differentiating Eq. 2-43 with respect to β gives

$$\sum_{k=1}^L \sum_{i=1}^p \sum_{j=1}^n \frac{1}{\sigma_{kij}^2} (\hat{c}_{kij} - c_{kij}(\beta)) \frac{\partial c_{kij}(\beta)}{\partial \beta} = 0 \quad (2-44)$$

If one further assumes that σ_{kij} is not varying with respect to time and space, Eq. 2-44 can be written as

$$\sum_{k=1}^L \frac{1}{\sigma_k^2} \sum_{i=1}^p \sum_{j=1}^n (\hat{c}_{kij} - c_{kij}(\beta)) \frac{\partial c_{kij}(\beta)}{\partial \beta} = 0 \quad (2-45)$$

This is equivalent to the weighted least-squares problem (Eq. 2-37) with weights

$$\hat{W}_k = 1/\hat{\sigma}_k^2 \quad (2-46)$$

Differentiating Eq. 2-43 with respect to σ_{kij} and assuming σ_{kij} are not varying with respect to time and space leads to

$$\hat{\sigma}_k^2 = \frac{1}{pn} \sum_{i=1}^p \sum_{j=1}^n (\hat{c}_{kij} - c_{kij}(\beta))^2 \quad (2-47)$$

which shows that the model error variance is the mean residual variance. Eq. 2-47 gives a meaningful result. For the state variable associated with large errors, less weight is given.

A disadvantage of Eq. 2-47 is that it holds only for the true parameter β . The implement of the result is not straightforward because one does not know the true parameter β , thus $\hat{\sigma}_k$ remains an unknown variable. van Straten and Carrera

suggested updating $\hat{\sigma}_k$ during the optimization. However, they both showed that a

continuous weight update turned out to be very insensitive to the choice of the parameter values and led to a poor parameter estimation. It should be noted that

updating $\hat{\sigma}_k$ during optimization process implies that $\hat{\sigma}_k$ is a function of parameter

β , which conflicts with the assumptions. Moreover, the cost function (Eq. 2-37) becomes a constant when updating $\hat{\sigma}_k$ during optimization, i.e.

$$J = \sum_{k=1}^L pn = pnL \quad (2-48)$$

thus, the cost function becomes insensitive to the parameter values. This suggests that a continuous update $\hat{\sigma}_k$ is not a proper technique. In a case without model structure

errors, $\hat{\sigma}_k$ can be estimated by observation errors. However, the observation errors are

often unknown in reality. $\hat{\sigma}_k$ remains an unknown variable. Although it is difficult

to use Eq. 2-47 in the model, Eq. 2-47 gives a guideline for choosing weights. With no knowledge of sampling errors and random errors, weights can be possibly estimated on a try-and-error basis based on Eq. 2-47, the error residual variance of the model.

2.6 Preconditioning Method

The success of the inverse model (minimization of Eq. 2-14) is dependent on the condition of the Hessian matrix, the second derivative of the cost function with respect to the parameters. A sufficient condition for a unique solution is that the Hessian matrix is positive defined (Carrera et al. 1986). Convergence properties of the

minimization are determined by the eigenvalue spectrum of the Hessian matrix and speed of convergence is related to the Hessian condition number, the ratio between its maximum and minimum eigenvalues. If the Hessian matrix is ill-conditioned, calculated descent direction is almost quasi-orthogonal to the optimal direction resulting in slow convergence or no convergence. A way to improve ill-conditioning of the Hessian is to introduce a preconditioner so that the new condition number of preconditioned Hessian is close to unity.

Preconditioning has been used in applications of minimization in meteorological problems (Axellsson and Barker 1984; Conn et al., 1992; Courtier et al. 1994; Li et al. 1994). Two methods of preconditioning introduced are: using weights to modify the cost function (Courtier et al. 1994); and applying parameter transformation so that the Hessian has better condition with respect to the new parameter (Li et al. 1994; Carrera et al. 1986). The purpose of the parameter transformation is to scale the parameters and the gradients so that the gradients of the cost function with respect to the scaled parameters have the same order of magnitude.

For the present inverse model, the parameter transformation method is used to construct a preconditioner. If one knows the true Hessian, an ideal preconditioner would be the Hessian itself. Let J_{β}'' be the Hessian matrix of the cost function with respect to the original parameter β and assume that it is positively defined. A linear transformation can be applied to the parameter β , i.e.,

$$\beta = J_{\beta}''^{-\frac{1}{2}} Y \quad (2-49)$$

where $J_{\beta}''^{-\frac{1}{2}}$ is the preconditioner and Y is the new parameter vector. The gradient of

the cost function with respect to Y is

$$\nabla J_Y = J_{\beta}''^{-\frac{1}{2}} \nabla J_{\beta} \quad (2-50)$$

The new Hessian matrix J_Y'' obtained after linear transformation is

$$J_Y'' = J_{\beta}''^{-\frac{1}{2}} J_{\beta}'' J_{\beta}''^{-\frac{1}{2}} = (J_{\beta}''^{-\frac{1}{2}} J_{\beta}''^{\frac{1}{2}}) (J_{\beta}''^{\frac{1}{2}} J_{\beta}''^{-\frac{1}{2}}) = I \quad (2-51)$$

It shows that the condition number of the preconditioned Hessian with respect to the new parameter is unity (eigenvalues are equal to unity). This means that minimization can be obtained in one iteration. However, for the present inverse model, the Hessian matrix is unknown. The basic issue is whether the unknown Hessian can be estimated. Although estimation of the Hessian is very difficult for a nonlinear system, the Hessian can be estimated in some special cases and the estimated Hessian provides some useful information to relax the ill-conditioning of the Hessian.

For a nonlinear model, the Hessian can be written as

$$\frac{\partial^2 J}{\partial \beta_i \partial \beta_j} = \frac{\partial C^T}{\partial \beta_i} W \frac{\partial C}{\partial \beta_j} + (C - \hat{C})^T W \frac{\partial^2 C}{\partial \beta_i \partial \beta_j} \quad (2-52)$$

where C and \hat{C} are the column vectors of the concentrations of the state variables and observations over all sample locations, respectively; W is a weight matrix. Assuming that the system is a quasi-linear system, the second term (second derivative) on the right-hand-side of Eq. 2-52 can be neglected, i.e.,

$$\frac{\partial^2 J}{\partial \beta_i \partial \beta_j} = \frac{\partial C^T}{\partial \beta_i} W \frac{\partial C}{\partial \beta_j} \quad (2-53)$$

If we further assuming that the Hessian is weakly dependent on the parameter β , the gradient can be expanded at a certain point β_0 , thus

$$\frac{\partial C^T}{\partial \beta_i} = \frac{\partial C^T}{\partial \beta_i} \Big|_{\beta_0} + \frac{\partial^2 C}{\partial \beta_i \partial \beta_j} \Delta \beta \quad (2-54)$$

Substituting Eq. 2-54 into Eq. 2-53 and neglecting the second order derivative term gives

$$\frac{\partial^2 J}{\partial \beta_i \partial \beta_j} \approx \frac{\partial C^T}{\partial \beta_i} W \frac{\partial C}{\partial \beta_j} \Big|_{\beta_0} \quad (2-55)$$

Eq. 2-55 shows that the Hessian can be estimated at a certain point β_0 if linearization around the parameter values is reasonable. With a quasi-linear assumption, the error covariance matrix is the inverse of the Hessian (Rabier et al. 1992). Let β_t be the true parameter and $\hat{\beta}_t$ be the result of the minimization, then

$$E\{(\hat{\beta}_t - \beta_t)(\hat{\beta}_t - \beta_t)^T\} = \hat{J}''^{-1} \quad (2-56)$$

where

$$E\{(\hat{\beta}_t - \beta_t)(\hat{\beta}_t - \beta_t)^T\}$$

is the covariance matrix. \hat{J}''^{-1} is the estimated inverse Hessian. With the assumption

that the Hessian is weakly dependent on the parameters, the inverse Hessian can be estimated at β_0

$$E\{(\hat{\beta}_0 - \beta_0)(\hat{\beta}_0 - \beta_0)^T\} = \hat{J}''^{-1} \quad (2-57)$$

Eq. 2-57 provides a way to estimate the Hessian since the covariance matrix can be estimated using the method given in Chapter 4 or the method given by Courtier et al. (1994). It should be noted that this result is reasonable only if the linearization around the parameter values is reasonable. In case of pronounced nonlinear behavior, Eq. 2-57 may yield the wrong estimation. The experiments show (see section 3.1.2) that using Eq. 2-57 to estimate the Hessian and using Eq. 2-49 as the parameter transformation does not improve the speed of convergence of the present inverse model. The reason is nonlinearity of the system. Using Eq. 2-49, parameters are very sensitive to the precondition matrix. Errors in estimating the precondition matrix result in the wrong estimation of the gradients. Instead of using the whole matrix of the estimated

Hessian, the diagonal of the Hessian can be used to construct a preconditioner since the diagonal of the estimated Hessian provides the basic information of the Hessian.

In this study, linear transformation is applied to the original parameter β , thus

$$\beta = LY \quad (2-58)$$

where Y is the new parameter and L is a preconditioner which is a diagonal matrix.

With the linear transformation, the cost function with respect to the new parameter Y is

$$\Delta J_Y = L \Delta J_\beta \quad (2-59)$$

and the new parameters can be written as

$$Y = L^{-1} \beta \quad (2-60)$$

Three methods are introduced to specify the L matrix and each method is tested. The convergence of the inverse model with respect to each method is compared in section 3.1.2.

The first method uses the diagonal of the estimated Hessian to calculate L so that

$$L = \text{diag}(\hat{J}''^{-1/2}) \quad (2-61)$$

The second method uses empirical scales of the parameters to scale the parameters.

The L matrix can be written as

$$L = \begin{bmatrix} l_1 & 0 & 0 \\ \cdot & \cdot & \cdot \\ 0 & l_k & 0 \\ \cdot & \cdot & \cdot \\ 0 & 0 & l_m \end{bmatrix} \quad (2-62)$$

where $l_k = \beta_k^0 / K_{gr}^0$; β_k^0 = the scale value of the k th parameter; K_{gr}^0 = the scale value of the optimum phytoplankton growth rate. The third method uses the following matrix to specify L

$$L = \begin{bmatrix} v_1 l_1 & 0 & 0 \\ \cdot & \cdot & \cdot \\ 0 & v_k l_k & 0 \\ \cdot & \cdot & \cdot \\ 0 & 0 & v_m l_m \end{bmatrix} \quad (2-63)$$

where l_k is the same as Eq. 2-61 and v_k 's are the empirical coefficients to be determined through the model experiments so that the gradients of the cost function with respect to the scaled parameters have the same order of magnitude, or the estimated Hessian has the smallest condition number.

III. INVERSE MODEL EXPERIMENTS

The test inverse model used the tidal Rappahannock River, one of the western shore tributaries of the Chesapeake Bay, as a prototype estuary. The estuary was divided into 71 segments ($\Delta x = 2.5\text{km}$) with up to 10 layers vertically ($\Delta z = 2\text{m}$). The model transects in the tidal Rappahannock River are shown in Fig. 3-1. The two-dimensional eutrophication model developed by Park and Kuo, hereafter referred to as the original model, has been calibrated, verified and applied successfully to study hypoxic conditions in the river (Park and Kuo 1993b, 1996). Their model calibrated parameter values were adopted in the present inverse model study as the basic set of parameter values. The parameters used in the inverse model are listed in Table 1. The parameters marked " * " are to be estimated in the present inverse model study. Several numerical experiments were conducted to study the feasibility of parameter estimation by the inverse model. The numerical model experiments were designed to determine the response of the model to different scenarios of the estuary. In the following sections, the results of numerical experiments with several different hypothetical data sets under different boundary conditions are presented.

3.1 Experiments With Constant Boundary Conditions

3.1.1 Test model description

For the experiments using constant boundary conditions, the inverse model was forced by an M_2 tide with a tidal amplitude of 18.3 cm at the mouth. The freshwater discharge

was $48 \text{ m}^3\text{s}^{-1}$, the long-term average. The point source loads were located at 7.5km, 10km, 12.5km, and 15km from the head of tide, respectively. Monthly mean loads of point sources, and nonpoint source during period June 6 to July 5, 1990 (the same period for the original model calibration) were used as constant loads. The downstream boundary conditions of the state variables were specified using the mean values of the slack water surveys of June 6 and July 5, 1990. Constant solar radiation and light extinction coefficients as well as zero benthic fluxes were used throughout the model experiments. The time series data of velocities and dispersion coefficients to drive the transport portion of the model were computed from the hydrodynamic model and saved to a database for frequent retrieval during inverse modeling processes. The initial conditions were compiled from the slack water survey of June 6, 1990. Examples of the surface and bottom concentrations of state variables as the initial conditions are shown in Fig. 3-2. These initial conditions were used for the model experiments with constant boundary conditions.

Sample prototype data required for the inverse model experiments were generated by running the inverse model forward with the original model calibrated parameters, except a constant settling velocity K_{p22} of $20 \text{ (cm day}^{-1}\text{)}$ was used instead of using spatially varying parameter values. At particular times, based on different model experiments, original model outputs were saved as "field" data sets. Each data set included concentrations of eight state variables at each cell vertically at seven locations along the estuary. The locations of the sample stations, denoted by "+", are shown in Fig. 3-4. The parameter values used to generate sample data were treated as the "true" values. Using model generated data to investigate the strategy of inverse modeling has three advantages.

First, it is possible to study the identifiability of the unknown parameter values for different conditions because the "true" parameter values are known. Second, the model generated data are consistent with the model so that the problem of mechanisms not modeled can be eliminated. Third, the model generated data are void of sampling errors which are inherent to prototype data.

The initial guess values of the unknown parameters for the inverse model were specified using mean values based on the data compiled from an EPA report (Johnson et al. 1985) and other published results (Table 2). The parameter values were bounded by upper-limit and lower-limit values to ensure that the estimated parameter values were within the acceptable range. The maximum values in Table 2 were used as upper-limit of the parameters and zeros were used as lower-limit of the parameters. The estimated maximum concentrations of state variables in the estuary were used to calculate scale factors.

3.1.2 Test of preconditioning

Before starting the inverse model experiments, the different methods of preconditioning were tested. Three test runs for a ten-day model simulation were conducted with constant boundary conditions and initial conditions described in the last section. In these runs, the mean values of the parameter listed in Table 2 were used as initial guess values and it was assumed that one sample data set was available at the beginning of day 10. Run P1 used Eq. 2-61 as the preconditioner. The Hessian was estimated using Eq. 2-57 at β_0 , the initial guess values. Run P2 used Eq. 2-62 as the preconditioner. The maximum values

listed in Table 2 were used as parameter scale values. Run P3 used Eq. 2-63 as the preconditioner. The scales for each parameter were round up values of those used in Run P2. The coefficients v_k were adjusted based on the estimated condition number and the gradients of the cost function with respect to the parameters in the first few iterations so that the gradients have the same magnitude. Because calculated gradients of the cost function with respect to the settling velocities and denitrification rate are an order of magnitude smaller than the gradients with respect to the rest of the parameters, large coefficients associated with settling velocity were used. The scale values and coefficient v are listed in Table 3. The estimated condition numbers for Run P1, P2, and P3 are listed in Table 4.

Two test runs, one without the preconditioner and one with the preconditioner using a full estimated matrix of the Hessian (Eq. 2-57), were also tested. The inverse model was not convergent for both runs. With proposed preconditioning, the inverse model was convergent. The relative errors of the cost function, the error of total data misfit at the last iteration divided by the total data misfit at the beginning of the iteration, for Run P1, P2, and P3 are compared in Fig. 3-3. It shows that the rate of convergence for Run P1 and P2 are almost the same, while Run 3 has the quickest convergence speed. The results suggest that a proper preconditioner is very important for the convergence of the inverse model. The estimated condition number corresponding to the new parameters also indicates that the condition of the Hessian matrix with respect to the new parameters is improved with a proper preconditioning (Table 4). The preconditioner used in Run P3 is used for the rest of the inverse model experiments and the model calibration with field data.

3.1.3 Basic parameter estimation tests

To ensure the inverse model functions properly, three experiments for a ten-day model simulation were conducted to test the response of the model to different initial guess of the parameters and to different environments. Run C1 used the mean values listed in Table 2 as the initial guess parameter values and Run C2 used either maximum or minimum values listed in Table 2 as the initial guess parameters (Table 5). In both runs, it was assumed that three sample data sets, as described in the aforementioned paragraph, were available at the beginning of day 3, day 6, and day 10, respectively. The original model calibrated parameters served as "true" parameters and the original model results with true parameters were considered as true results. The comparisons of the daily surface maximum and bottom minimum concentrations of the state variables over the 10th day between model results with initial guess parameters for Run C1 and the true results are shown in Fig. 3-4. It shows that the model results are far away from the true results if the wrong parameter values are used. Run C3 used a new set of parameters (Table 6), which were either maximum or minimum values listed in Table 2, as "true" parameters to create a very different environment from Run C1 and Run C2. The initial guess parameters for Run C3 were the same as those for Run C1. The percentage error in the estimated parameter is calculated by the following equation:

$$\frac{|True\ value - Estimated\ value|}{True\ value} \times 100\% \quad (3-1)$$

The results of Run C1, Run C2, and Run C3 are listed in Tables 5 and 6, respectively.

The results indicate that the inverse model is convergent with different initial guess parameters (Run C1 vs. Run C2) and for different environments (Run C1 vs. Run C3). The relative errors are on the order of 1×10^{-7} after more than 200 iterations (exclude unsuccessful gradient search) for Run C1 and Run C2. It take 476 iterations to reach relative errors on the order of 1×10^{-6} for Run C3. If higher accuracy is desired, more iterations have to be conducted. It can be seen that speed of convergence is affected by the initial guess parameters and varies with different environments. The errors in the estimated parameters are up to 1% in 219 iterations for Run C1 and are up to 6% in 476 iterations for Run C3, except for K_{bod} . The graphical presentations of the inverse model results from Run C1, Run C2 and Run C3 are all indistinguishable from those of true results and, hence, they are not presented.

Since the model sensitivity to each parameter is different in the system, the errors in the estimated parameters are not the same. The errors in estimated settling velocities are large compared to other parameters for Run C1 and Run C2 and are on the same order as others for Run C3. The settling velocity of CBOD, K_{bod} , has the largest error among the parameters. The large error of K_{bod} suggests that the model is not sensitive to the settling velocity of K_{bod} . This is confirmed by a sensitivity experiment. The sensitivity experiment was conducted by varying K_{bod} from 0.0 to 0.45 (true value is 0.02) while true values were used for all other parameters. The results showed that the relative errors due to change of K_{bod} were less than 1×10^{-7} . It indicates that the model is not sensitive to K_{bod} . For the model setup, the magnitude of K_{bod} used in the model was very small. As a consequence, no measurable data misfit is sensed by the model within the error criterion

of 1×10^{-7} . It suggests that the accuracy of parameter estimation is dependent on how sensitive the system is with respect to the particular parameter and what error criterion is given in the model. No unique solution of a particular parameter may be obtained if the system is not sensitive to that parameter within the given error criterion. The sensitivity is directly related to the parameter uncertainty. For an insensitive parameter, it is characterized by its large uncertainty. The parameter uncertainty will be further discussed in Chapter 4.

Fig. 3-5 plots the relative error of the cost function as a function of the number of iterations for Run C1. Each iteration includes running the inverse model forward and backward several times to search out the gradients and step length. It shows that relative error is reduced very quickly within the first 25 iterations. The rate of error reduction slows down between iteration 25 and 160. Error reduction increases again after 160 iterations and becomes slow again after 170 iterations. The degradation of convergence occurs after the first 25 iterations. During this period, the number of forward and backward runs within each iteration to search out the new gradients are more than that required during the first 25 iterations. Sometimes a perturbation of a local minimum must be activated in order to search out the new gradients. The major causes of degradation of convergence are cross effects among parameters and multiple scales associated with the parameter system. Because the concentrations of the state variables depend on the combined effects of several parameters, a different set of parameters can provide equivalent results with the same total error of data misfit. For example, over estimated algal growth rate can be compensated by over estimating respiration rate and mortality

rate. Sometimes the local equilibrium cannot be broken without a perturbation of a local minimum. As a consequence, parameters often oscillate within their neighborhood during iteration processes and speed of convergence reduces drastically. On the other hand, the preconditioner used is an empirical method and it implies that the Hessian is not a function of the parameters. The preconditioner may become improper during iteration processes when the parameters converge to the new values which deviate from their initial values. Some parameters are over-corrected and some are under-corrected in each iteration. The over-correction or under-correction often causes more iterations to correct it. Although some degree of degradation of convergence may occur, the parameters can be correctly estimated by the inverse model.

3.1.4 Experiments with noisy data

In practice, the water quality data collected from the field are often associated with random and sampling errors. The feasibility and the accuracy of estimating model parameters by field data with a certain degree of error are very important in model calibration. For this scenario, it was assumed that sample data sets were associated with normally distributed random errors. Two model runs (Run C4 and Run C5) were conducted for this scenario. The true parameter values and their initial guess values for both runs were the same as Run C1. Three sample data sets were generated by adding a normally distributed random number with specified standard deviations to the sample data sets used in Run C1. The standard deviations for Run C4 and Run C5 are 10% and 20%, respectively, of mean concentrations calculated from the true sample data sets used in Run

C1. Since the relative errors of total misfit cannot be reduced after 55 iterations and 77 iterations for Run C4 and Run C5 respectively, the results at 54 and 77 iterations are treated as final results. The model results of Run C4 and Run C5 are presented in Table 7. The comparisons of instantaneous surface and bottom concentrations of state variables at the 10th day between the inverse model results (Run C4 and Run C5) and the true results are shown in Figs. 3-6 and 3-7, respectively. The sample data with random errors are also plotted in the figures. Figures show that the inverse model results agree with true results better than with the data used for parameter estimation, i.e., the data with random errors.

Using sample data with 10% random error, the errors in estimated parameters are less than 10% except settling velocity K_{Chl} , K_{bod} and denitrification rate K_{n33} . Although the errors in parameters K_{Chl} and K_{n33} are relatively large, model results are very satisfactory (Fig. 3-6). Again K_{bod} can not be recovered due to model insensitivity. The errors in the estimated parameters increase when sample data with 20% random error were used (Table 7). Although a graphic match (Fig. 3-7) can be obtained, the errors in some estimated parameters are very large. In this case, it was found that multiple sets of optimal parameters can be obtained if starting with a different set of initial guess parameter values. Unique solution cannot be obtained by using three sample data sets with more than 20% random error. It can be seen from Table 7 that large errors are often associated with the settling velocities in the experiments because the model is less sensitive to these parameters for a given error criteria. Fig. 3-8 is the scatterplots of the inverse model results of Run C4 vs sample data and true results. It shows that the inverse model has a smoothing effect. The noise within the sample data are smoothed out as the inverse model

reaches its convergence. However, caution must be exercised when using noisy data, since errors in estimated parameters may be large for those parameters to which a model is not sensitive and a unique solution may not be guaranteed even though a graphic match is satisfactory. The problem of the uniqueness will be further discussed in the section 3.2.3.

3.1.5 Long period simulation with limited data sets

One difficulty in inverse water quality modeling is that available field data for the model calibration are often limited. Long period model simulation is often required in order to calibrate the model. For this scenario, Run C6 was conducted. Run C6 was the same as Run C1, except the inverse model was run for a 30-day model simulation with only one sample data set available at the beginning of the 30th day. After 63 iteration, the errors in the estimated parameters are already less than 10% (Table 5) except for K_{bod} and the relative error is 3.1810×10^{-4} . The results shows that parameter values can be estimated with one sample data set. It suggests that more sample data sets are not necessary. The comparisons of the daily surface maximum and bottom minimum concentrations of state variables over the 30th day between the inverse model results and the true results are presented in Fig. 3-9. It shows that the results are very satisfactory. Again K_{bod} cannot be recovered due to model's insensitivity as discussed earlier. The results suggest that the inverse model can be useful to aid model calibration for long period simulation.

TABLE 1. Parameter Values Used in The Inverse Model^a

Name	Eq.	Values	Name	Eq.	Values
a_c	A-7	0.05 mg C per μg Chl	θ_4	A-2	1.04
a_n	A-2	0.007 mg N per μg Chl	Kh12	A-2	1.0 mg l^{-1}
a_p	A-5	0.001 mg P per μg Chl	θ_5	A-3	1.04
a_t	A-2	1.0	K_{h23}	A-4	1.0 mg l^{-1}
PQ	A-8	1.0 moles O ₂ per mole C	K_{nit}	A-5	2.0 mg l^{-1}
RQ	A-8	1.33 moles CO ₂ per mole O ₂	θ_6	A-5	1.046
K_{mn}	A-1	0.025 mg l^{-1}	K_{h33}	A-5	0.5 mg l^{-1}
K_{mp}	A-1	0.001 mg l^{-1}	F_n	A-3	0.75
θ_1	A-1	1.066	BenN1	A-2	0.0 g $\text{m}^{-2} \text{day}^{-1}$
I_t	A-1	250 langleys day^{-1}	BenN2	A-2	0.0-0.05 g $\text{m}^{-2} \text{day}^{-1}$
$K_{e,Chl}$	A-1	0.00018 $\text{l} \mu\text{g}^{-1} \text{cm}^{-1}$	BenN3	A-3	0.0 g $\text{m}^{-2} \text{day}^{-1}$
θ_2	A-1	1.08	* $K_{n12}(20)$	A-2	0.04 mg $\text{l}^{-1} \text{day}^{-1}$
θ_3	A-1	1.0	* $K_{n23}(20)$	A-3	0.3 mg $\text{l}^{-1} \text{day}^{-1}$
* K_{gr}	A-1	2.0 day^{-1}	* K_{n11}	A-2	8.0 cm day^{-1}
* K_{Chl}	A-1	10.0 cm day^{-1}	* $K_{n33}(20)$	A-4	0.35 day^{-1}
* R_{20}	A-1	0.17 day^{-1}	θ_7	A-5	1.04
* P_{20}	A-1	0.02 day^{-1}	K_{ph12}	A-5	1.0 mg l^{-1}
θ_8	A-7	1.047	F_p	A-5	0.55
K_{ro}	A-8	393	BenP1	A-5	0.0 g $\text{m}^{-2} \text{day}^{-1}$
θ_9	A-8	1.024	BenP2	A-6	0-0.005 g $\text{m}^{-2} \text{dat}^{-1}$
K_{DO}	A-7	0.5 mg l^{-1}	* $K_{p12}(20)$	A-5	0.06mg $\text{l}^{-1} \text{day}^{-1}$
SOD	A-7	2.0 g $\text{m}^{-2} \text{day}^{-1}$	* K_{p11}	A-5	10 cm day^{-1}
* K_{bod}	A-7	0.02 cm day^{-1}	* K_{p22}	A-6	0-20 cm day^{-1}
* $K_c(20)$	A-7	0.1 day^{-1}			

a see Park and Kuo 1993b

* the parameters to be estimated.

TABLE 2. Values of Parameters for Eutrophication Model

Name	Unit	Range	Mean	Reference ^a
K_{gr}	day ⁻¹	0.410 - 3.000	1.70	EPA
R_{20}	day ⁻¹	0.030 - 0.460	0.16	EPA
P_{20}	day ⁻¹	0.030 - 0.460	0.16	(1) (2) (3) (4)
$K_{n12}(20)$	mg l ⁻¹ day ⁻¹	0.001 - 0.400	0.07	EPA
$K_{n23}(20)$	mg l ⁻¹ day ⁻¹	0.025 - 5.700	0.90	EPA
$K_{n33}(20)$	day ⁻¹	0.002 - 0.350	0.16	EPA
$K_{p12}(20)$	mg l ⁻¹ day ⁻¹	0.001 - 0.800	0.17	EPA
K_c	day ⁻¹	0.010 - 4.250	0.46	EPA
K_{chl}	cm day ⁻¹	5.000 -80.000	18.00	EPA
K_{n11}	cm day ⁻¹	1.000 -50.000	10.00	(1) (2) (3) (4)
K_{p11}	cm day ⁻¹	1.000 -50.000	10.00	(1) (2) (3) (4)
K_{p22}	cm day ⁻¹	1.000 -50.000	10.00	(1) (2) (3) (4)
K_{bod}	cm day ⁻¹	1.000 -50.000	10.00	(1) (2) (3) (4)

- a (1) Thomann, R. and J. A. Mueller, 1987.
 (2) Kuo, A. Y. et al. 1991a.
 (3) Park, K. and A. Y. Kuo, 1993b.
 (4) Cerco, C. F. and Cole, T. M., 1994.

TABLE 3. Parameter Scale Values and Empirical Coefficients for Run P3

Parameter Name	Scale Values	Coefficient ν
K_{gr}	5.0	1
R_{20}	0.5	1
P_{20}	0.5	1.5
$K_{n12}(20)$	0.5	1
$K_{n23}(20)$	5.0	1
$K_{n33}(20)$	1.0	10
$K_{p12}(20)$	1.0	0.6
K_c	4.0	0.5
K_{chl}	50.0	10
K_{n11}	50.0	5
K_{p11}	50.0	10
K_{p22}	50.0	10
K_{bod}	50.0	20

TABLE 4. Condition Number of Test Runs

Without Preconditioning	P1	P2	P3
899000	534	360	125

TABLE 5. Estimated and True Values of the Parameters for Run C1, Run C2, and Run C6

Par. Name	True value	Run C1 (219 iterations)			Run C2 (254 iterations)			*Run C6 (66 iterations)	
		Ini. value	Res.	Error %	Ini. value	Res.	Error%	Res.	Error%
K_{gr}	2.00	1.70	1.9983	0.085	0.400	1.9970	0.150	1.9359	3.21
R_{20}	0.17	1.16	0.1696	0.235	0.460	0.1710	0.588	0.1579	7.12
P_{20}	0.02	0.16	0.0200	0.000	0.460	0.0200	0.000	0.0214	7.00
$K_{n12}(20)$	0.04	0.07	0.0400	0.000	0.001	0.0397	0.750	0.0379	5.25
$K_{n23}(20)$	0.30	0.90	0.3002	0.067	0.025	0.2986	0.467	0.2898	3.40
$K_{n33}(20)$	0.35	0.16	0.3513	0.371	0.002	0.3457	1.229	0.3574	2.11
$K_{p12}(20)$	0.06	0.17	0.0600	0.000	0.800	0.0596	0.667	0.0571	4.83
K_c	0.10	0.46	0.1001	0.100	4.200	0.0999	0.100	0.1016	1.60
K_{chl}	10.0	18.00	10.1109	1.109	1.000	9.2608	7.392	10.9971	9.97
K_{n11}	8.00	10.00	7.9458	0.678	1.000	8.2164	2.705	7.5971	5.04
K_{p11}	10.0	10.00	9.9707	0.293	1.000	10.3647	3.647	10.0961	0.96
K_{p22}	20.0	10.00	19.9917	0.042	1.000	19.6489	1.756	18.6822	6.59
K_{bod}	0.02	10.00	0.0000	100.00	1.000	0.4166	**	0.0413	**
Relative error		3.2020×10^{-7}			5.9060×10^{-7}			3.1810×10^{-4}	

** error is more than 100%.
a initial guess values are same as Run C1

TABLE 6. Estimated and True Values of The Parameters for Run C3

Parameter Name	Initial value	Result (476 iterations.)	True value	Error (%)
K_{gr}	1.70	2.7828	2.80	0.61
R_{20}	0.16	0.4128	0.40	3.20
P_{20}	0.16	0.3798	0.40	5.05
$K_{n12}(20)$	0.07	0.3474	0.35	0.74
$K_{n23}(20)$	0.90	4.8592	5.00	2.82
$K_{n33}(20)$	0.16	0.1938	0.20	3.10
$K_{p12}(20)$	0.17	0.5955	0.60	0.75
K_c	0.46	3.9055	4.00	2.36
K_{Chl}	18.00	37.6938	40.00	5.77
K_{n11}	10.00	41.3328	40.00	3.33
K_{p11}	10.00	40.2912	40.00	0.73
K_{p22}	10.00	40.3548	40.00	0.89
K_{bod}	10.00	13.2643	40.00	66.8
relative error		7.4060×10^{-6}		

TABLE 7. Estimated and True Values of The Parameters for Run C4 and Run C5

Par. Name	Initial value	True value	Run C4 (55 iterations)		Run C5 (77 iterations)	
			Result	Error %	Result	Error %
K_{gr}	1.70	2.00	1.8961	5.20	1.9540	2.30
R_{20}	0.16	0.17	0.1607	5.47	0.1916	12.71
P_{20}	0.16	0.02	0.0210	5.00	0.0080	60.00
$K_{n12}(20)$	0.07	0.04	0.0401	0.25	0.0369	7.75
$K_{n23}(20)$	0.90	0.30	0.3259	8.63	0.2984	0.53
$K_{n33}(20)$	0.16	0.35	0.4041	15.46	0.2826	19.26
$K_{p12}(20)$	0.17	0.06	0.0556	7.33	0.0573	4.50
K_c	0.46	0.10	0.1027	2.70	0.0872	12.80
K_{Chl}	18.0	10.0	6.8468	31.53	0.0024	99.98
K_{n11}	10.0	8.00	8.4266	5.33	12.9478	61.84
K_{p11}	10.0	10.0	9.7661	2.34	8.9826	10.16
K_{p22}	10.0	20.0	21.279	6.40	24.1299	20.64
K_{bod}	10.0	0.02	0.0031	84.50	4.5287	**
Relative error			0.05030		0.1729	

Figure 3-1 The model transects in the tidal Rappahannock River.

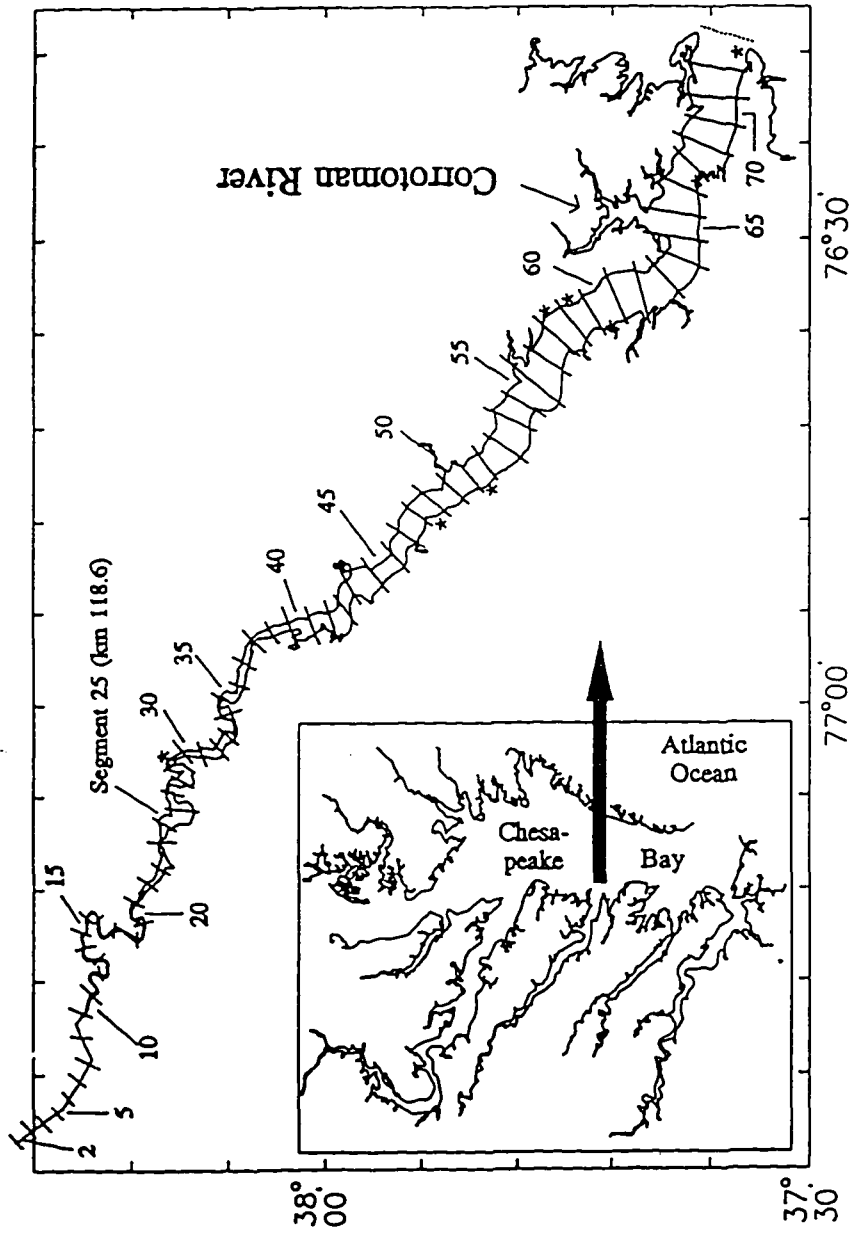
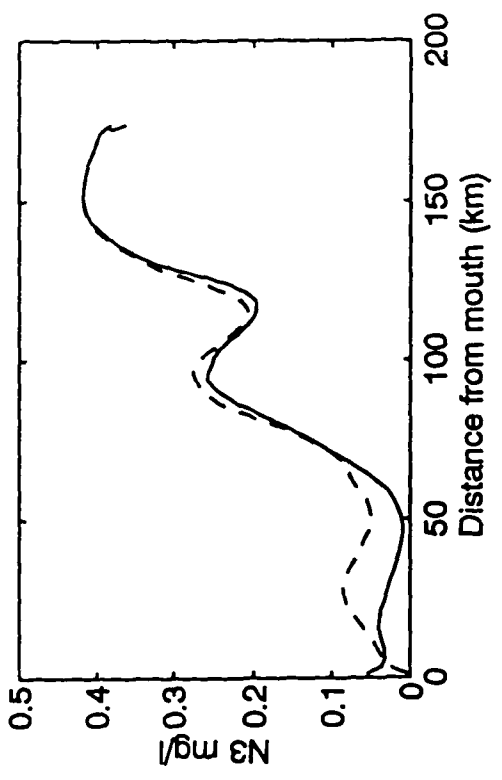
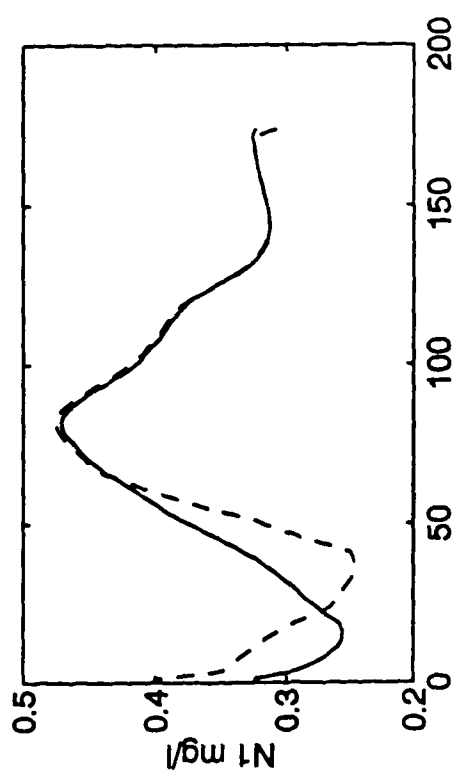
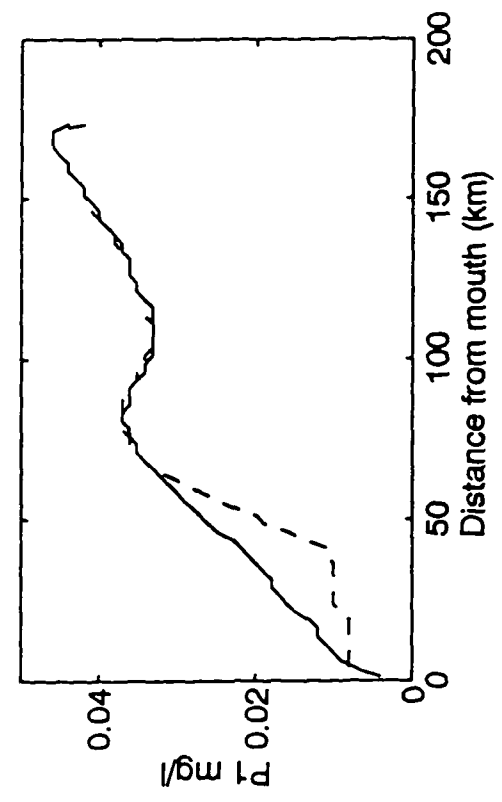
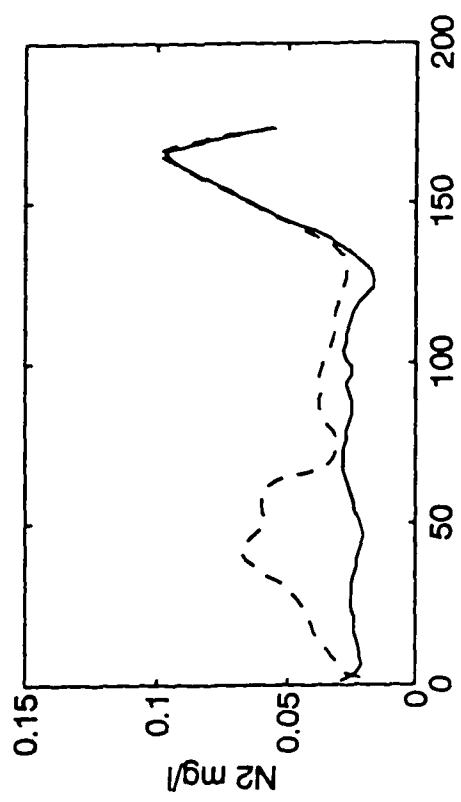


Figure 3-2 Distributions of initial concentrations at the surface and the bottom layers for experiments with constant boundary conditions. (Solid lines are the surface concentrations and dashed lines are the bottom concentrations, N1 = organic nitrogen; N2 = ammonium nitrogen; N3 = nitrite-nitrate nitrogen; P1 = organic phosphorus; P2 = inorganic phosphorus; Chl = phytoplankton; CBOD = carbonaceous biochemical oxygen demand; and DO = dissolved oxygen).



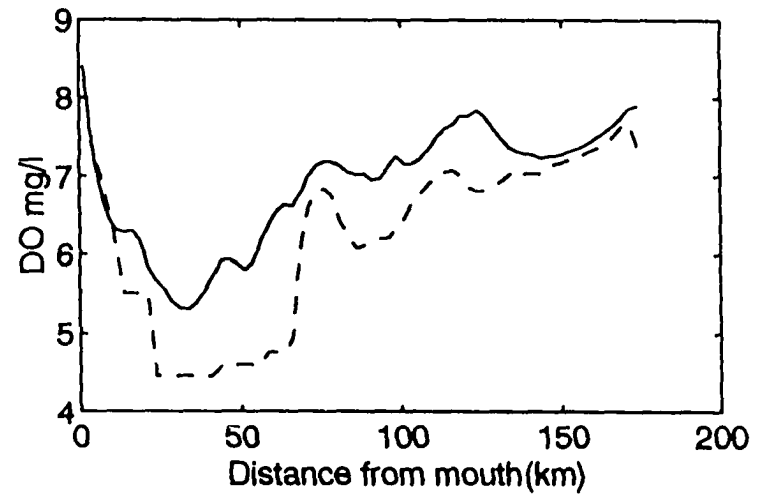
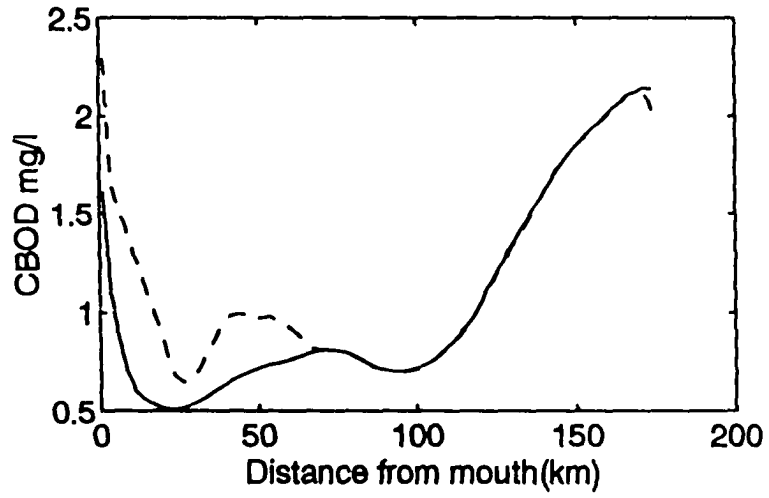
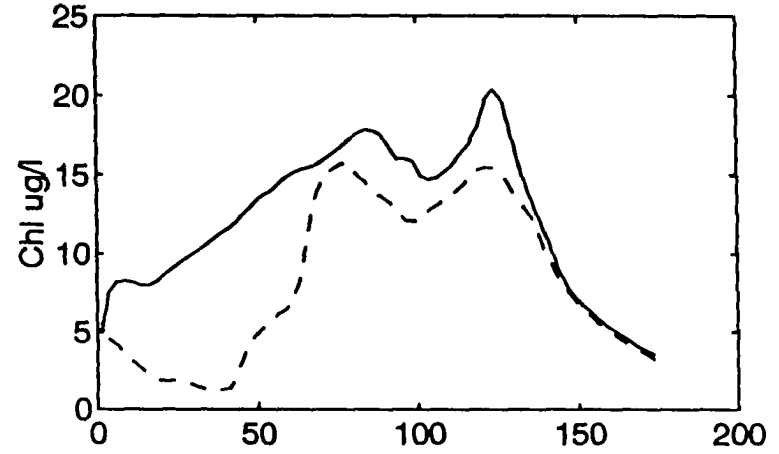
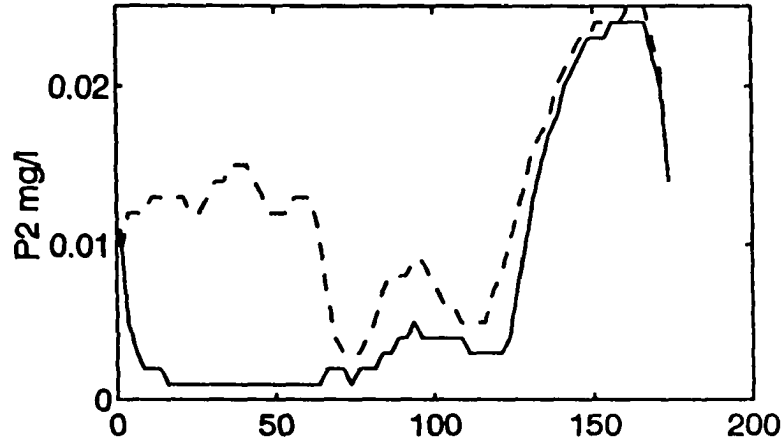


Figure 3-3 Comparisons of the rate of convergence of different preconditioning methods (dotted line = Run P1; dash-dotted line = Run P2; and solid line = Run P3)

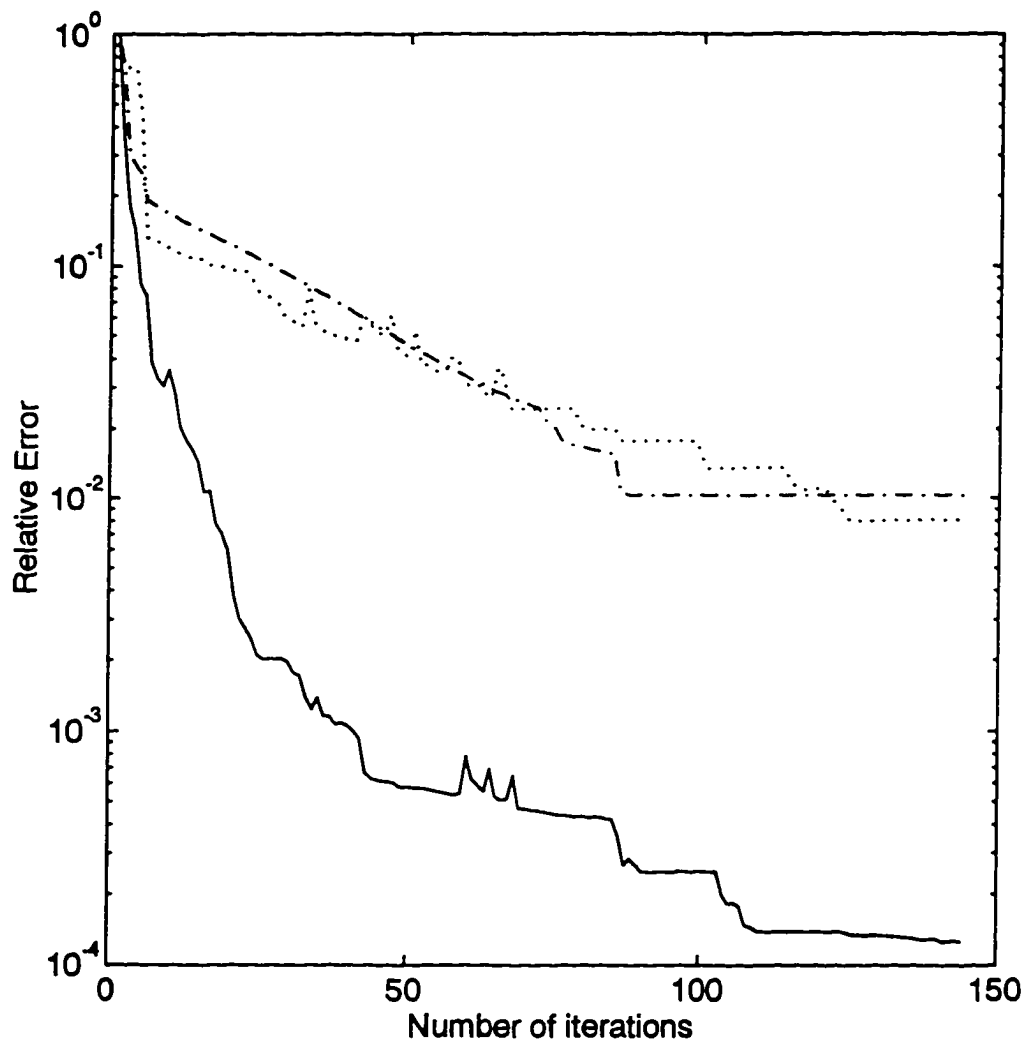
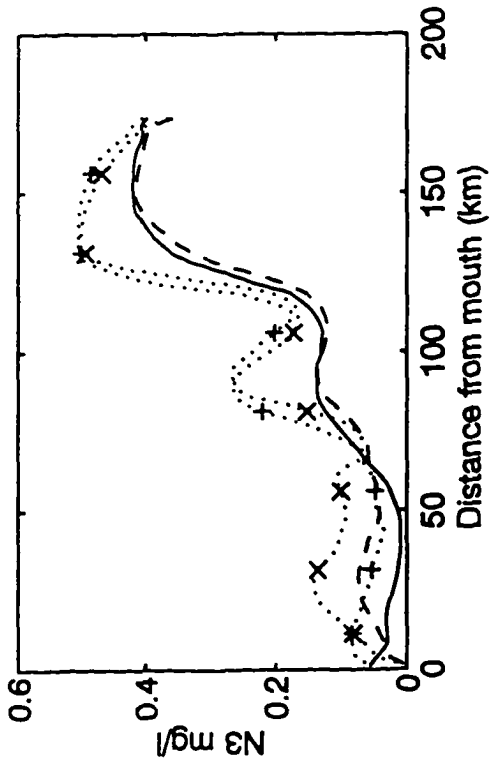
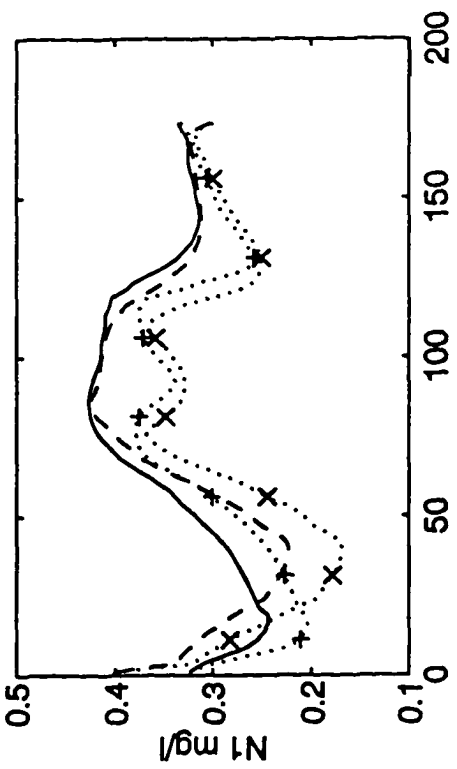
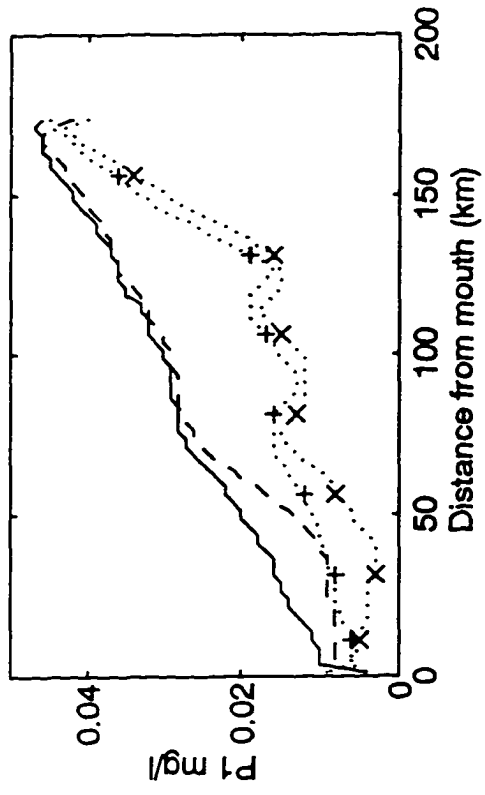
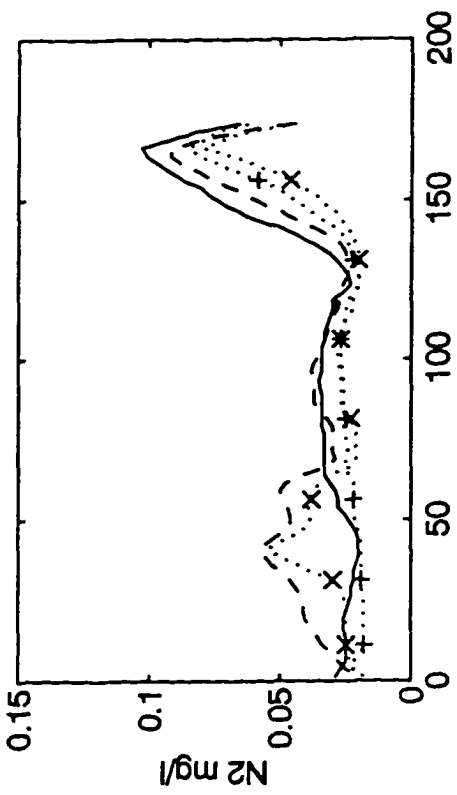


Figure 3-4 Comparisons of the daily surface maximum and bottom minimum concentrations of the state variables between the model results (Run C1) with initial guess parameter values and the true results over the 10th day (solid lines are the true surface maximum concentrations; dashed lines are the true bottom minimum concentrations, dot lines with '+' are the model surface maximum concentrations, and dot lines with 'x' are the model bottom minimum concentrations. The +'s are the locations of sample stations).



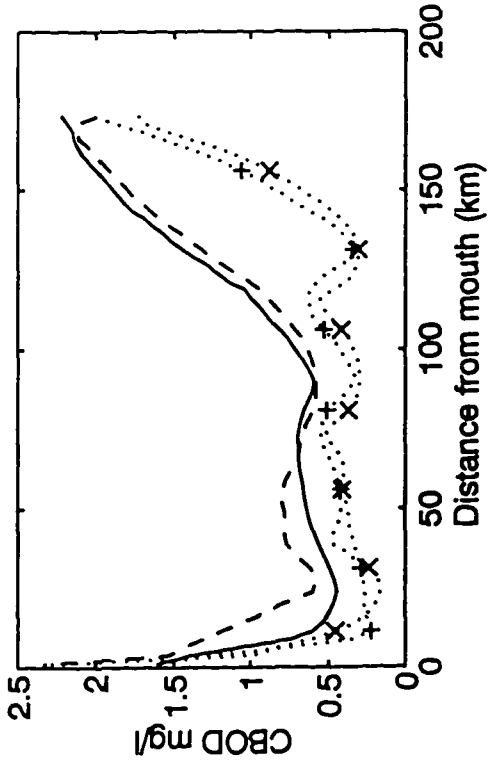
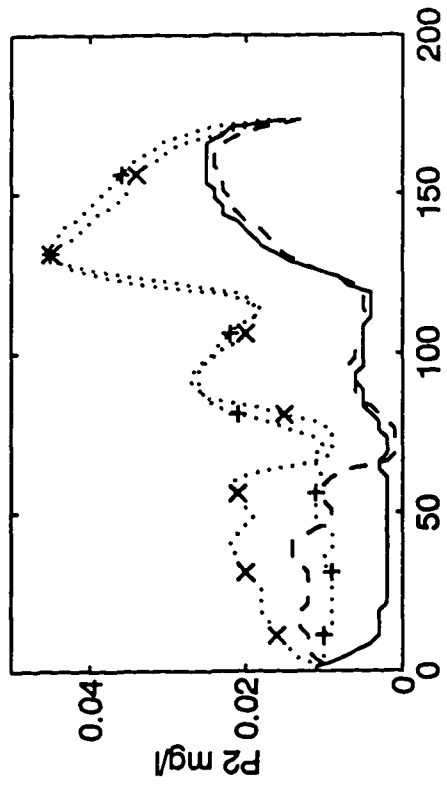
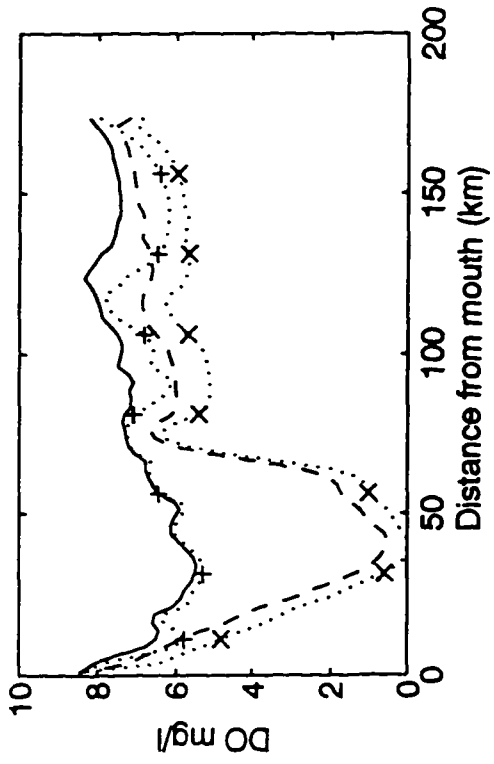
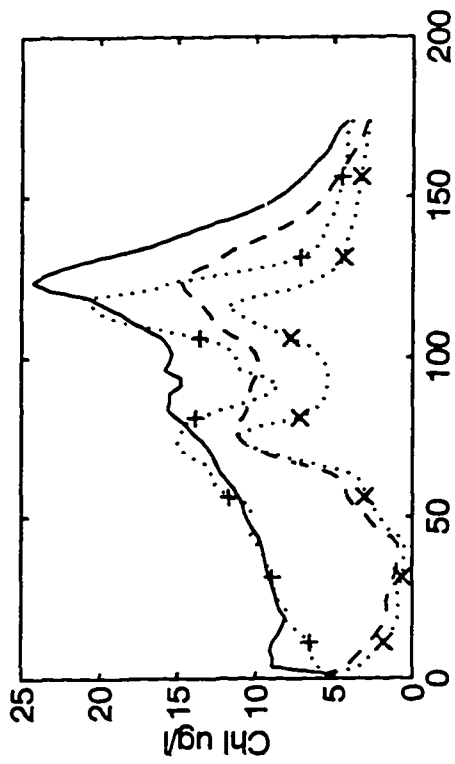


Figure 3-5 The relative error of cost function as a function of the number of iterations for Run C1.

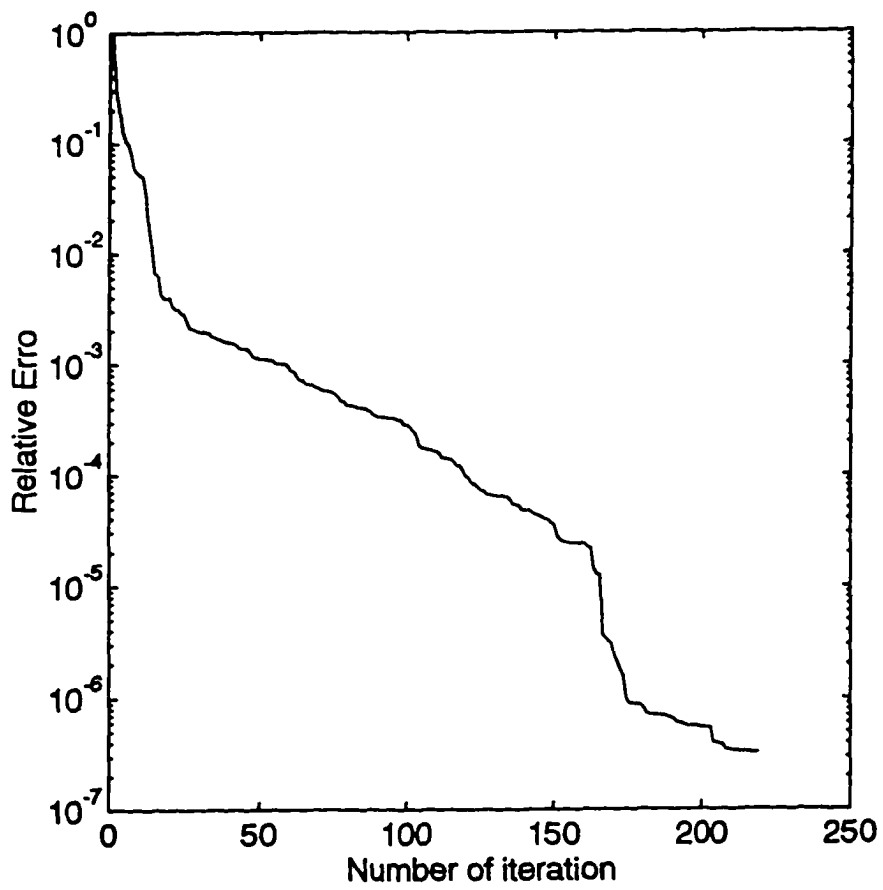
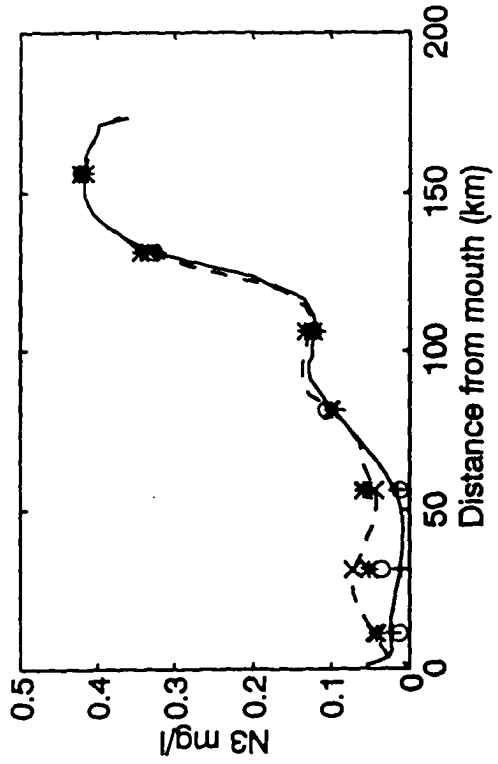
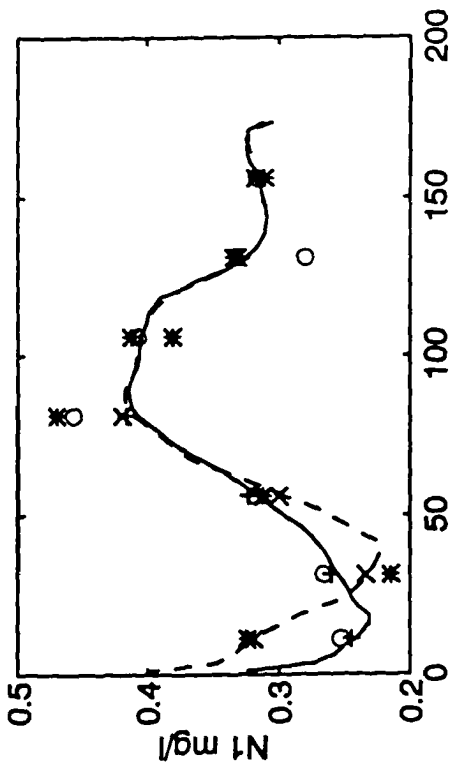
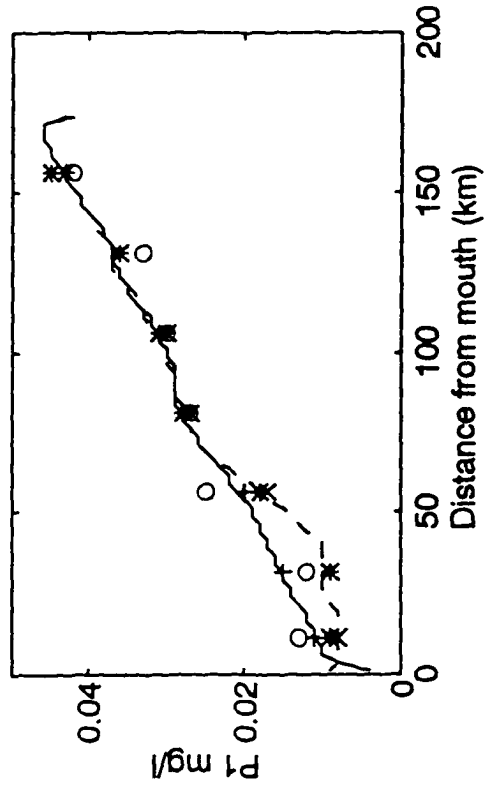
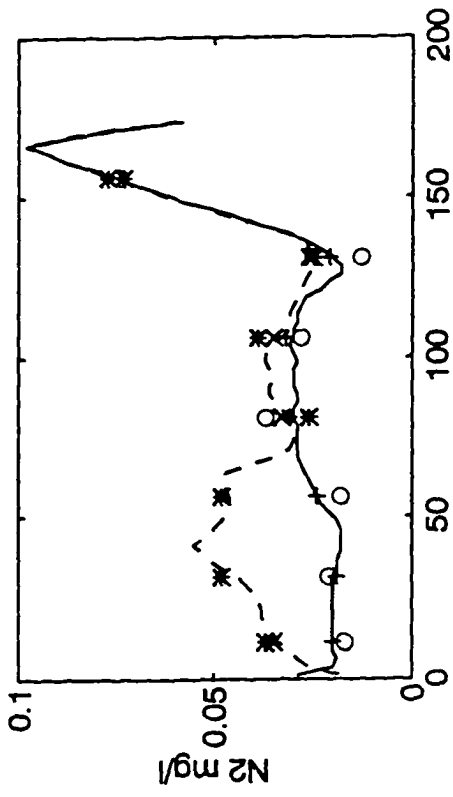


Figure 3-6 Comparisons of instantaneous surface and bottom concentrations of the state variables between the inverse model results (Run C4) and the true results together with sample data (with 10% error) at the 10th day (solid lines are the model results at surface, dashed lines are the model results at bottom, +’s and x’s are the true results at the surface and the bottom, respectively, and o’s and *’s are the sample data at the surface and the bottom, respectively).



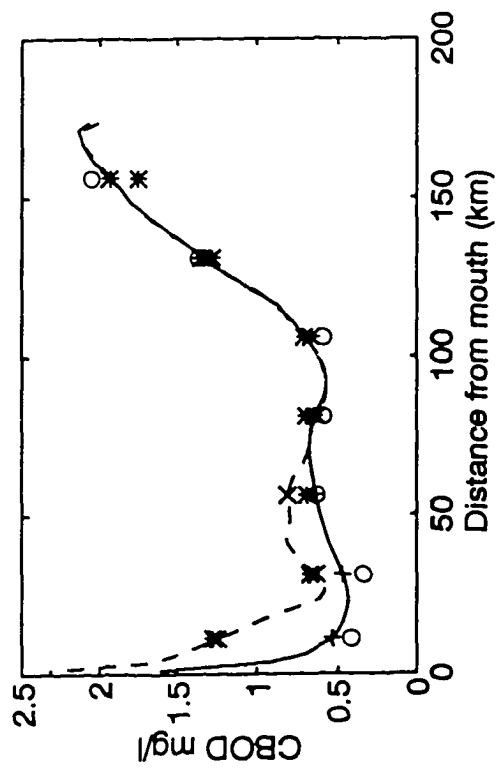
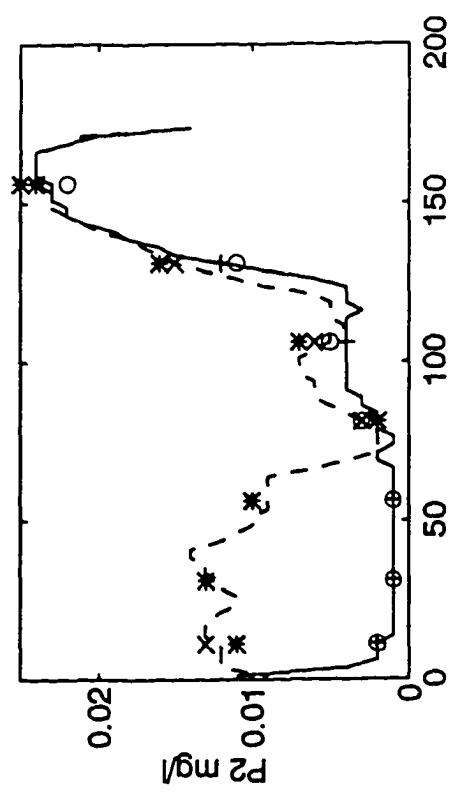
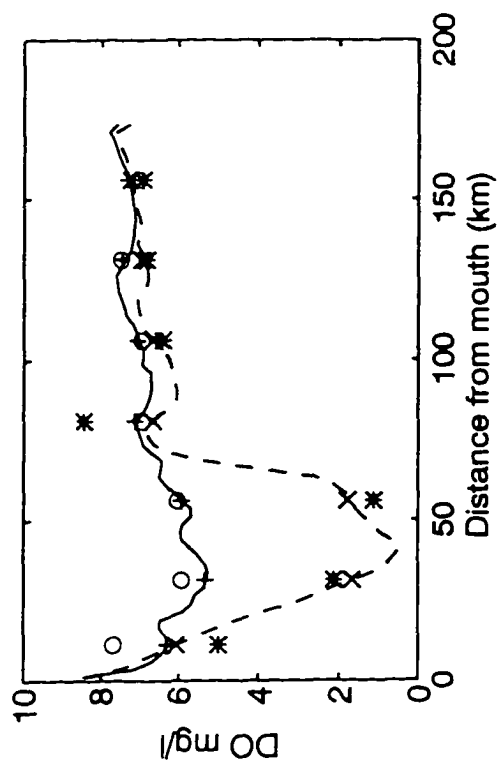
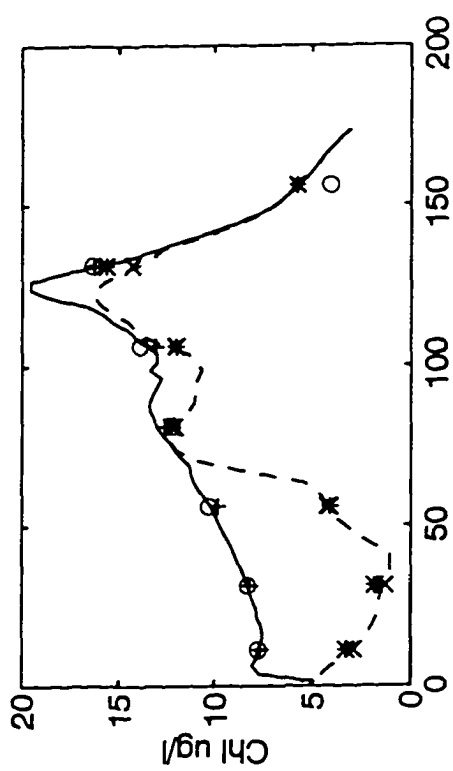
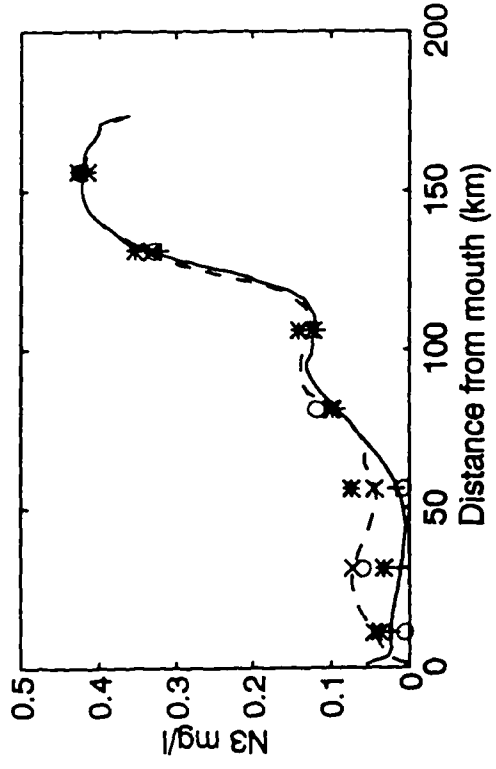
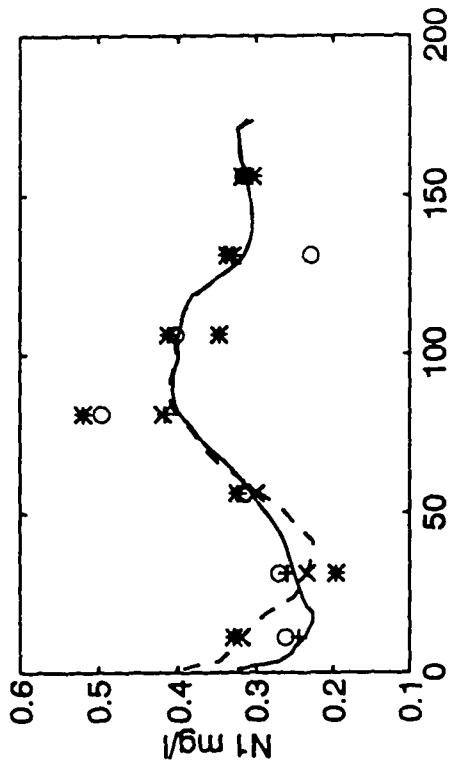
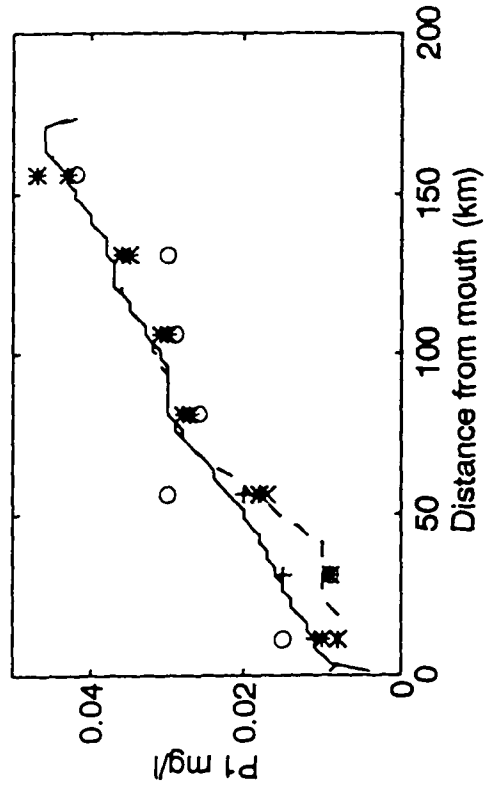
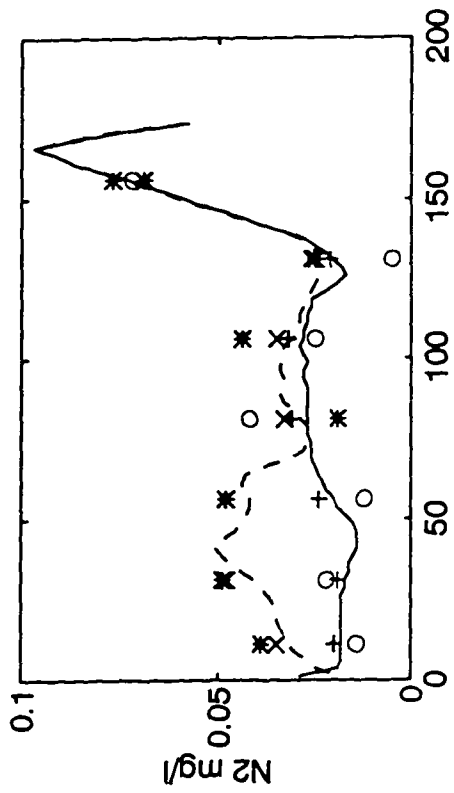


Figure 3-7 Comparisons of instantaneous surface and bottom concentrations of the state variables between the inverse model results (Run C5) and the true results together with sample data (with 20% error) at the 10th day (refer to Fig. 3-6 for symbol description).



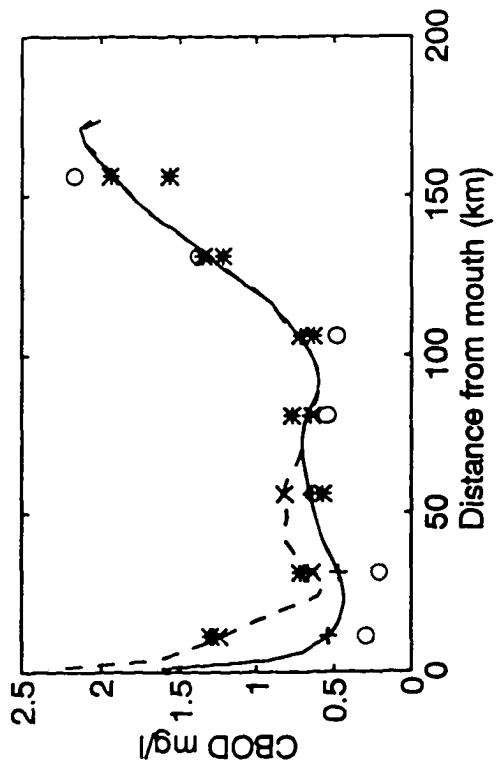
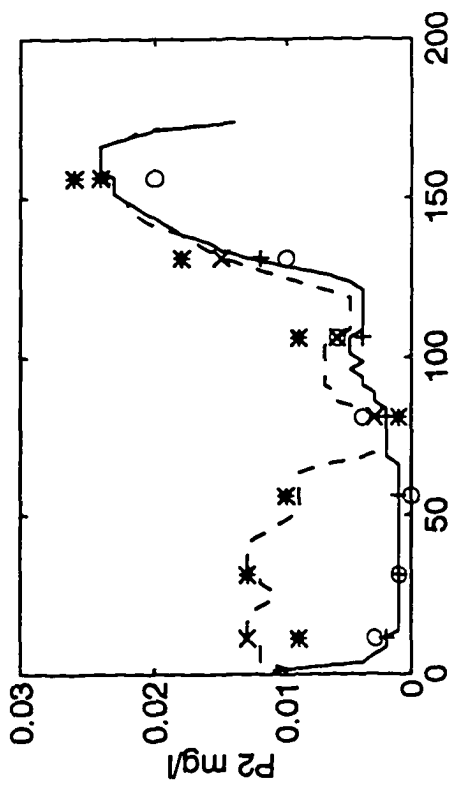
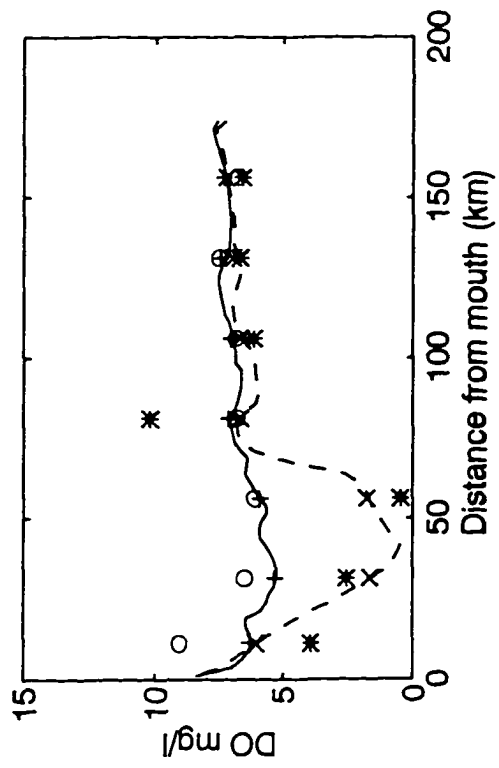
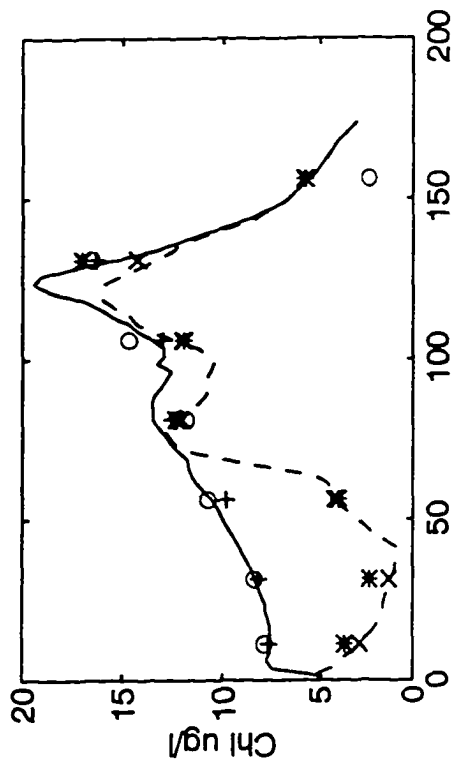
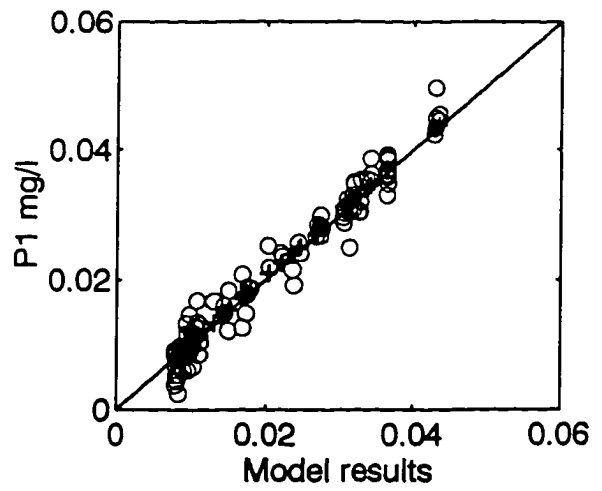
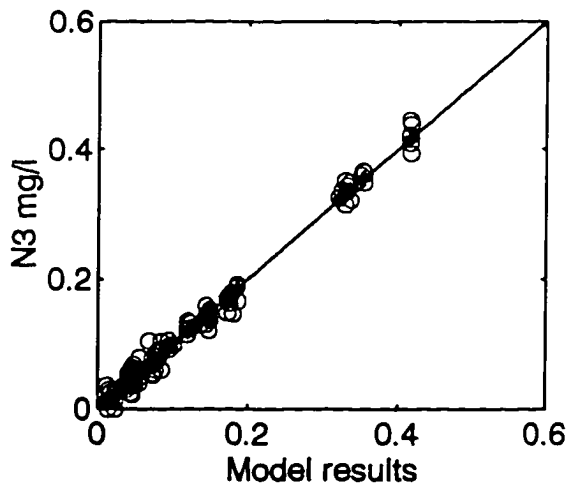
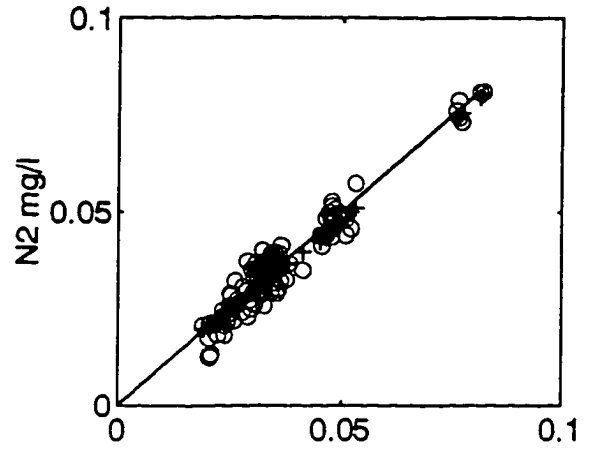
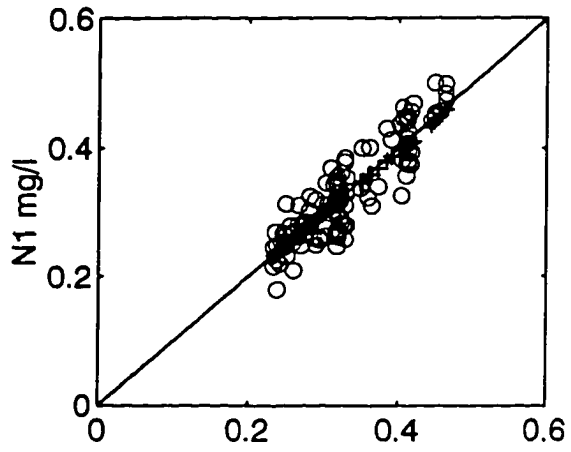


Figure 3-8 Scatterplots of the inverse model results (Run C4) vs. true results and sample data ('+' s are the model result vs. true results, circles are the model results vs. sample data (with 10% error), and solid lines indicate one to one correspondence).



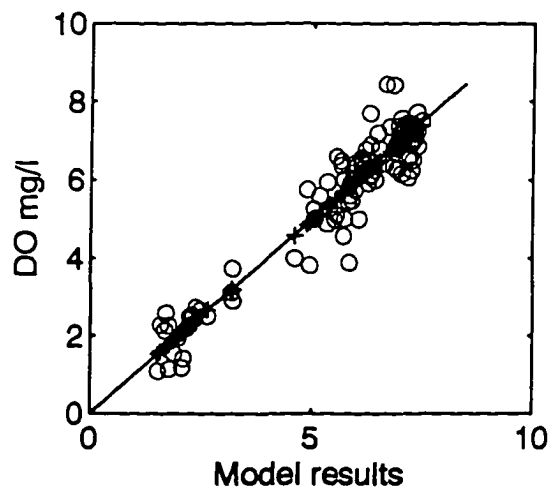
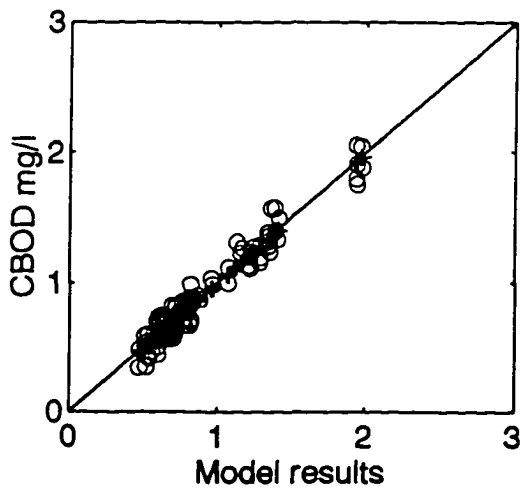
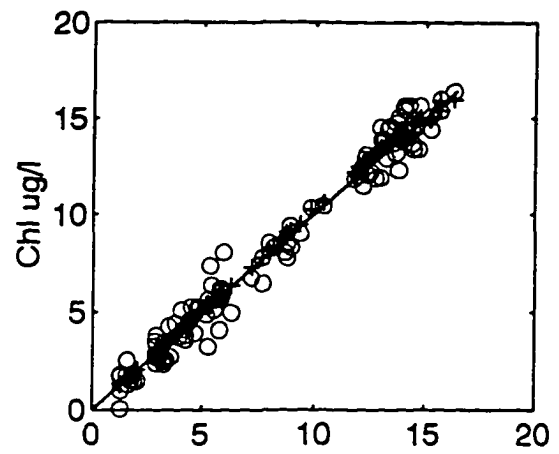
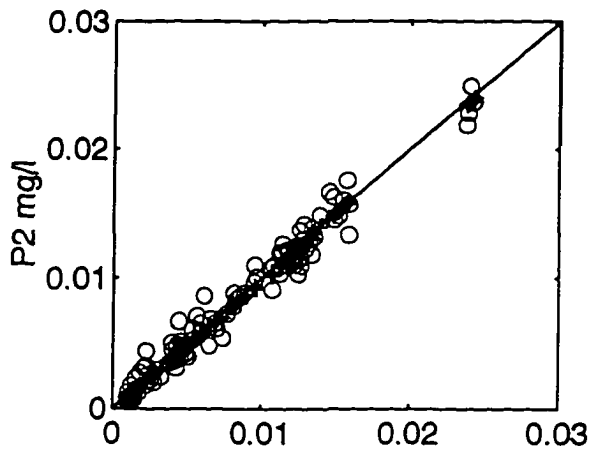
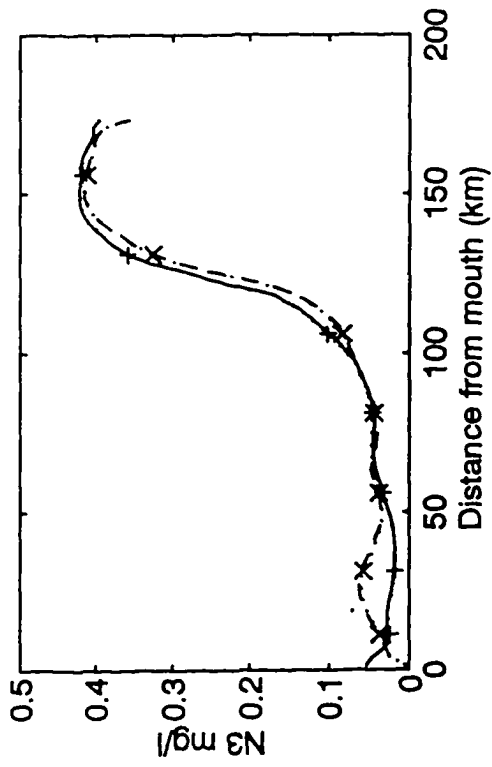
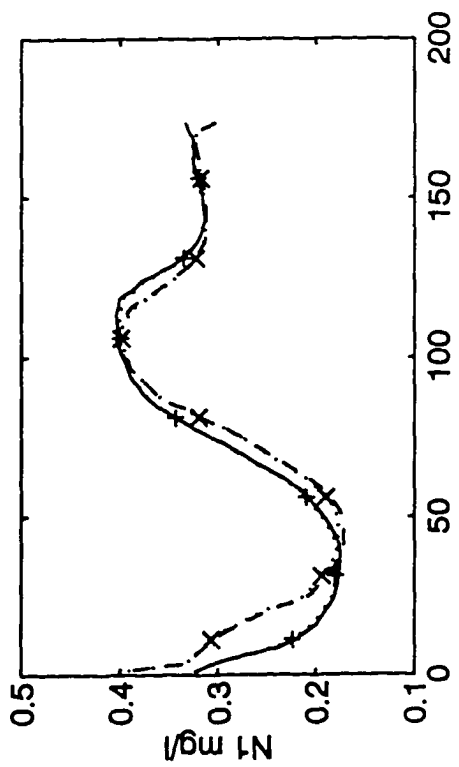
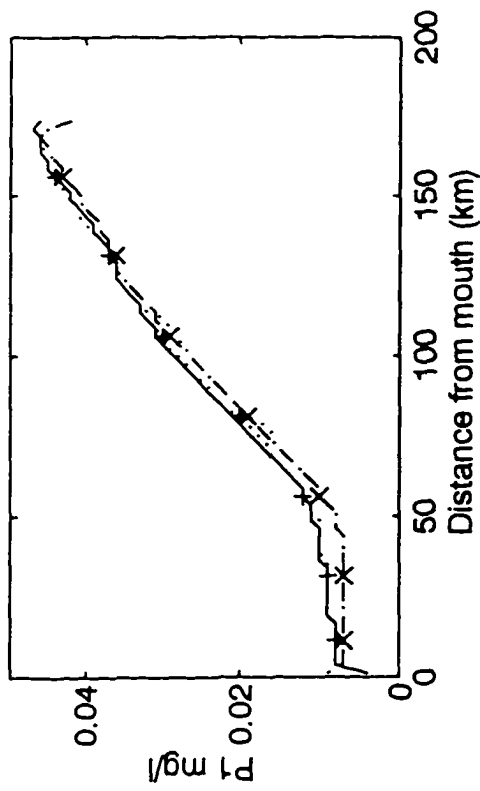
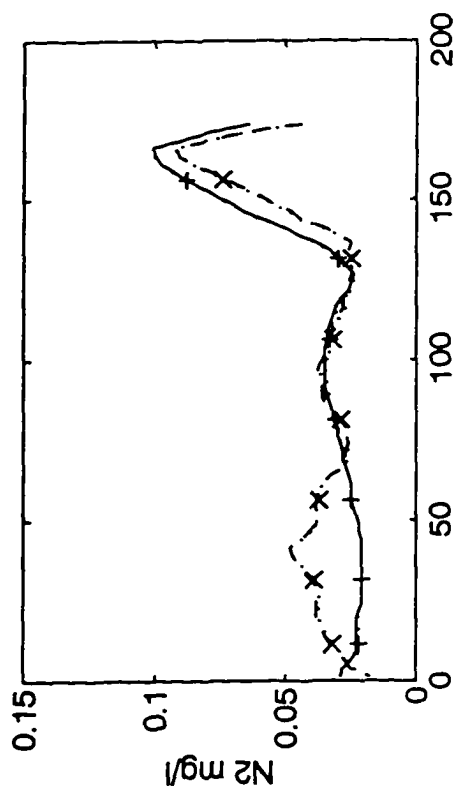
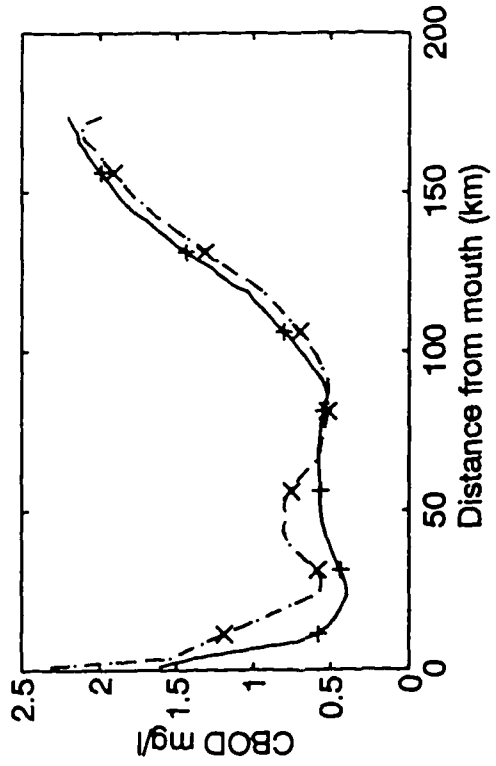
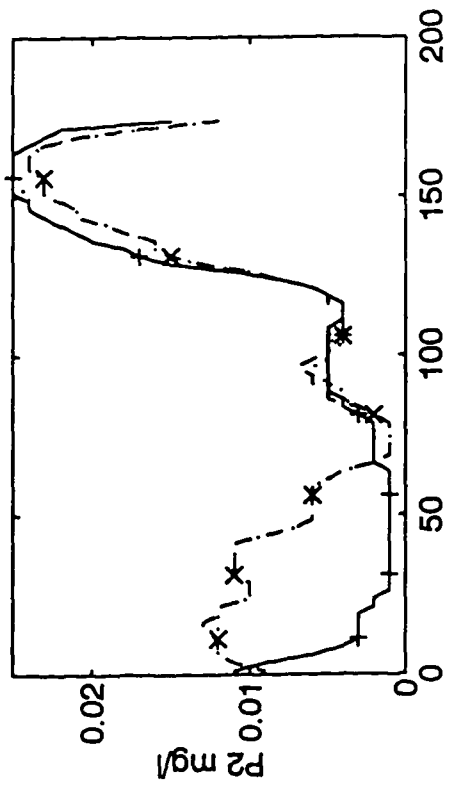
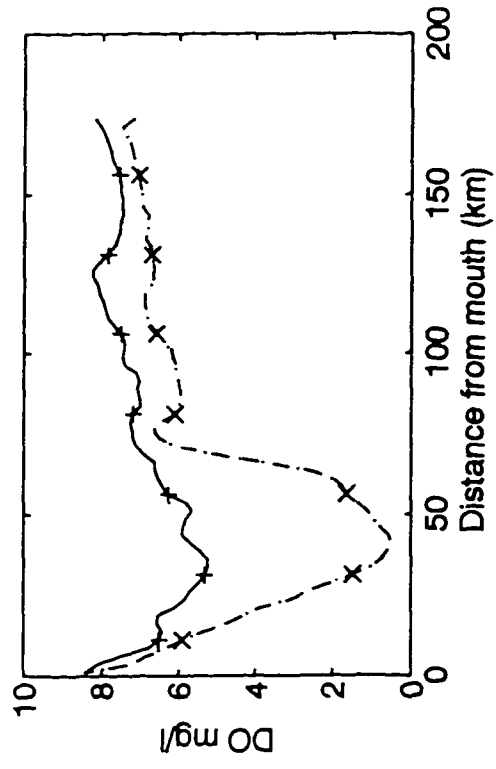
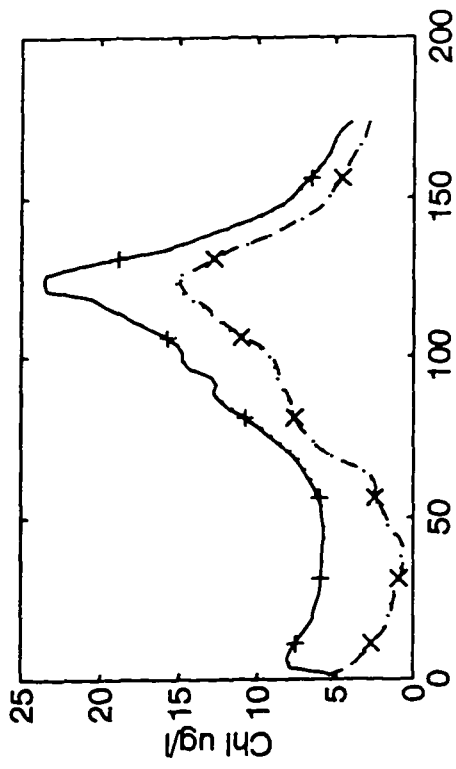


Figure 3-9 Comparisons of daily surface maximum and bottom minimum concentrations of the state variables between the inverse model results (Run C6) and the true results over the 30th day (refer to Fig. 3-4 for lines description).





3.2 Experiments With Time Varying Boundary Conditions

3.2.1 Model boundary conditions and sample data description

The model experiments with time-varying boundary conditions were conducted for the period during June 6 to July 5, 1990 (the same period for the original model calibration). The model setup for the present study is exactly the same as the original eutrophication model. The field data collected by Virginia Institute of Marine Science (VIMS) during that period were used for the model boundary conditions. They included upstream and downstream boundary conditions, sediment oxygen demand (SOD), benthic fluxes and light intensity related parameters. The full description of the field surveys and data were presented in Kuo et al. (1991a) and Park and Kuo (1993b).

A. Upstream and Downstream Boundary Conditions: Three time-varying boundary conditions controlled the hydrodynamic model, freshwater inflow through the upstream boundary, tide and salinity at the mouth. They were specified for the hydrodynamic model. The upstream boundary condition was specified with daily freshwater discharge measured at the Fredericksburg gauge station (USGS 1991). The model updated the freshwater discharge by linear interpolation over a 2 hour period from 0000 to 0200 hours, and then held it constant for the remaining 22 hours. Hourly tidal elevation measured at the mouth was used for the downstream boundary condition. The model linearly interpolated the hourly data to obtain the boundary condition every time step. Three slackwater surveys were conducted at the slack before flood (SBF) on June 6 and July 5. The salinity measurements at the mouth were linearly interpolated in time and used for the boundary condition. The water quality conditions at the mouth between those slackwater

surveys were also linearly interpolated in time and used for the daily downstream boundary conditions for eight water quality state variables.

B. Nonpoint and Point Source Loads: The nonpoint source contribution from the watershed above the fall line was evaluated from freshwater discharge rates and concentrations of water quality state variables at the fall line. Results from a regression analysis were used for the concentrations of all nutrient forms including N1, N2, N3, P1, and P2 (Kuo et al. 1991a). Daily input for the concentrations of Chl, CBOD and DO was obtained from the linear interpolation of monitoring data. During the sampling period, four sewage treatment plants (Claiborne Run, FMC, Fredericksburg, and Massaponax STP's) discharged waste water into the uppermost 10 km reach of the river. The monitoring data from the STP's were linearly interpolated in time and used for the daily input of the point source loadings.

C. Benthic Fluxes: The original model (Park and Kuo 1993b) calibrated results of benthic nutrient fluxes including N1, N2, N3, P1, P2 and SOD were specified for the inverse model. These fluxes remained constant throughout the model experiments.

D. Light Conditions: The measurements of daily inputs of I_a , t_v and t_d at VIMS were used to calculate solar radiation. The original model calibrated light extinction coefficients were used for the present model.

E. Initial Conditions: The field data collected on June 6 slackwater survey were used in the present model to specify the initial conditions. The distribution of surface and bottom concentrations of eight state variables are shown in Fig. 3-10. These initial conditions of state variables were used for both the inverse model experiments and sample data

generation.

The sample data were generated by running the original model from June 6 to July 5, 1990 with time-varying boundary conditions and initial conditions described in the last paragraph. The original model calibrated parameter values (Table 1), except settling velocity K_{p22} , were used as "true" parameter values to generate sample data. A constant 20 cm day^{-1} was used for K_{p22} instead of using spatial varying values. At the beginning of day 32 (July 5) after the model started, the model output was saved as "field" data set. The data set included the concentrations of eight state variables at each cell vertically at seven locations along the estuary. The locations of the sample stations denoted by '+' are showed in Fig. 3-11.

3.2.2 Basic parameter estimation tests

As experiments conducted with constant boundary condition, two experiments (Run T1 and Run T2) were conducted to test the response of the inverse model to the different initial guess of parameter values. The initial guess values of parameters for Run T1 and Run T2 were the same as those used in Run C1 and Run C2. The model simulations were conducted from June 6 to July 5, 1990. The sample data set saved at day 32, i.e., July 5, was used as "field sample data" and the parameter values used to generate "field" data were treated as "true" values. The results of estimated parameter values together with true values and initial guess values are listed in Table 8. The results show that the inverse model is convergent after 141 iterations for Run T1 and Run T2. The errors in the estimated parameter values are less than 4% for Run T1 except for the settling velocity

K_{bod} . The errors in the estimated parameters for Run T2 are relatively larger, especially some settling velocities. If better accuracy is desired, more iterations have to be conducted. Again, a good initial guess of parameter values significantly increases the speed of convergence. Since the model is less sensitive to the settling velocities, convergence of the settling velocities are relatively slow. The graphical presentations of the inverse model results from Run T1 and Run T2 are all indistinguishable from those of true results and, hence, they are not presented.

3.2.3 Experiments with noisy data

As experiments conducted in section 3.1.4, random errors with 10% of the mean concentration as standard deviation for each state variable were added to the data set used in Run T1. The results of the estimated parameter values are listed in Table 9 and the comparison of instantaneous results between the inverse model and data with random errors together with the true results are shown in Fig. 3-11. Although most estimated parameter values are close to the true parameter values, errors in some estimated parameter values are relatively large, such as P_{20} and K_{bod} even though the graphic match is very satisfactory. It suggests that unique solutions for some parameters cannot be guaranteed for long period simulation with limited sample data set with random errors.

The unique solutions are difficult to obtain, particularly for the system where several parameters are strongly correlated as van Straten (1983) pointed out in his research. For example, the kinetic equation (Eq. A-3) of N_2 is given as

$$\frac{d(N2)}{dt} = -\frac{K_{n23}N2}{K_{h23}+N2} \frac{DO}{K_{nu}+DO} + \frac{K_{n12}N1}{K_{h12}+N1} + \text{other terms}$$

where ammonification rate (K_{n12}) and nitrification rate (K_{n23}) are highly correlated. $N2$ concentration is dependent on the net results of the rate of ammonification and nitrification rather than on individual parameter K_{n12} and K_{n23} . To determine individual parameter, it must rely on additional governing equations. For example, the ammonification and nitrification rate are incorporated in the mass balance equation of $N1$ and $N3$ (A-2 and A-4). If there are no errors in the sample data, the differences between the sample data and the calculated concentrations of $N1$ and $N3$ will provide additional information through λ_{N1} and λ_{N3} to correct K_{n12} and K_{n23} through Eqs. 2-20 and 2-21. However, if there are errors associated with sample data $N1$ and $N3$, the error messages will continuously feedback from data misfit even as the parameters converge to the true values. Consequently, the parameters converge to the values which give the best fit of the field data in a sense of minimum error of misfit. Some individual parameters may not close to their "true" values while the model results can be very good in a sense of least-squares criterion. On the other hand, the accuracy of parameter estimation also depends on the model sensitivity with respect to individual parameter within the error criteria. Because of the errors in the sample data, the cost function cannot be reduced to zero. Within certain error misfit, the inverse model may be not sensitive to some individual parameters, such as K_{bod} . Because the parameter estimation by the inverse model is based on a best fit criterion, increased sample data can be expected to improve the accuracy of

parameter estimation if errors associated with sample data are normally distributed.

However, increased sample data may not be feasible practically. For those parameters with large uncertainty, accuracy estimation may not be guaranteed even though more sample data are used. For large random errors, the inverse model may not converge without alteration of the cost function. This can be more clearly seen during the inverse model calibration with field data in Chapter 5.

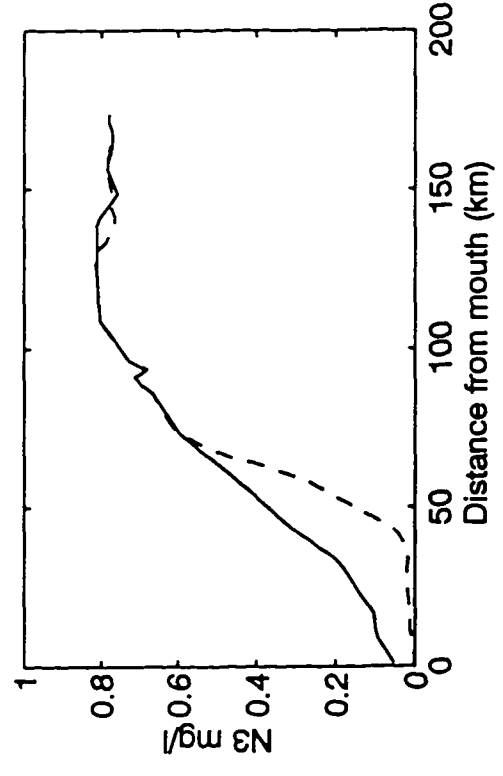
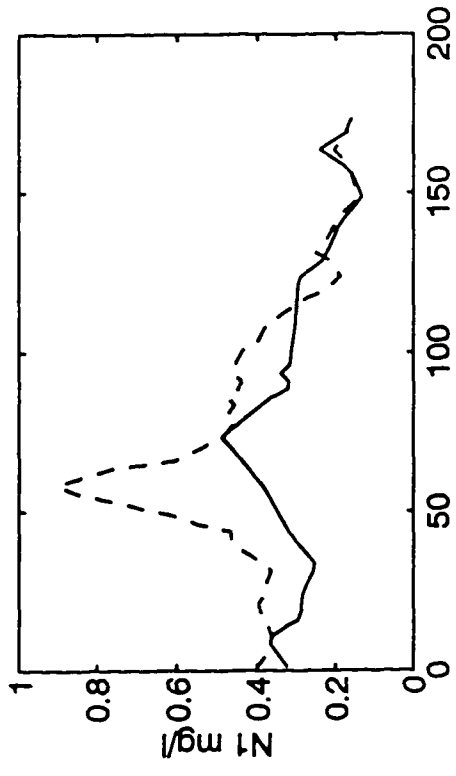
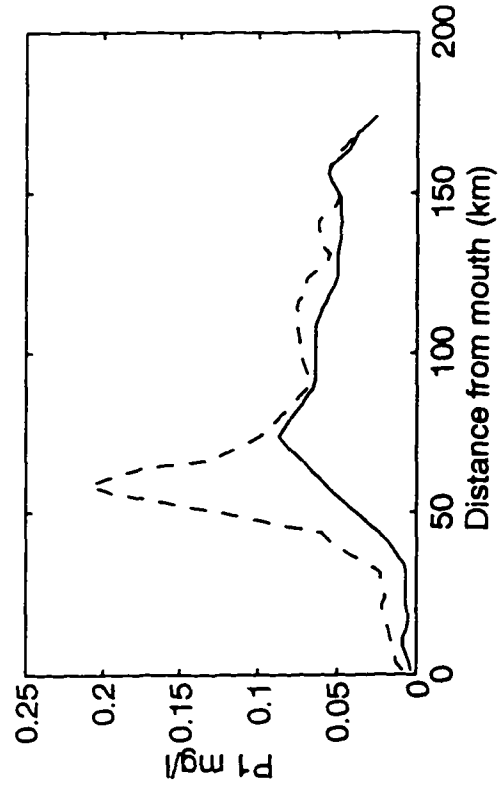
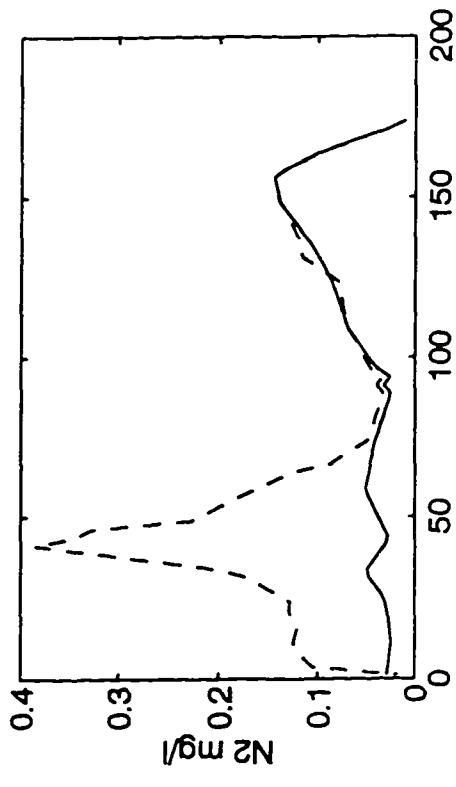
TABLE 8. Estimated and True Values of Parameters for Run T1 and Run T2
(basic parameter estimation tests with time vary boundary conditions)

Par. Name	True value	Run T1 (141 iterations)			Run T2 (141 iterations)		
		Ini. value	Res.	Error %	Ini. value	Res.	Error %
K_g	2.00	1.70	1.9877	0.62	0.400	2.0221	1.11
R_{20}	0.17	0.16	0.1659	2.41	0.460	0.1778	4.59
P_{20}	0.02	0.16	0.0204	2.00	0.460	0.0192	4.00
$K_{n12}(20)$	0.04	0.07	0.0395	1.23	0.001	0.0405	1.25
$K_{n23}(20)$	0.30	0.90	0.2996	0.13	0.025	0.2996	0.47
$K_{n33}(20)$	0.35	0.16	0.3531	0.89	0.002	0.3376	3.54
$K_{p12}(20)$	0.06	0.17	0.0593	1.17	0.800	0.0605	0.83
K_c	0.10	0.46	0.0993	0.70	4.200	0.0974	2.60
K_{chl}	10.0	18.00	10.1202	1.20	1.000	9.3815	9.38
K_{n11}	8.00	10.00	7.6769	4.04	1.000	8.3206	4.01
K_{p11}	10.0	10.00	9.7591	2.41	1.000	11.0404	10.40
K_{p22}	20.0	10.00	19.9616	0.19	1.000	19.6268	1.87
K_{bod}	0.02	10.00	1.3857	**	1.000	1.4525	**
Relative error		3.49200×10^{-5}			5.6490×10^{-6}		

TABLE 9. Estimated and True Value of Parameters for Run T3
(experiments with 10% random error data)

Parameter Name	Initial value	Result 63 iterations	True value	Error (%)
K_g	1.70	1.9453	2.00	2.74
R_{20}	0.16	0.1536	0.17	9.65
P_{20}	0.16	0.0341	0.02	70.50
$K_{n12}(20)$	0.07	0.0427	0.04	6.75
$K_{n23}(20)$	0.90	0.3136	0.30	4.53
$K_{n33}(20)$	0.16	0.3982	0.35	13.77
$K_{p12}(20)$	0.17	0.0624	0.06	4.00
K_c	0.46	0.1121	0.10	12.10
K_{chl}	18.00	9.3339	10.00	6.66
K_{n11}	10.00	7.4688	8.00	6.64
K_{p11}	10.00	10.3596	10.00	3.60
K_{p22}	10.00	22.8105	20.00	14.05
K_{bod}	10.00	8.6871	0.02	**
Relative error		1.1650×10^{-2}		

Figure 3-10 Distributions of initial concentrations at the surface and the bottom layers for experiments with time vary boundary conditions and field data calibration. (Solid lines are the surface concentrations and dashed lines are the bottom concentrations, N1 = organic nitrogen; N2 = ammonium nitrogen; N3 = nitrite-nitrate nitrogen; P1 = organic phosphorus; P2 = Inorganic phosphorus; Chl = phytoplankton; CBOD = carbonaceous biochemical oxygen demand, DO = dissolved oxygen).



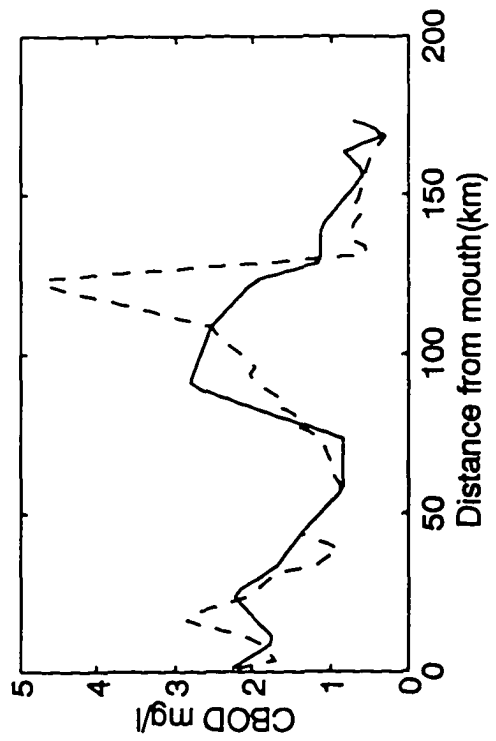
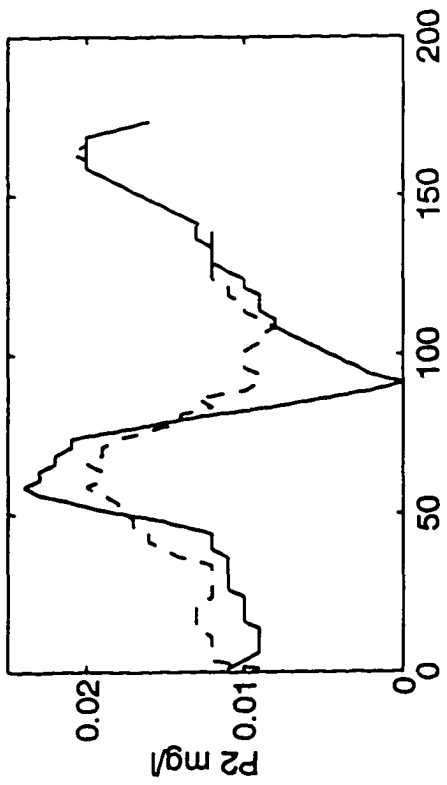
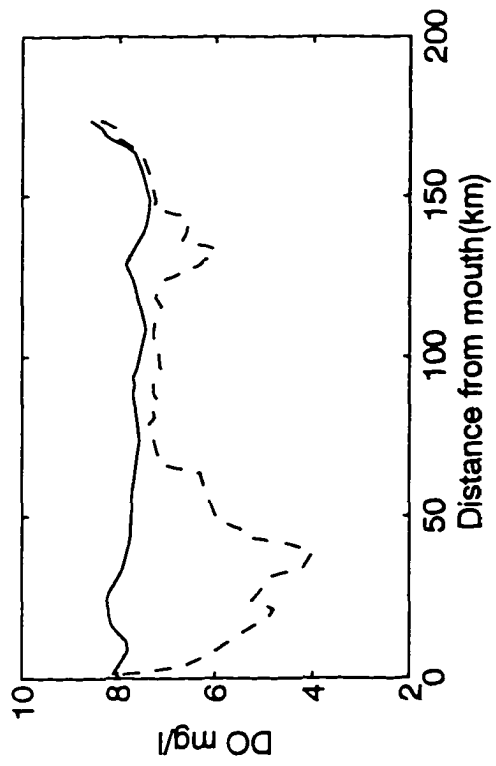
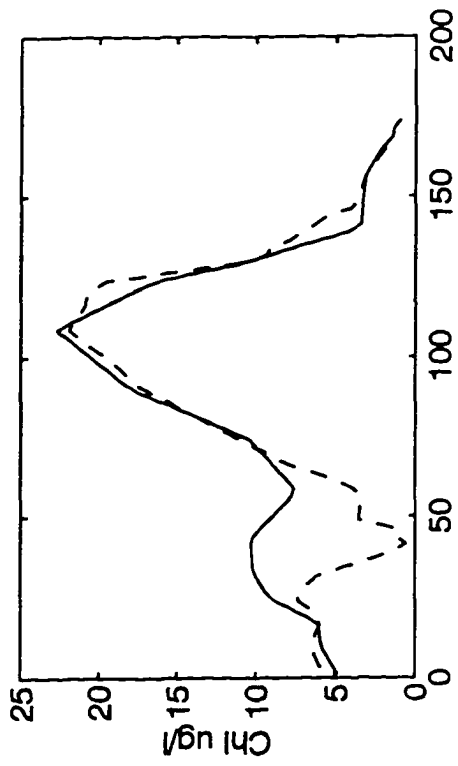
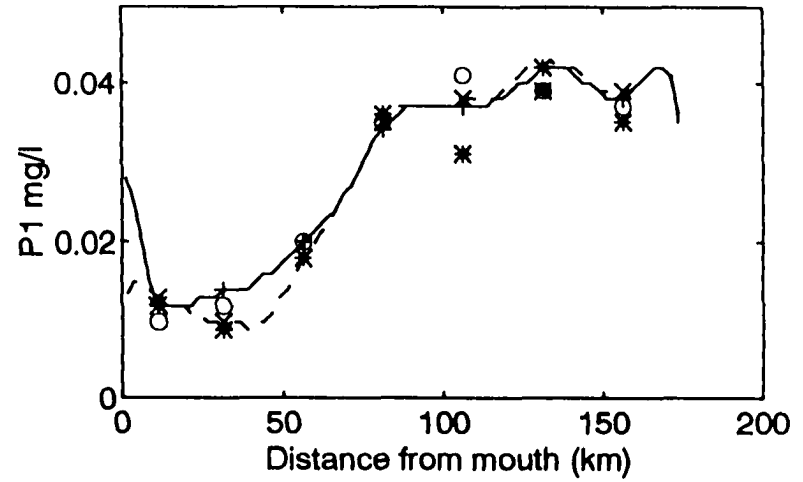
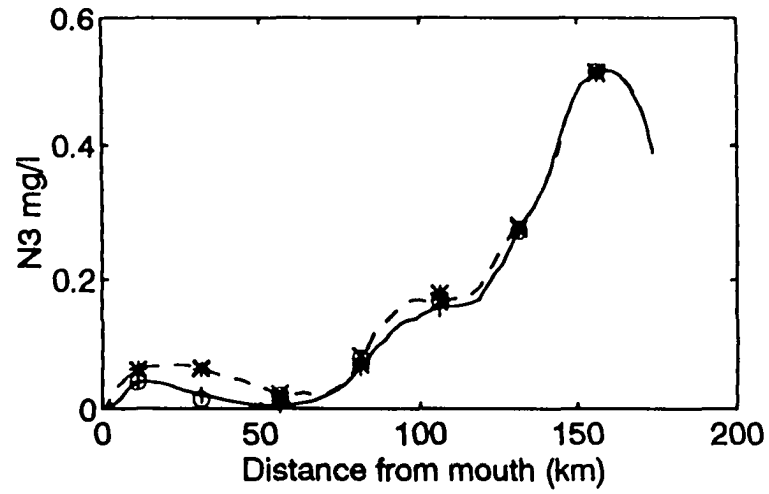
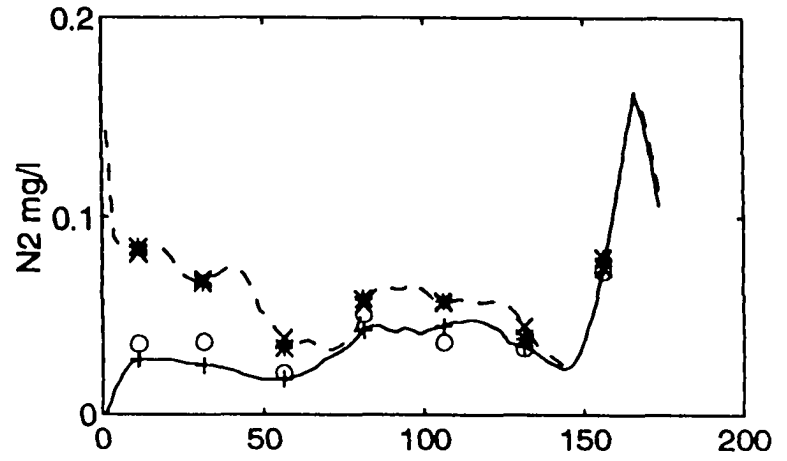
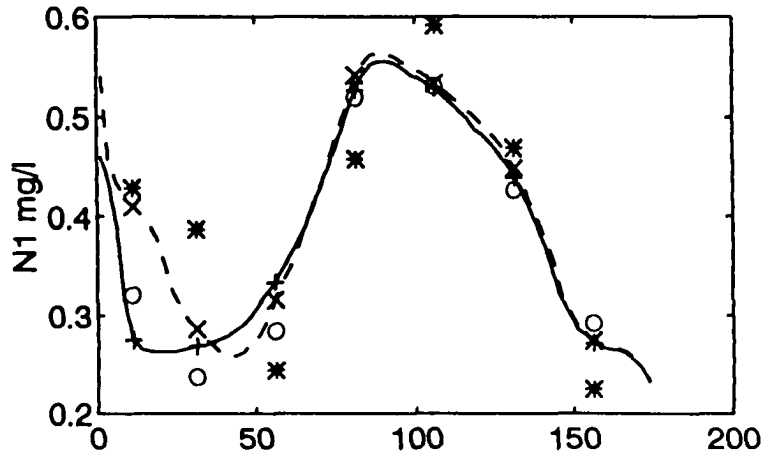
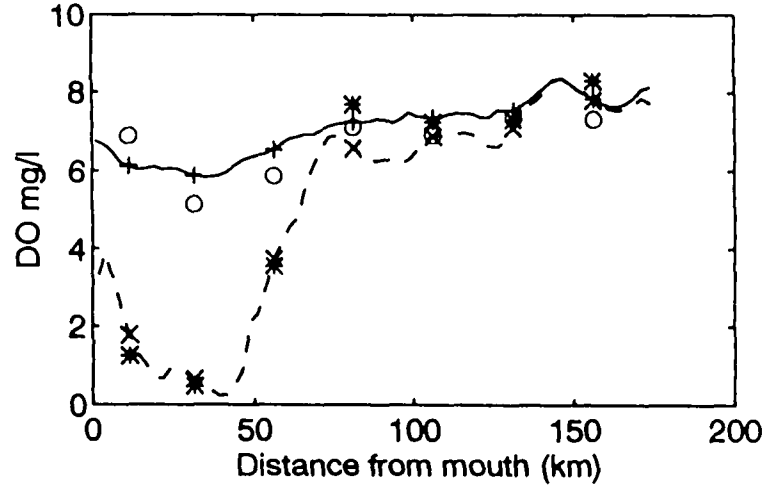
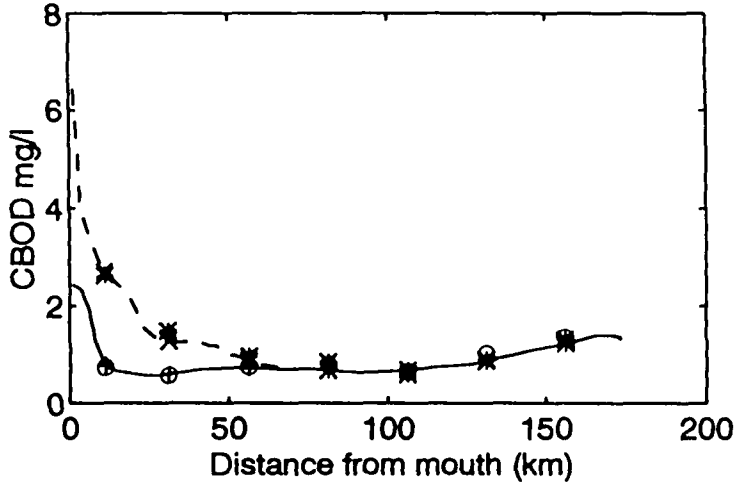
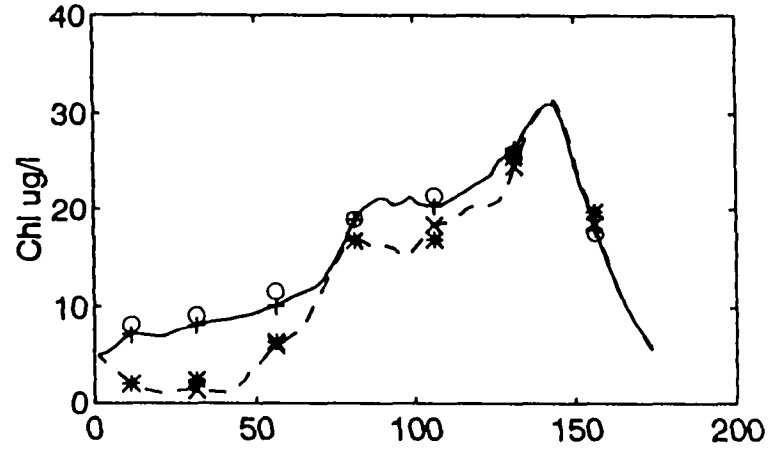
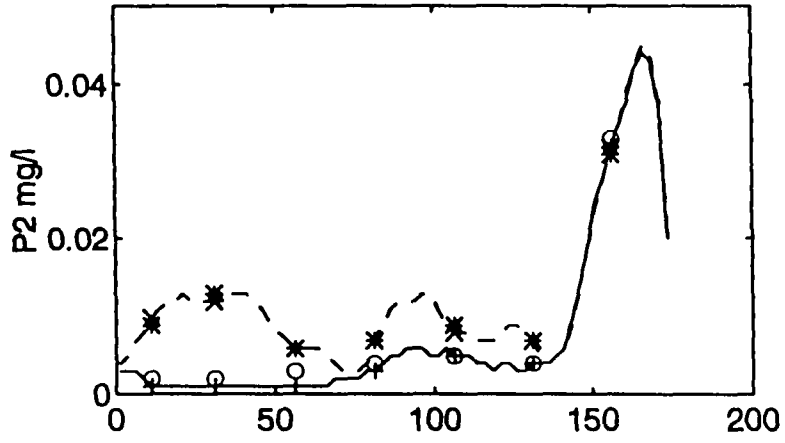


Figure 3-11 Comparisons of instantaneous surface and bottom concentrations of the state variables between the inverse model results (Run T3) and the true results together with sample data (with 10% error) at the 30th day (solid lines are the model results at surface, dashed lines are the model results at bottom, +'s and x's are the true results at the surface and the bottom, respectively, and o's and *'s are the sample data at the surface and the bottom, respectively).





IV. THE UNCERTAINTY OF THE PARAMETER

4.1 Parameter Uncertainty

To understand the behavior of the parameters in the system in detail, it is important to study the uncertainty of each parameter and the relations among the parameters in the system. The uncertainty of the parameters, or errors associated with the estimated parameter values, can be estimated by the covariance matrix of the estimated parameters. The covariance matrix of the estimated parameters is defined by:

$$Cov(\hat{\beta}) = E[(\beta - \hat{\beta})(\beta - \hat{\beta})^T] \quad (4-1)$$

where β is the true parameter, $\hat{\beta}$ is the estimated parameter, E is mathematical expectation, and superscript T denotes the transpose of a vector. With the assumption of uncorrelated errors, an approximation of the covariance matrix of the estimated parameters in nonlinear regression can be obtained by the following equation (Bard 1974; Yeh 1986):

$$Cov(\hat{\beta}) = \frac{J(\hat{\beta})}{N-m} [A(\hat{\beta})]^{-1} \quad (4-2)$$

where $J(\beta)$ is the least squares error, N is the number of observations; m is the parameter dimension; $\mathbf{A} = [\mathbf{A}_s^T \mathbf{A}_s]$; and \mathbf{A}_s is the Jacobian matrix, or sensitivity matrix, i.e., the gradients of the concentrations of the state variables with respect to the parameter β . Eq. 4-2 gives a lower-bound for the parameter variance-covariance, the actual covariance may be higher than that given by Eq. 4-2 because errors are often correlated. A well-estimated parameter is generally characterized by a small variance as compared to an insensitive parameter which is associated with a large variance.

The sensitivity matrix can be obtained by the influence coefficient method or variational method (e.g. Yeh 1986). The influence coefficient method uses the concept of parameter perturbation and the element of \mathbf{A}_s is approximated by:

$$a_{sj}^k = \frac{\partial C_i^k}{\partial \beta_j} = \lim_{\Delta \beta_j \rightarrow 0} \frac{C_i^k(\beta_j + \Delta \beta_j) - C_i^k}{\Delta \beta_j} \quad (4-3)$$

for each $j = 1, 2, \dots, m$; $i = 1, 2, \dots, n$; $k = 1, 2, \dots, L$; and $s = k_1, k_2, \dots, k_i, \dots, k_n$

where a_{sj}^k is the sensitive coefficient of the k th state variable at the sample location i with respect to the parameter β_j ; $\Delta \beta_j$ = a small increment of β_j ; C_i^k is the k th state variable at the sample location i ; L = the number of state variables; n = the number of sample stations; and m = the number of parameters. Using matrix notation, Eq. 4-3 can be expressed as:

$$(\mathbf{A}_s)_{N \times m} \Delta \beta_{m \times m} = \Delta \mathbf{C}_{N \times m} \quad (4-4)$$

where $N = n \times L$; and $\Delta\beta =$ a diagonal matrix with $\Delta\beta_{ii} = \Delta\beta_i$ for $i = j$ and 0 for others.

For the inverse model experiment with time varying boundary conditions (Run T1), the parameter uncertainty is provided by the diagonal terms of the sensitivity matrix (here the factor $J(\beta)/(N-m)$ was omitted). The uncertainties associated with the parameters are shown in Table 10. It can be seen that the large uncertainties of the parameters are associated with the settling velocities. These parameters are so uncertain that they are not identifiable without applying parameter transformation. This result is consistent with results of the test runs presented in section 3.1.2, which show that the inverse model is not convergent without preconditioning. A large uncertainty of individual parameter also indicates that the model is not sensitive to that parameter. It is perhaps more appropriate to speak of sensitivities rather than uncertainties when the estimated parameters are not close to the "true" values (van Straten 1983). After applying parameter transformation, parameters become identifiable in the new parameter space (Table. 11). In fact, the parameter transformation used in this study is equivalent to scale the parameters based on their physical scales and their contributions in the system so that the contributions of the scaled parameters are comparable in the new parameter space. For an individual parameter, it may not be considered identifiable in the original parameter system, while it is identifiable in the new parameter system. For instance, the estimated value of K_{bod} is about 1.4 in Run T1. It deviates from the true parameter value of 0.02 if viewing it in the original parameter space. However, it is considered identifiable in the new parameter space because the difference between estimated value and the true value is on the order of

1×10^{-3} (see Table 3, the scale for K_{bod} is 1×10^3). In other words, the error due to wrong estimation of K_{bod} is negligible.

4.2 Parameter Correlation and Singular Value Decomposition

With the result of the covariance matrix, one can obtain the correlation matrix of the estimated parameters. The correlation matrix is defined as:

$$R = \begin{bmatrix} \frac{c_{11}}{(c_{11}c_{11})^{1/2}} & \dots & \frac{c_{1m}}{(c_{11}c_{mm})^{1/2}} \\ \cdot & \dots & \cdot \\ \frac{c_{m1}}{(c_{m1}c_{11})^{1/2}} & \dots & \frac{c_{mm}}{(c_{mm}c_{mm})^{1/2}} \end{bmatrix} \quad (4-5)$$

where c_{ij} 's are the elements of the covariance matrix of the estimated parameters. A correlation analysis of the estimated parameters will indicate the degree of interdependence among the estimated parameters in the parameter system. For a system with high correlations among parameters, it can result in a slow rate of convergence or even nonoptimal parameter estimation (Yeh 1986). The correlation matrix of the parameters (Run T1) is shown in Table 12. The results show that many parameters are correlated with each other, such as R_{20} , K_{n11} , and K_{chl} ; P_{20} and K_{bod} ; K_{n12} , and K_{n23} ; and K_{p12} , K_{p11} and K_{chl} . Many settling velocities are highly correlated with other parameters. Because of the high correlations among the parameters, the concentrations of the state variables are dependent on the combined net effects of several parameters rather than on the individual parameter. In other words, the model predicted concentrations may not be affected significantly if the combined net effects

of the correlated parameters are the same even though the parameter values deviate from their "true" values. This phenomenon can be seen more clearly in the experiments with noisy data, in which the model predictions are very satisfactory even though errors in some estimated parameters are relatively large (Table 9).

To understand the relations among the parameters in detail, the singular value decomposition (SVD) method is introduced here to further investigate the relations among the parameters in the system. The SVD method was previously used by Wiggins (1972) and Uhrhammer (1980) to calibrate seismologic parameters and recently used by Lal (1995) to study the river roughness. Using SVD method, one can diagnose the sensitivity matrix and understand the parameters of the model in great detail (Lal 1995).

The SVD is based on the theorem that a matrix A_s can be decomposed into three matrices U , Λ , and V such that

$$A_s = U\Lambda V^T \quad (4-6)$$

where U , $V = N \times N$ and $m \times m$ matrixes of orthogonal singular vectors, respectively; and $\Lambda =$ an $N \times m$ diagonal matrix of singular values of A_s (Noble and Daniel 1975).

With symmetric matrix, SVD provides eigenvalues and eigenvectors.

Assuming ϵ_s^k is the differences between model results and the sample data for

the k th state variable at location i , then,

$$\epsilon_s^k = \epsilon_k^k = (C_i^k - \hat{C}_i^k) \quad (4-7)$$

for each $s = k_1, k_2, \dots, k_p, \dots, k_n; i = 1, 2, \dots, n; k = 1, 2, \dots, L,$

where C_i^k 's and \hat{C}_i^k 's are the model results and the sample data, respectively.

Recalling Eq. 4-3, the corrections in parameter $\Delta\beta$ required to make $\epsilon_i^k=0$ can be

approximated by the set of following equations (Wiggins 1972; Lal 1995):

$$a_{sj}^k \Delta\beta_j = -\epsilon_s^k \quad (4-8)$$

or, in matrix form

$$A_s \Delta\beta = -\epsilon \quad (4-9)$$

where ϵ = error matrix. Using SVD method, Eq. 4-9 can be expressed as

$$\Lambda \Delta Z = -\Delta D \quad (4-10)$$

where

$$\Delta Z = V^T \Delta\beta \quad (4-11)$$

$$\Delta D = U^T \epsilon \quad (4-12)$$

Eq. 4-10 tells us that the errors of data misfit (ΔD) are dependent on the new linearly independent parameter corrections ΔZ , which is the linear combination of the difference between the true parameters and the estimated parameters (Eq. 4-11). For a system with parameters correlated with each other, the system can be described by

only m_p ($m_p < m$) dominant new independent parameters. The contribution of the new independent parameter correction Δz_j is given by its corresponding singular value λ_j . Applying SVD to the original parameter system, i.e., without parameter transformation, the calculated first four vectors of V , which correspond to the four largest singular values, are shown in Table 13. The independent parameter corrections (ΔZ) can be calculated by linear combination of the difference between the true parameters and estimated parameters (Eq. 4-11). The coefficients of each linear combination, listed in Table 13, can be treated as weights corresponding to the parameter deviations shown in column a . The first four independent new parameter corrections contribute 99.37% of the error information to the system. It suggests that the correlations among the original parameters can be represented by these four new independent parameters which contribute 99.37% of the error of data misfit. In other words, the model will give a good prediction (99.37% accuracy) as long as these new independent parameter corrections are very small even though an individual parameter may deviate from its true value. For instance, two different sets of parameters may give the same error of the data misfit if their corresponding new independent parameter corrections are very close.

The coefficients listed in Table 13 not only give the information about correlations among parameters but also give the information indicating importance of the individual parameter. For example, column 1 shows that K_{n12} and K_{p12} are the key parameters in the model. Column 2 shows that K_{gr} , R_{20} , P_{20} , K_{n12} , K_{p12} , K_{n23} , and K_c are the key parameters in the model. These seven parameters are very important in the system. They indicate the relations among growth, respiration, and mortality and the

relations among nutrients recycling and mineralizations. For example, column 2 shows that the growth rate has the opposite sign as the respiration rate and mortality rate, so that the net error will not increase if an increase of growth rate, respiration rate, and mortality rate occur simultaneously. It indicates that an increase of growth rate can be compensated by an increase of respiration and mortality rates to keep the net effect unchanged. Notice that R_{20} and P_{20} in column 2 have the opposite sign as K_{p12} and K_{n12} . The large values of R_{20} and P_{20} also indicate the quick nutrient recycling back to the system. However, an increase of nutrients recycling can be balanced by an increase in the rate of mineralization processes resulting in no net change in terms of error. The accuracy of model prediction is about 83.4% if these seven parameters can be estimated accurately. All the settling velocities are associated with small coefficients which indicate that these parameters are not very important in the system. A wrong estimation of these parameters will not increase the error of data misfit significantly resulting in a high uncertainty of these parameters. The results of SVD of the new parameter system are shown in Table 14. The results show that the first four independent new parameters only contribute 85.51% of the error information to the system. It took ten independent new parameters to have the total contribution of 98.77%. This indicates that the new parameters are almost independent in the new parameter system after parameter transformation. Examining the weights associated with the parameters, they are on the same order of magnitude so that each parameter is important in the new parameter system. The results of SVD suggest that applying parameter transformation can also reduce correlations among parameters resulting in increased speed of convergence.

TABLE 10. Parameter Uncertainty (diagonal terms) of Run T1

Parameter Name	Uncertainty (%)	Parameter Name	Uncertainty (%)
K_{gr}	0.596	K_c	0.021
R_{20}	0.024	K_{chl}	7732.35
P_{20}	0.007	K_{n11}	799.55
$K_{n12}(20)$	0.002	K_{p11}	2487.44
$K_{n23}(20)$	0.170	K_{p22}	4432.51
$K_{n33}(20)$	0.882	K_{bod}	11027.15
$K_{p12}(20)$	0.006		

TABLE 11. Parameter Uncertainty (diagonal terms) of New Parameters After Parameter Transformation (Run T1).

Parameter Name	Uncertainty (%)	Parameter Name	Uncertainty (%)
K_{gr}	0.60	K_c	0.03
R_{20}	0.59	K_{chl}	0.77
P_{20}	0.17	K_{n11}	0.08
$K_{n12}(20)$	0.32	K_{p11}	0.99
$K_{n23}(20)$	0.17	K_{p22}	0.44
$K_{n33}(20)$	0.22	K_{bod}	0.28
$K_{p12}(20)$	0.14		

TABLE 12. Correlation Matrix of The Estimated Parameters
(Run T1 in absolute values)

	K_{gr}	R_{20}	P_{20}	K_{n12}	K_{n23}	K_{n33}	K_{p12}	K_{chl}	K_{n11}	K_{p11}	K_{p22}	K_c	K_{bod}
1 K_{gr}	1.00												
2 R_{20}	0.33	1.00											
3 P_{20}	0.03	0.25	1.00										
4 K_{n12}	0.26	0.06	0.08	1.00									
5 K_{n23}	0.04	0.05	0.02	0.74	1.00								
6 K_{n33}	0.51	0.22	0.07	0.29	0.39	1.00							
7 K_{p12}	0.49	0.12	0.02	0.37	0.12	0.46	1.00						
8 K_{chl}	0.33	0.60	0.02	0.28	0.08	0.19	0.68	1.00					
9 K_{n11}	0.00	0.61	0.02	0.51	0.43	0.35	0.37	0.74	1.00				
10 K_{p11}	0.28	0.52	0.01	0.38	0.17	0.14	0.70	0.92	0.72	1.00			
11 K_{p22}	0.22	0.28	0.02	0.04	0.06	0.06	0.44	0.25	0.26	0.48	1.00		
12 K_c	0.02	0.00	0.25	0.06	0.05	0.05	0.03	0.08	0.04	0.06	0.03	1.00	
13 K_{bod}	0.01	0.15	0.81	0.09	0.01	0.09	0.05	0.10	0.03	0.08	0.04	0.65	1.00

TABLE 13. The Coefficients of the First Four Vectors of V Matrix

a	1	2	3	4
ΔK_{gr}	0.0069	-0.0125	0.0134	-0.1053
ΔR_{20}	-0.0163	0.2418	0.1677	0.9106
ΔP_{20}	-0.0003	0.8351	-0.4628	-0.0537
ΔK_{n12}	-0.8957	-0.1983	-0.3812	0.0944
ΔK_{n23}	-0.0334	0.0150	0.0450	-0.0854
ΔK_{n33}	0.0199	-0.0062	-0.0134	0.0262
ΔK_{p12}	0.4426	-0.3974	-0.7651	0.2364
ΔK_{Chl}	-0.0006	0.0006	0.0008	0.0018
ΔK_{n11}	-0.0003	-0.0002	-0.0001	-0.0003
ΔK_{p11}	-0.0010	-0.0004	-0.0005	0.0013
ΔK_{p22}	-0.0004	-0.0002	0.0004	0.0000
ΔK_c	-0.0077	-0.2157	0.1579	0.2899
ΔK_{bod}	0.0000	-0.0006	0.0005	0.0006
λ (%)	45.59	37.89	14.64	1.25
sum	45.59	83.48	98.12	99.37

TABLE 14. The Coefficients of the First Four Vectors of V Matrix of New Parameters after transformation

a	1	2	3	4
ΔK_{gr}	0.0288	-0.0407	0.0131	-0.1954
ΔR_{20}	-0.0785	0.0698	-0.1008	0.3732
ΔP_{20}	0.2737	0.2705	-0.0704	0.3283
ΔK_{n12}	-0.1245	0.1592	-0.1308	-0.2247
ΔK_{n23}	0.0110	0.0219	0.1537	-0.0712
ΔK_{n33}	0.0366	-0.0450	0.3309	0.3178
ΔK_{p12}	0.2929	-0.3277	0.3932	0.4855
ΔK_{Chl}	-0.3856	0.4396	-0.0971	0.4291
ΔK_{n11}	-0.2795	0.4100	0.7802	-0.2193
ΔK_{p11}	-0.2155	0.2517	-0.1851	0.2543
ΔK_{p22}	-0.1517	0.1716	-0.1639	-0.0375
ΔK_c	-0.6268	-0.5113	0.0203	0.1516
ΔK_{bod}	-0.3554	-0.2636	0.0162	-0.0348
λ (%)	45.98	19.38	9.82	10.33
sum	45.98	65.36	75.18	85.51

V. MODEL CALIBRATION WITH FIELD DATA

In this chapter, using the inverse model to calibrate the eutrophication model of the Rappahannock River with field data will be discussed. The eutrophication model was calibrated with a simulation of distributions of the state variables from June 6 to July 5, 1990. The boundary conditions, initial conditions, and benthic fluxes are described in section 3.2.1, which were the same as those used for the experiments with time-varying boundary conditions. The results of the slackwater survey conducted on July 5 was used for the model calibration. The eutrophication model was verified by using data collected on August 7, 1990.

5.1. Model Calibration

To calibrate a model with field data accurately, the effects of observation errors, model structure errors, and random variability of the nature that can not be reproduced by a deterministic model should be considered. A way to reduce these errors is to treat them as a combined random error and introduce weight to the cost function based on the likelihood theory. Because these random errors associated with each state variables were unknown, the proper weights were determined based on a trial-and-error basis, while using Eq. 2-47 as a guideline.

A trial run was first conducted by using all the data available on July 5 and unit

weights for all the state variables. The inverse model simulated the distributions of the state variables from June 6 to July 5, 1990 with initial guess parameter values used in Run T1, i.e., mean values compiled from published results. The results of the trial run were not satisfactory. The errors between the observations and model predictions associated with N₂, CBOD, Chl, and P₂ were very large. By examining the field data carefully, it was found that some unusual data values occurred in the measurements of N₂ and CBOD. The unusual high values of N₂ between km 140 to 160 were noted by Park and Kuo (1993b). By comparing point source loading and concentrations of N₂ and Chl between the field surveys on July 5 and August 8, they concluded that there might be some errors in the measurements of N₂ between km 140 to 160 on July 5. High concentrations of the bottom N₂ also occurred between km 0 to 40. The main reason for this was due to an increase of benthic release of N₂ (Park and Kuo 1993b). During the period of field survey, the concentration of DO near the bottom was almost zero (see Fig. 5-1). The anoxic condition resulted in increasing the release of N₂ from the bottom. However, the present model does not model this mechanism and the benthic flux of N₂ was treated as a constant release, i.e., not as a function of DO. Discrepancy between the model predictions and field observations was expected. High concentrations of CBOD at the surface between km 0 to 60 on July 5 were also noted. Comparing the concentrations of CBOD between July 5 and August 7, no unusual high concentration of CBOD near the surface was observed on August 7. The concentration of CBOD near the surface was on the same order as that at the bottom between km 0 to 60 on August 7, even though the DO concentration was almost the same as that on July 5. The reason for causing high concentration of CBOD on July 5

is not known. To reduce the model structure errors and observation errors associated with the field data, the final data used for the inverse model calibration excluded those data of N₂ with concentration higher than 0.25 mg l⁻¹ and data of CBOD with concentration higher than 4 mg l⁻¹.

From the trial calibration, it was also found that the model fit one state variable better than another. It was difficult to make the inverse model fitting all the state variables equally well because the random variability were different with respect to each state variable. Since it is important to model Chl, N₂, P₂, and DO accurately, higher priority was given to N₂, P₂, Chl, and DO. In order to do this, the global weights associated with each state variable were objectively specified. The weights corresponding to N₁, N₂, N₃, P₁, P₂, Chl, CBOD, and DO were 0.05, 0.15, 0.10, 0.05, 0.15, 0.25, 0.05, 0.2 respectively. The weights of Chl and DO were emphasized. With new weights and corrected field data, the second trial run was conducted. The calibration results were much improved this time. The calculated error residual variances showed that large errors between the model predictions and observations occurred mainly in P₂, N₂, CBOD, and Chl. The inverse model predicted relatively low concentrations of N₂ between km 140 to 160 and km 0 to 50, low surface concentrations of CBOD from the km 0 to 60, and low concentration of Chl and P₂ between km 90 to 140. N₂ had the largest error residual which was mainly due to the model structure error and observation errors as mentioned in the last paragraph. It suggested that the weight for N₂ should be decreased based on the likelihood theory. The low estimation of Chl was possibly due to the incorrect estimation of P₂ because P₂ was predicted too low between km 90 to 140. Since the system was phosphorus

limited, the concentration of Chl was very sensitive to the availability of P2. The weight for P2 should be increased. The concentration of DO was almost unchanged. It seems that DO was insensitive to the weight. As a matter of fact, the experiment showed that the prediction of DO was satisfactory even though the wrong parameters were used (Fig. 3-4). The reason is that the concentration of bottom DO is mainly controlled by the physical processes as Kuo *et. al.*, (1991b) pointed out, while the concentration of surface DO is mainly controlled by the temperature. The weights used for N1, N2, N3, P1, P2, Chl, CBOD, and DO were adjusted and the new values were 0.10, 0.07, 0.2, 0.1, 0.22, 0.15, 0.05, 0.15 respectively. Here, the weight for Chl was decreased so that high priority was given to P2. N3 had the smallest error residual so that the weight for N3 was increased.

With the adjusted weights, another trial run was conducted, the results were improved (not shown). The results showed that the estimated values of K_{n12} and K_{n23} were larger than the values obtained from the original model calibration. It was also found that the inverse model always attempted to reduce the values of the K_{n12} and K_{n23} during the iteration processes while the total misfit was increased as soon as these two parameter values were reduced. It seems that the results obtained might be a local minimum. It was decided that a new set of the initial guess parameters with small values was used for the calibration.

To find a new solution, the inverse model calibration Run IMC-1 was conducted with new weights and initial guess values. The calibration results of Run IMC-1 is shown in Fig. 5-1. The eight state variables (N1, N2, N3, P1, P2, Chl, CBOD, and DO) are presented in which the ranges over a day from the inverse model results at

the surface and bottom layers are compared with the field data along the distance from the river mouth. The results are satisfactory. The estimated parameter values of IMC-1 are listed in Table 15. To compare the present model calibration results with the original model results (Park and Kuo, 1993b), the model results with original model calibrated (OMC) parameter values are shown in Fig. 5-2 and the original model parameter values are also listed in Table 15.

Comparing the results of the inverse model calibration with the original model results (Figs. 5-1 and 5-2), there are four aspects to be noted: (1) the prediction of concentrations of Chl is improved by of IMC-1 comparing to that of OMC around km 100; (2) the prediction of concentrations of N2 is improved by IMC-1 comparing to that of OMC between km 140 to 160; (3) lower P2 concentration is predicted by IMC-1 than that of OMC around km 100; and (4) lower CBOD is predicted by IMC-1 than that of OMC near the mouth. One difference between IMC-1 and OMC was that a constant settling velocity K_{p22} of 40 cm day^{-1} was assumed for IMC-1 while OMC used variable K_{p22} . The value of 40 cm day^{-1} seems too high for all reaches, so another Run IMC-2 was conducted by varying K_{p22} along the channel. A value of 40 cm day^{-1} was used between km 140 to 160, and zero was used for the rest of the channel. The results of the IMC-2 calibration are shown in Fig. 5-3 and the estimated parameter values are listed in Table 15. Fig. 5-3 shows that the model prediction of P2 is improved but Chl prediction is not as good as IMC-1. There are not much difference for the rest of the state variables between IMC-1 and IMC-2. The improvement of predictions by IMC-2 is not evident.

5.2 Model Verification

Table 15 shows that the values of estimated parameters for both IMC are very different from that of OMC even though the total data misfit is very close. Some parameter values are different by an order of magnitude, such as K_{n12} and K_{n23} . It is hard to judge which set of parameter values is more appropriate without additional information. Since both the inverse model and original model were calibrated with one set of the field data, it does not guarantee that validity of the model can be extended beyond the data set used in the calibration processes. By verification tests, one may examine the response of the model, with a particular set of parameter values, to a different ambient condition.

The model runs, with different sets of parameter values (Table 15), were extended through August 7, 1990. The capability of the model, with respect to each set of parameter values, was tested through comparisons of the model predictions and the field data collected on August 7. The comparisons between the model results of IMC-1, OMC, and IMC-2 and field data are shown in Figs. 5-4, 5-5, and 5-6, respectively. It can be seen that low prediction of P2 by IMC-1 and high prediction of P2 by OMC are improved by IMC-2. The low prediction of N2 by OMC between km 140 to 160 can be well predicted by IMC-1 and IMC-2. IMC-1 gives the best prediction of Chl on August 7, while the predictions of Chl by IMC-2 and OMC are similar. OMC gives the best prediction of CBOD.

The model-data comparison of the results of calibration and verification can only provide a qualitative evaluation of the difference among different calibrations. The perceived agreement between predictions and the observations depend on the

viewpoint of the assessors. To evaluate the difference of the model predictions with different sets of the parameters obtained from different calibrations, quantitative assessments of the model accuracy are desirable. Many methods are available to quantify the model performance (Cercio and Cole 1994). In the present study, the root-mean-square, mean error, and relative error are used to evaluate the model results.

The root-mean-square error is defined:

$$RMS = \sqrt{\frac{\sum (O-P)^2}{n}} \quad (5-1)$$

where

RMS = root-mean-square; O = observation; P = model prediction; and n = the number of observations. The RMS is an indicator of the deviation between model predictions and observations.

The Mean error is defined:

$$MER = \frac{\sum (O-P)}{n} \quad (5-2)$$

where MER = mean error. Mean error provides the information of overprediction or underprediction. Positive mean error indicates model predictions are less than observations, on average. A negative mean error indicates model predictions exceed observations, on average.

The relative error is defined:

$$RER = \frac{\sum |O-P|}{\sum O} \quad (5-3)$$

where *RER* = relative error. The relative error is the ratio of the absolute mean error to the mean of the observations. It permits the comparisons of state variables with different units.

The calculated *RMS*, *MER*, and *RER* of the model results with the different sets of parameters obtained from the different model calibrations are listed in Tables 16, 17 and 18 respectively. The observations of July 5 and August 7 were used to calculate these errors. Those data excluded from the calibrations were not used in the error calculation.

Table 16 showed that root-mean-square error of IMC-1 and IMC-2 are less than that of OMC for most of the state variables. The differences between model predictions and observations of the state variables are reduced in IMC-1 except for CBOD. The results show that error reductions are mainly due to the improvement of the predictions of nitrogens and Chl. The improvements of P2 in IMC-1 was attributed to the reduction of P2 around km 150 which compensated low prediction of P2 around km 100. Based on the results of *RMS*, IMC-1 gives the best model prediction. However, the improvements results in a sacrifice of CBOD prediction.

The results of the mean errors showed that model prediction by IMC-1 was similar to that of OMC. The observations exceeded predictions by both IMC-1 and OMC for most of the state variables except for DO. The only difference was that IMC-1 gave a

underprediction of P2 while OMC gave a overprediction of P2. *MER* of IMC-1 in N1, N2, N3, P1, Chl, and DO were less than that of OMC while *MER* in P2 and CBOD were increase. *MER* of IMC-2 in N1, N2, P2, Chl and DO were reduced comparing with OMC, while *MER* in N3, P1, and CBOD were increase.

All calibrations showed that DO had the smallest relative errors. The low error was attributed to the nature of DO distributions. Surface DO is always near saturation, thus mainly controlled by the temperature, while bottom DO is mainly controlled by the estuarine circulation. The errors in CBOD were lagre for all three calibrations. It suggested that model predictions of CBOD were not satisfactory. Comparing the results of IMC and OMC, the relative errors in N1, N2, N3, P1, and Chl were reduced by IMC-1 while the relative errors in N1, N2, N3, P2, and Chl were reduced by IMC-2. Large error reductions were due to the improvement of model predictions of nitrogens by the inverse model calibrations, especially N1 and N3. The results of relative error showed evidence of improvement of the predictions by the inverse model calibration.

To compare the overall performance among the different calibrations, a paired comparisons between IMC-1 and OMC, IMC-2 and OMC, and IMC-1 and IMC-2 are listed in Table 19, in which "+" signs indicate that errors are decrease and "-" signs indicate that errors are increase. It shows that IMC-1 gives overall better result.

5.3. Calibration Summary

The results of the eutrophication model calibration and verification presented in the preceding sections show that the inverse model is a good tool to aid calibration of the eutrophication model and provides a new approach to the model calibration. With the use of the inverse model, the model calibration can be conducted more efficiently and systematically compared to traditional procedures.

The accuracy of the model calibration relies on the quality and quantity of field observations, model structure, and the nature of the system. Because of limited data sets and random variability in the nature, the unique solutions may not be guaranteed for those parameters to which the model is not sensitive. To overcome these weaknesses, the selection of the cost function and the previous knowledge of the range of the parameter values are very important. Because of the random variability that cannot be reproduced by a deterministic model, the accuracy of the inverse model calibration is dependent on what kind of cost function is selected. In the present inverse model calibration, the weighted least-squares was chosen as the cost function. Although the way of selecting weights was based on an engineering judgement and a try-and-error method, it did incorporate part of the random variability of the system into the cost function. The model calibration showed that the model can not be calibrated accurately without using proper weights. In processes of the inverse model calibrations, each parameter was bounded by its upper-bound and lower-bound. The previous knowledge of the range of parameter values in a particular system can successfully control the accuracy of parameter estimation. It is important to be aware that the parameters obtained from the inverse model calibration is based on the

assumption that other parameters and the boundary conditions are certain. It is expected that the model results may be improved by fine tuning the other parameters or by adjusting boundary conditions if measurements are available.

TABLE 15. Estimated Parameter Values of Model Calibration

Parm. Name	OMC Result	IMC-1		^a IMC-2
		Initial Guess	Result	Result
K_{gr}	2.00	1.000	1.3952	1.7580
R_{20}	0.17	0.100	0.0683	0.0988
P_{20}	0.02	0.100	0.0190	0.0590
$K_{n12}(20)$	0.04	0.010	0.0074	0.0222
$K_{n23}(20)$	0.30	0.100	0.0739	0.0847
$K_{n33}(20)$	0.35	0.100	0.3156	0.2436
$K_{p12}(20)$	0.06	0.100	0.0271	0.0502
K_c	0.10	0.100	0.2249	0.2466
K_{chl}	10.0	18.00	3.2446	9.1153
K_{n11}	8.00	10.00	8.5074	9.2172
K_{p11}	10.0	10.00	8.6867	11.8844
K_{p22}	20.0	10.00	39.998	40.000
K_{bod}	0.02	10.00	8.8272	10.1081
^b Error	0.178356		0.1835	0.16437

a: the initial guess values are same as IMC-1 and K_{p22} is specified (see text).

b: value of the cost function.

Table 16. Root-Mean-Square Errors Between the Observations and Model predictions

Name	n	IMC-1	IMC-2	OMC
N1	60	0.1396	0.1578	0.1781
N2	63	0.0496	0.0487	0.0576
N3	70	0.0733	0.0793	0.1032
P1	55	0.0187	0.0206	0.0198
P2	70	0.0074	0.0061	0.0081
Chl	60	5.9824	6.5200	6.9849
CBOD	61	1.6088	1.5947	1.4384
DO	70	1.0164	1.0262	1.0660

Table 17. Mean Errors Between the Observations and Model Predictions

Name	n	IMC-1	IMC-2	OMC
N1	60	0.0111	0.0106	0.0135
N2	63	0.0050	-0.0027	0.0107
N3	70	0.0065	0.0173	0.0136
P1	55	0.0045	0.0088	0.0064
P2	70	0.0033	-0.0000	-0.0018
Chl	60	1.8169	-3.1839	3.4080
CBOD	61	0.7432	0.6104	0.2362
DO	72	-0.1676	-0.1724	-0.2608

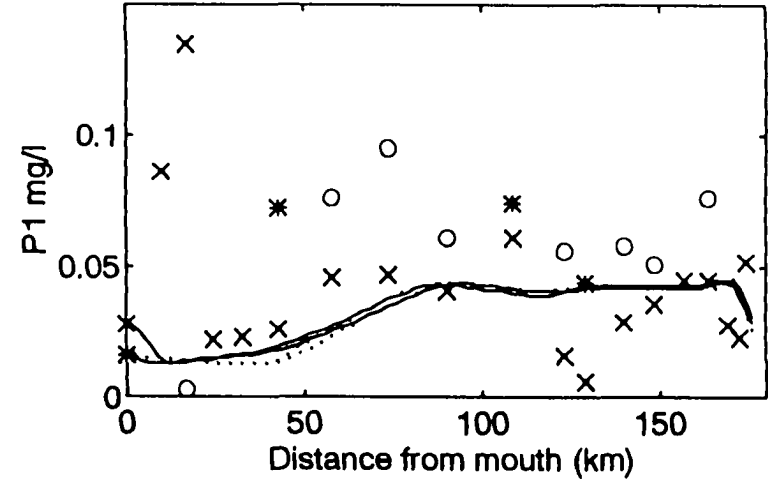
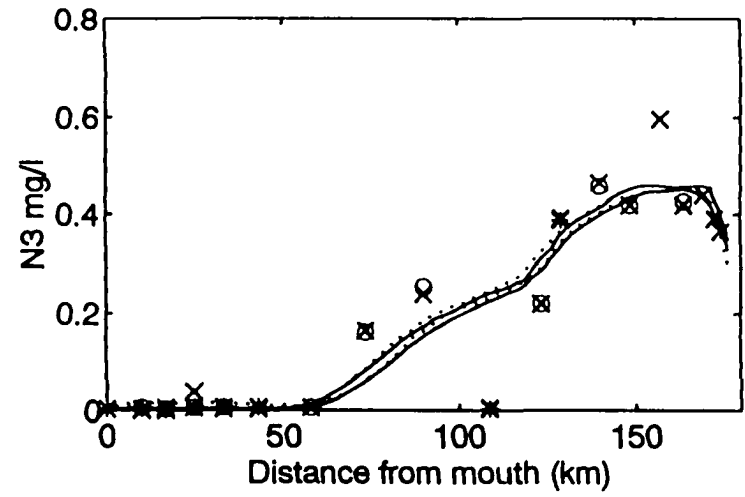
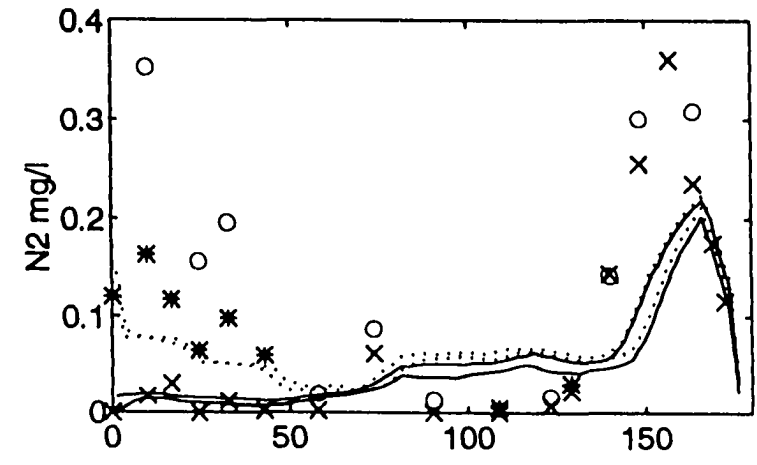
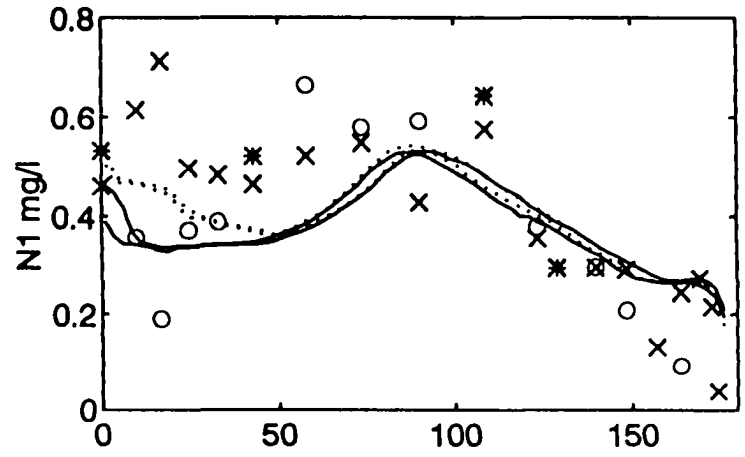
Table 18. Relative Errors Between the Observations and Model Predictions

Name	n	IMC-1	IMC-2	OMC
N1	60	0.2580	0.2925	0.3325
N2	63	0.5236	0.5282	0.6156
N3	70	0.3109	0.3427	0.4892
P1	55	0.3533	0.3910	0.3717
P2	70	0.5439	0.3931	0.4953
Chl	60	0.2671	0.2900	0.2933
CBOD	61	0.6565	0.6797	0.6004
DO	72	0.1353	0.1374	0.1442

Table 19. Comparisons of Errors Between Different Calibrations

	IMC-1 vs. OMC			IMC-2 vs. OMC			IMC-1 vs. IMC-2		
	<i>RMS</i>	<i>MER</i>	<i>RER</i>	<i>RMS</i>	<i>MER</i>	<i>RER</i>	<i>RMS</i>	<i>MER</i>	<i>RER</i>
N1	+	+	+	+	+	+	+	-	+
N2	+	+	+	+	+	+	-	-	+
N3	+	+	+	+	-	+	+	+	+
P1	+	+	+	-	-	-	+	+	+
P2	+	-	-	+	+	+	-	-	-
Chl	+	+	+	+	+	+	+	+	+
CBOD	-	-	-	-	-	-	-	-	+
DO	+	+	+	+	+	+	+	+	+
Total improvement	7	6	6	6	5	6	5	4	7

Figure 5-1. The inverse model (IMC-1) calibration results on 7/5/90 (daily maximum and minimum at the surface and bottom, solid lines are the model results at the surface layer, dashed lines are the model results at the bottom layer, x's are the field data at the surface, o's are field data at the bottom layer, and *'s are the field data at the middle layer).



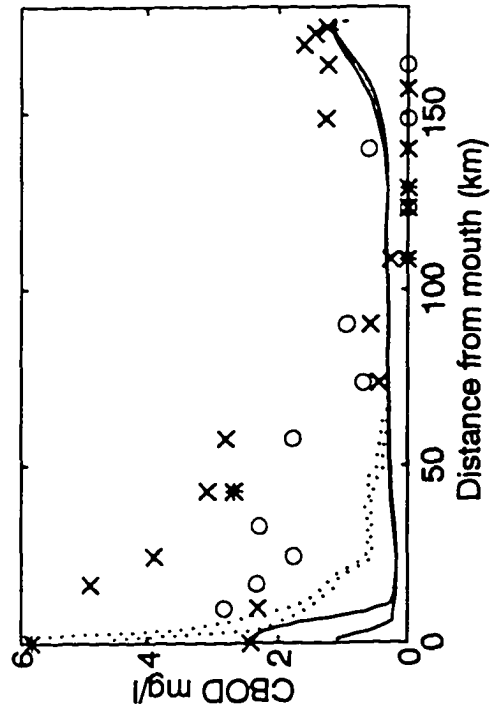
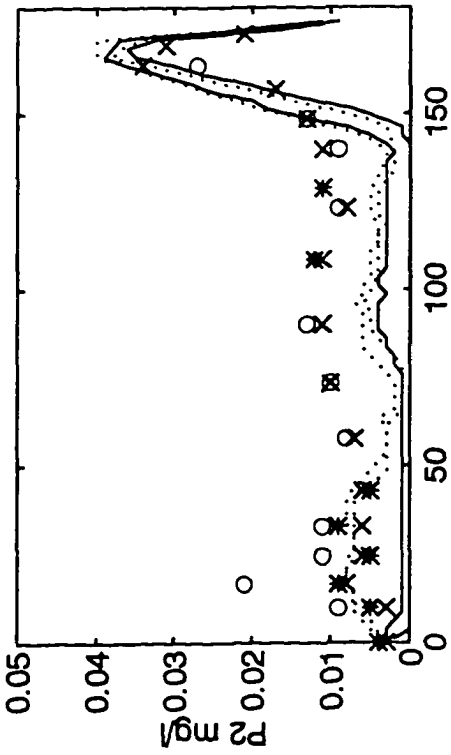
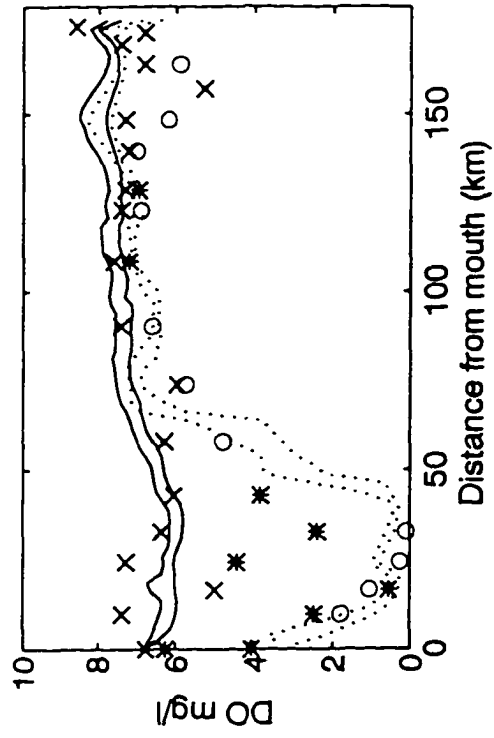
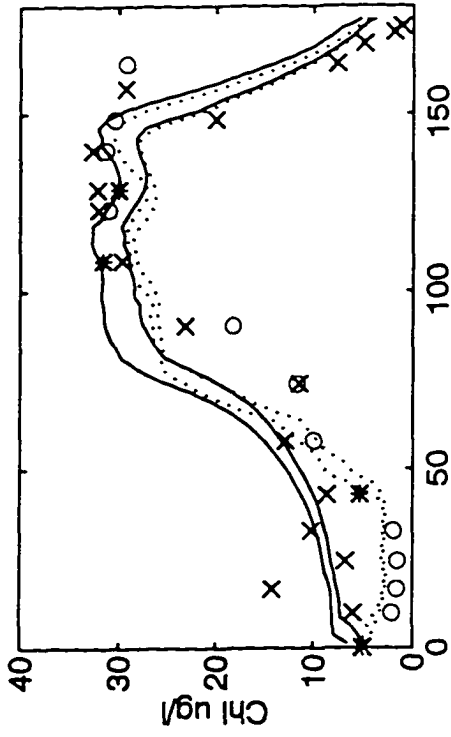
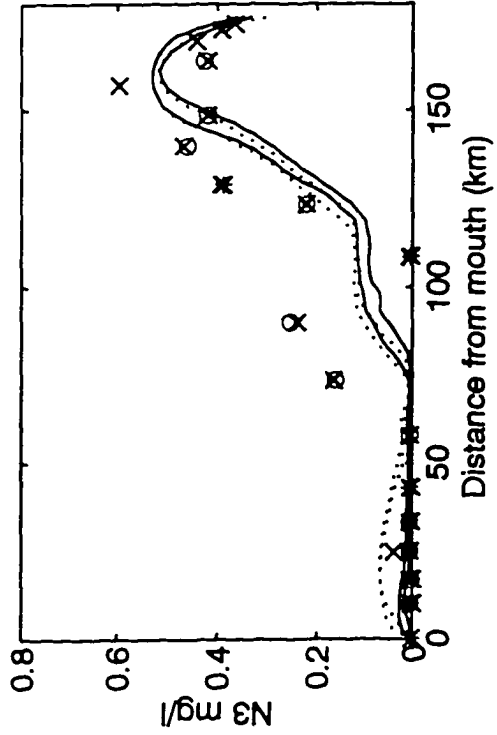
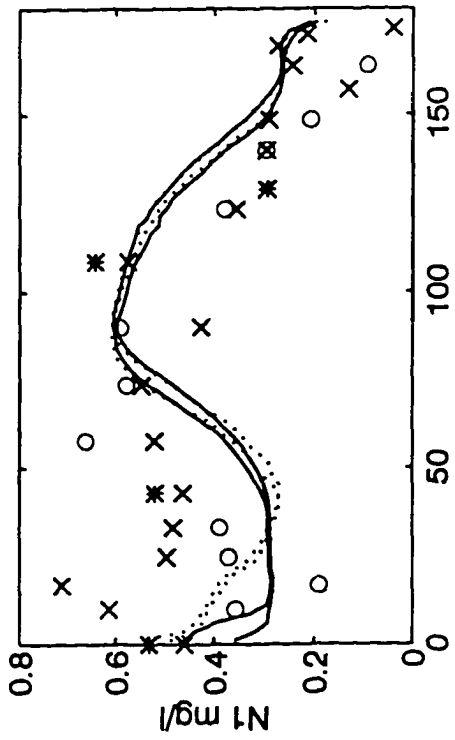
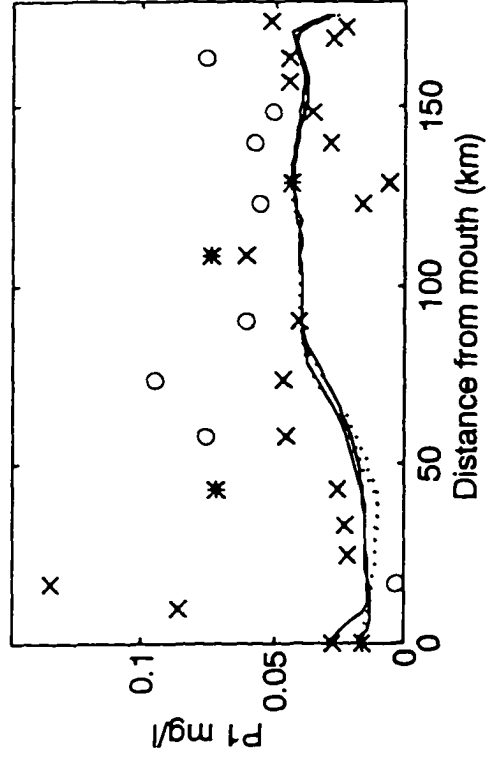
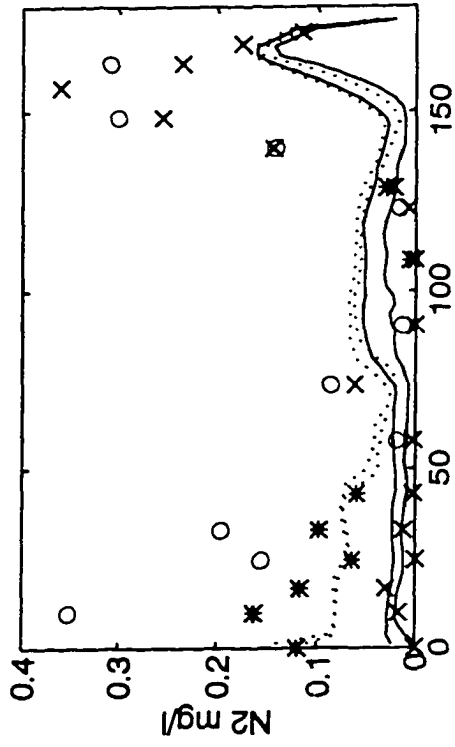


Figure 5-2. The original model (OMC) calibration results on 7/5/90 (daily maximum and minimum at the surface and bottom, refer to Fig. 5-1 for line and symbol description).



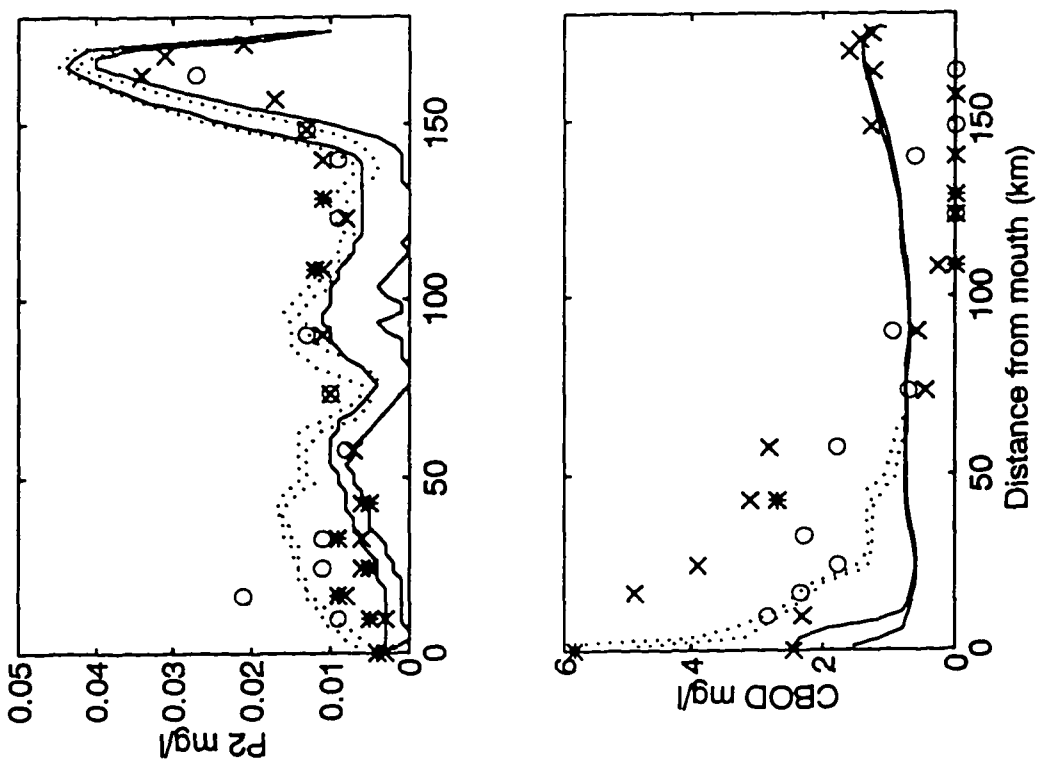
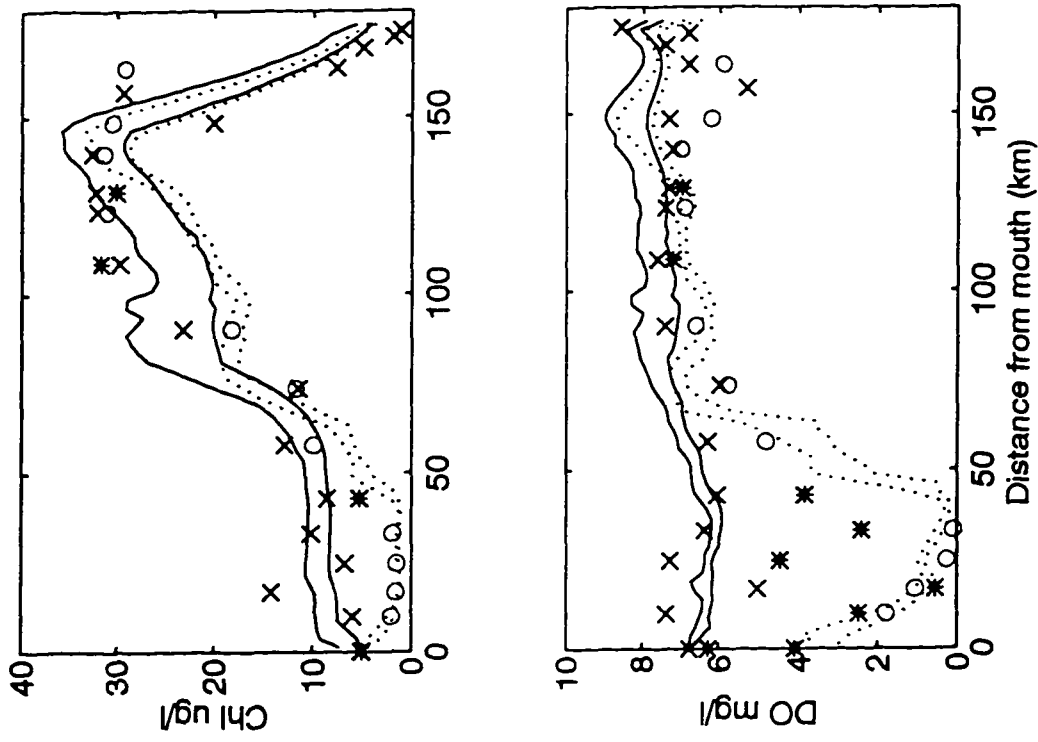
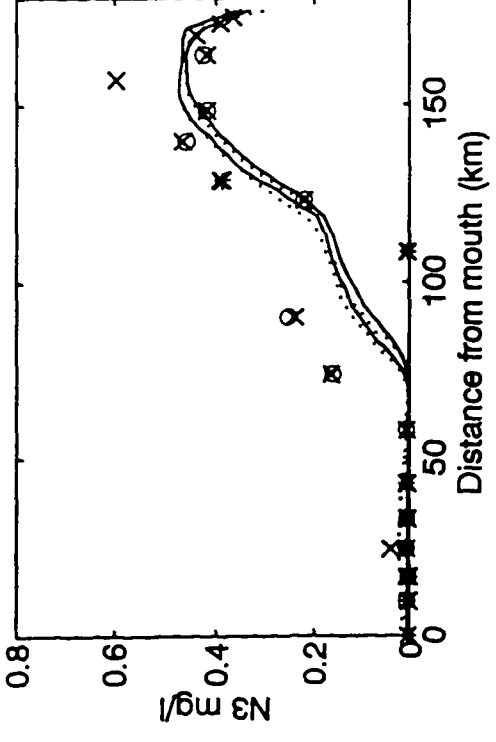
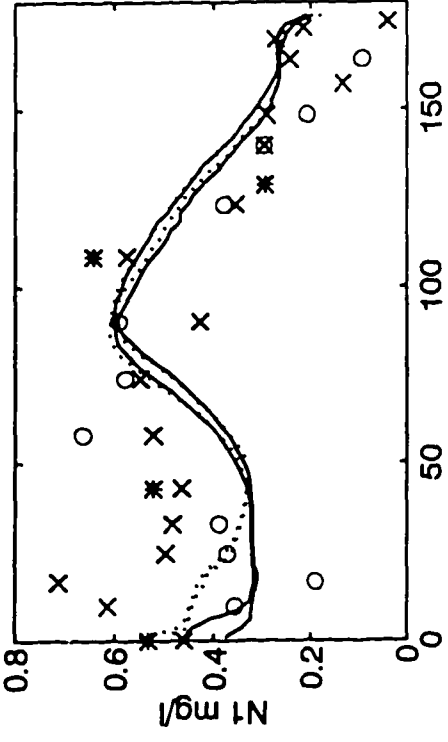
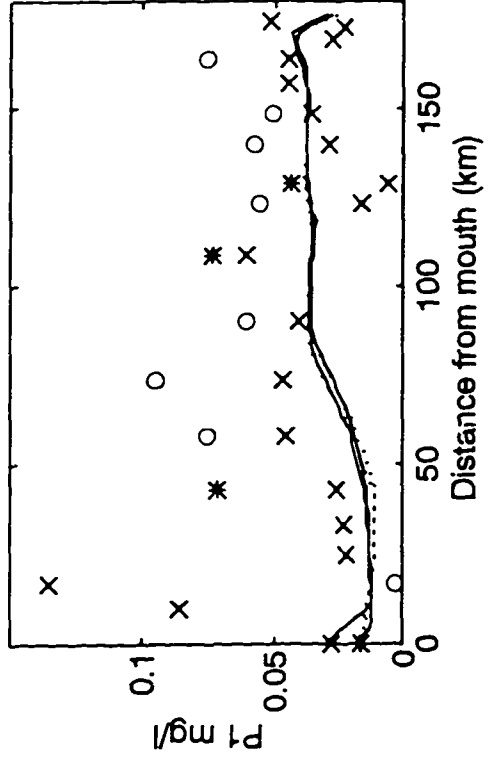
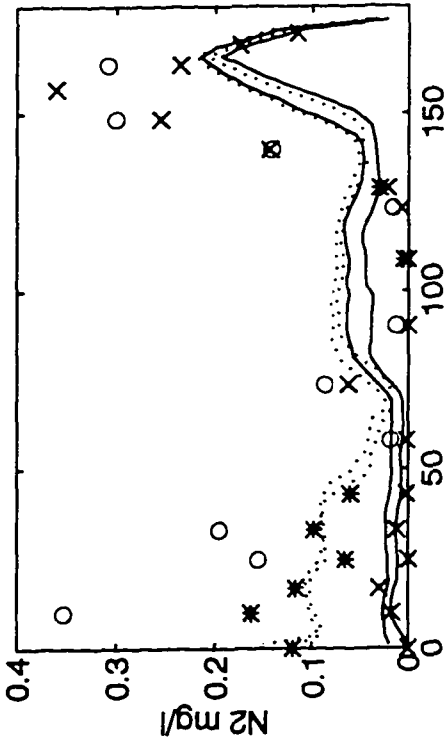


Figure 5-3 The inverse model (IMC-2) calibration results on 7/5/90 (daily maximum and minimum at the surface and bottom, refer to Fig. 5-1 for line and symbol description).



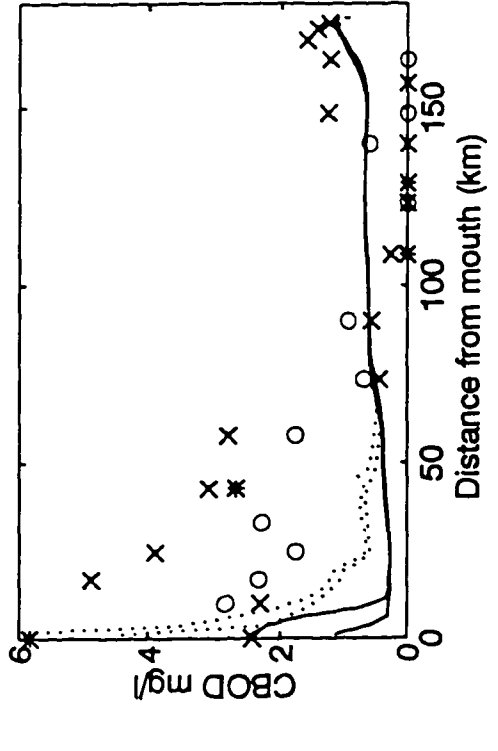
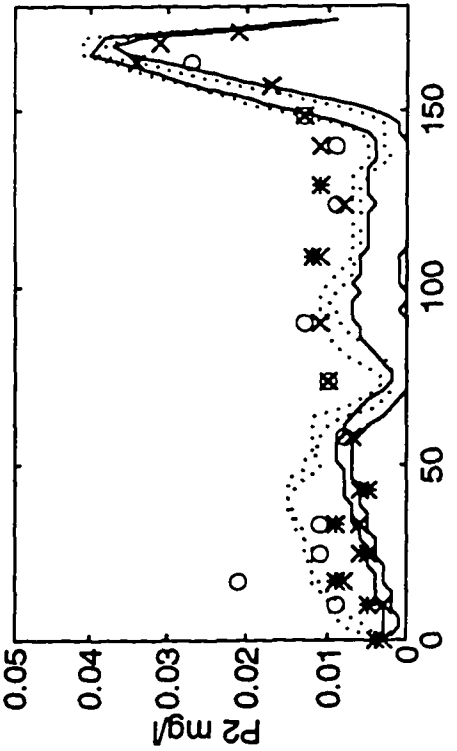
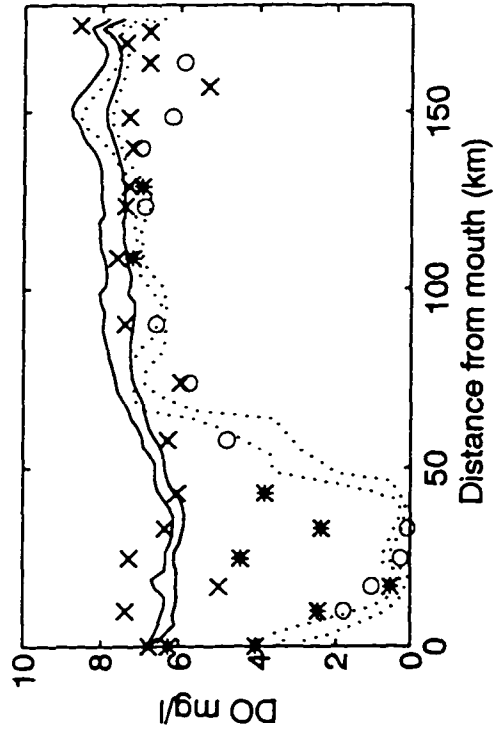
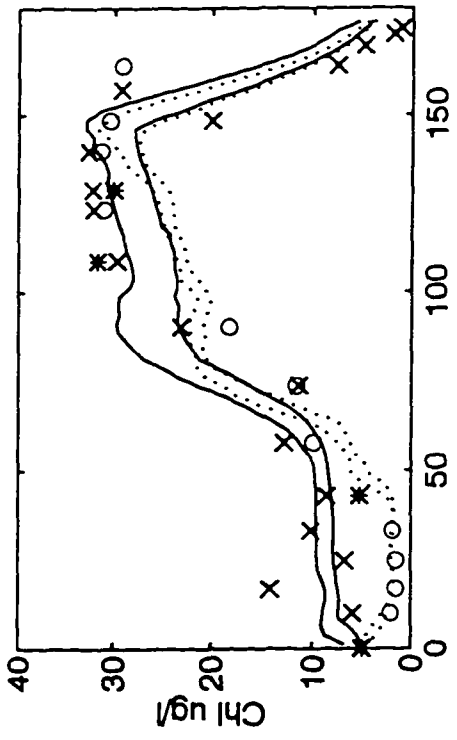
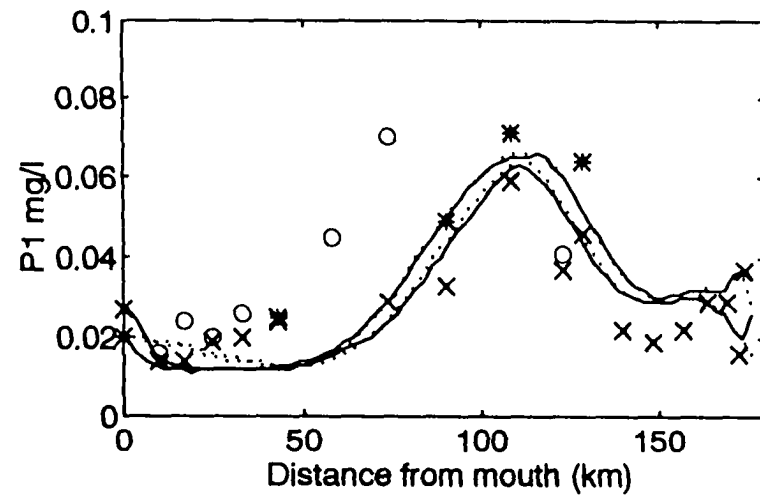
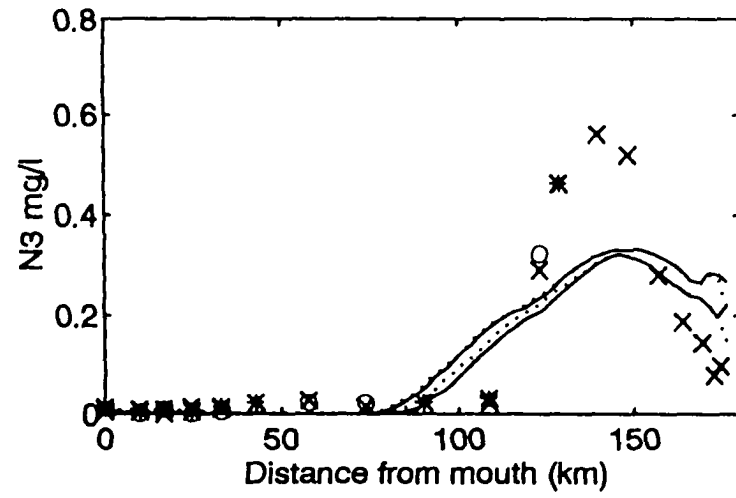
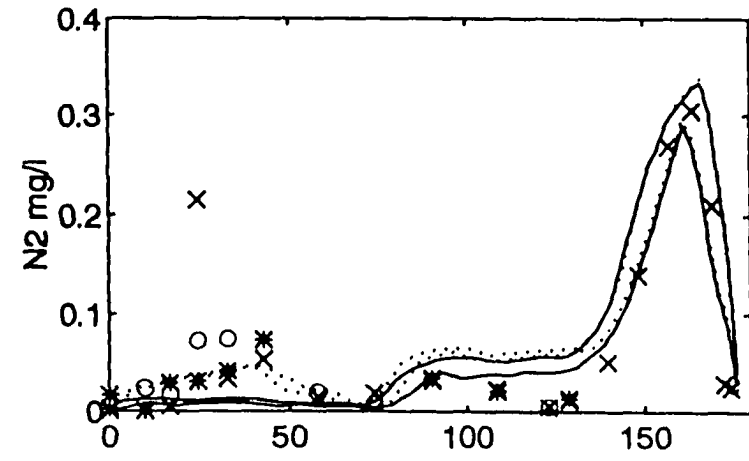
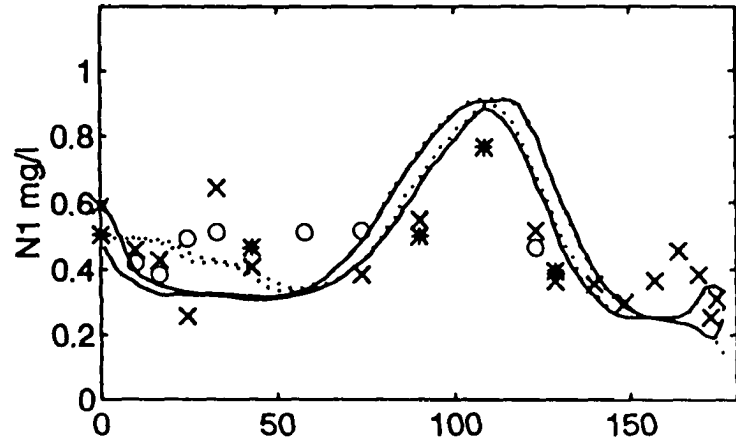


Figure 5-4 The inverse model (IMC-1) verification results on 8/7/90 (daily maximum and minimum at the surface and bottom, refer to Fig. 5-1 for line and symbol description).



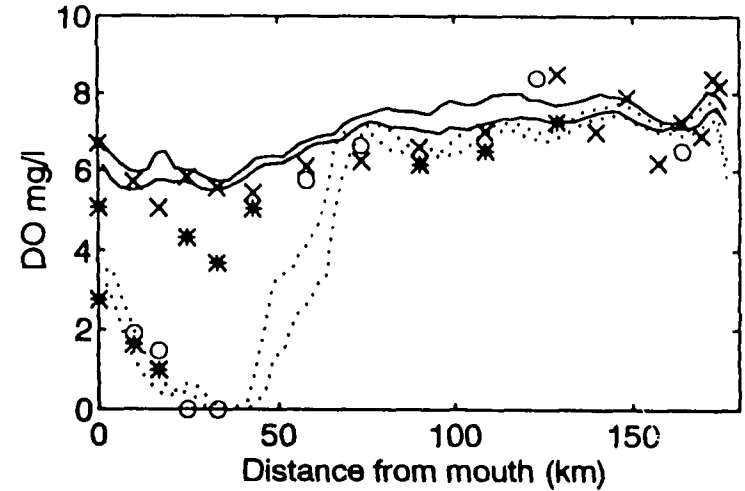
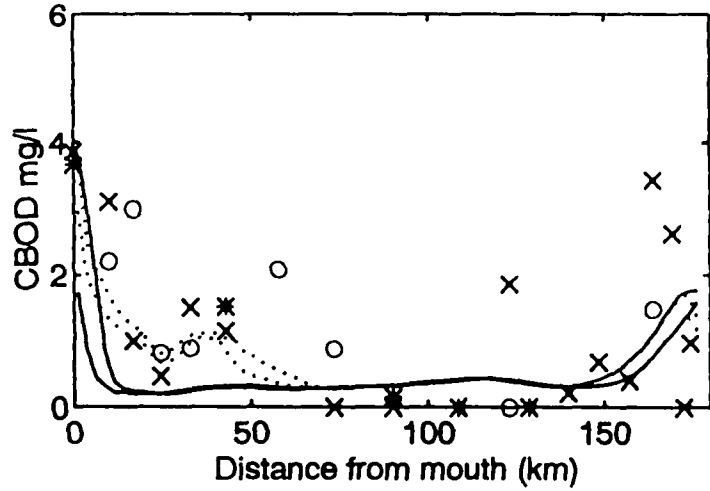
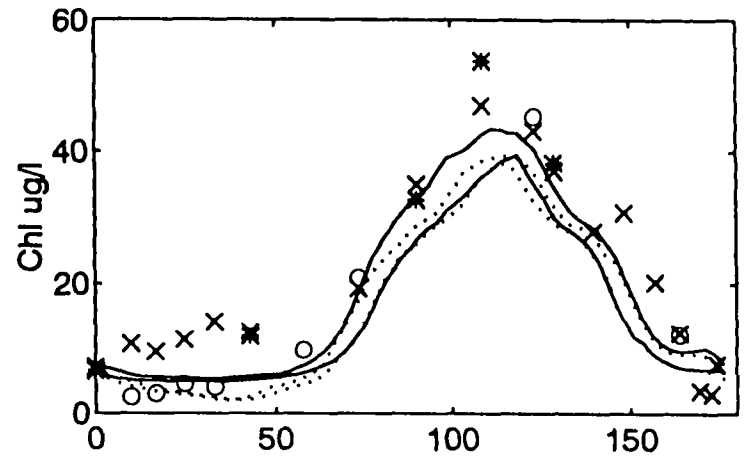
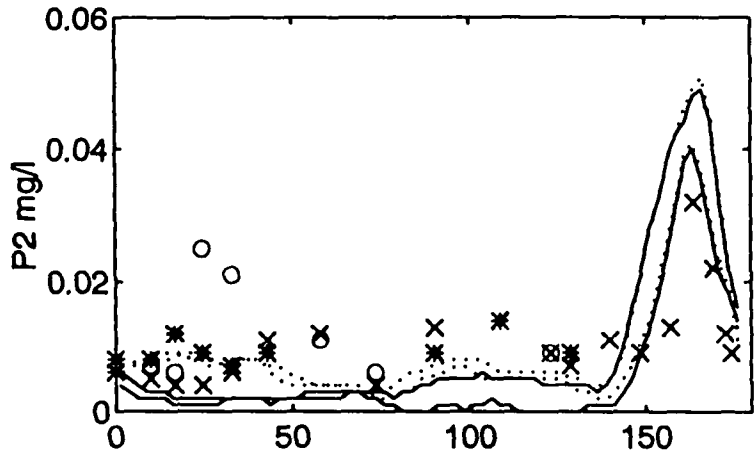
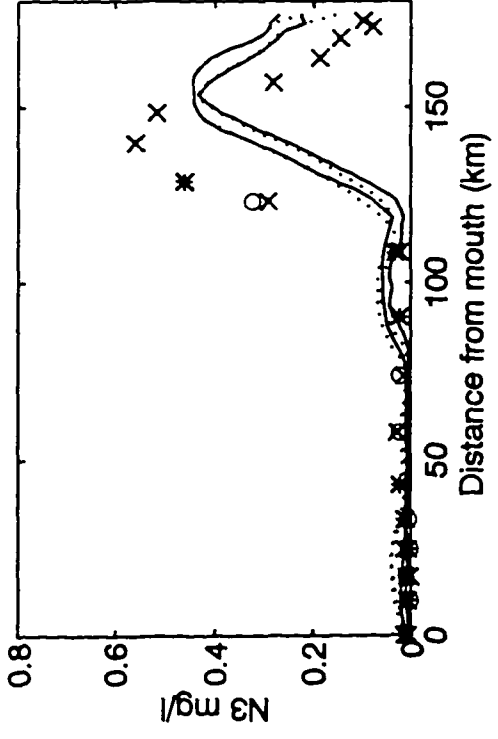
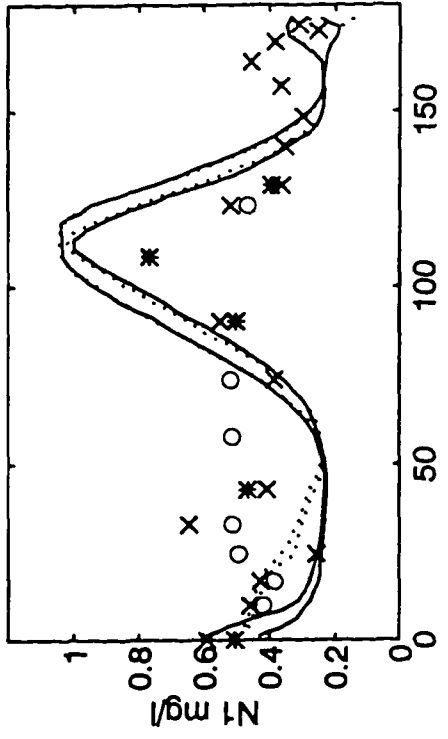
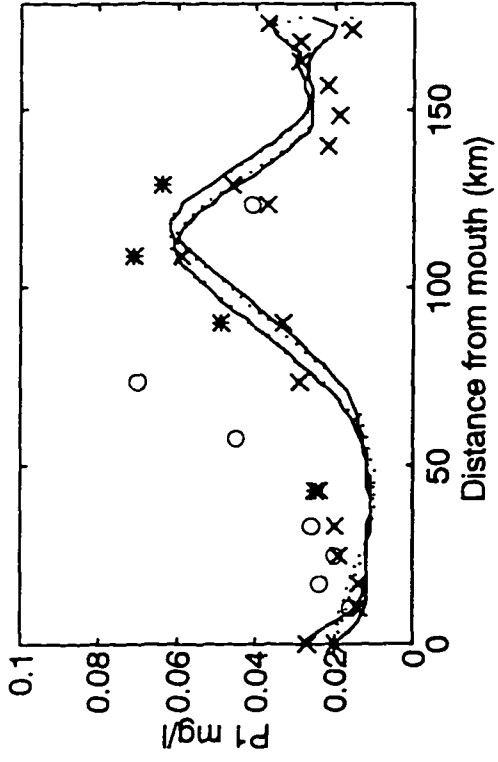
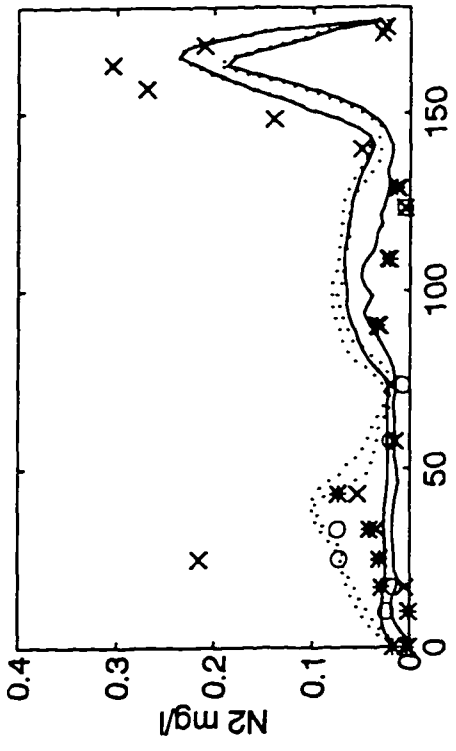


Figure 5-5 The original model (OMC) verification results on 8/7/90 (daily maximum and minimum at the surface and bottom, refer to Fig. 5-1 for line and symbol description).



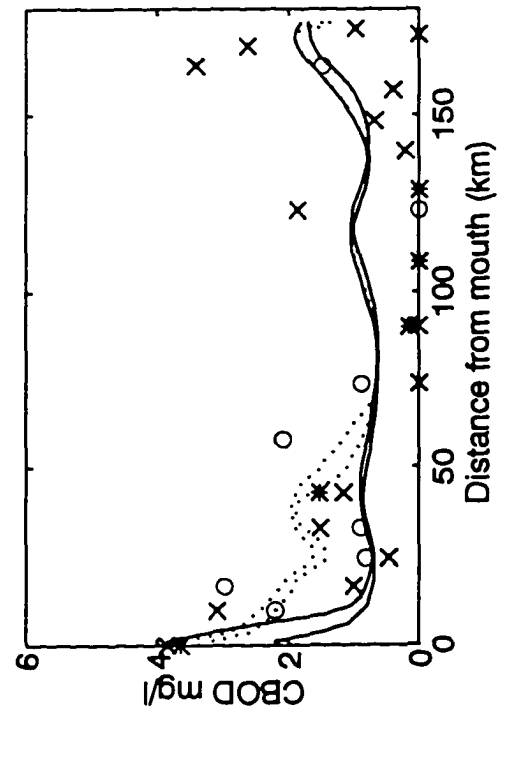
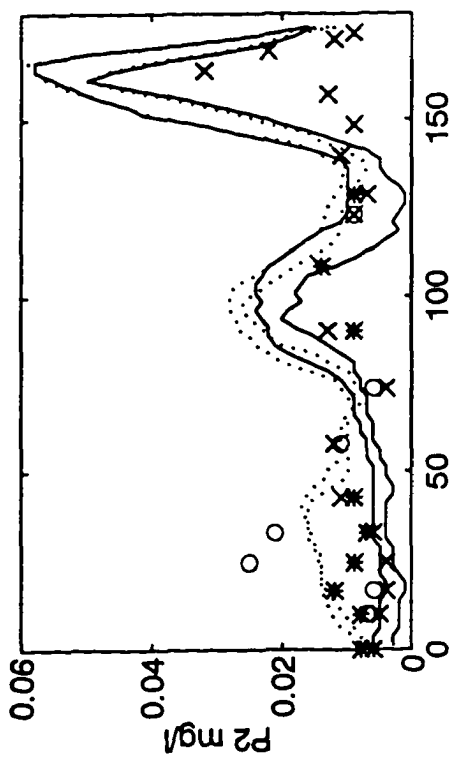
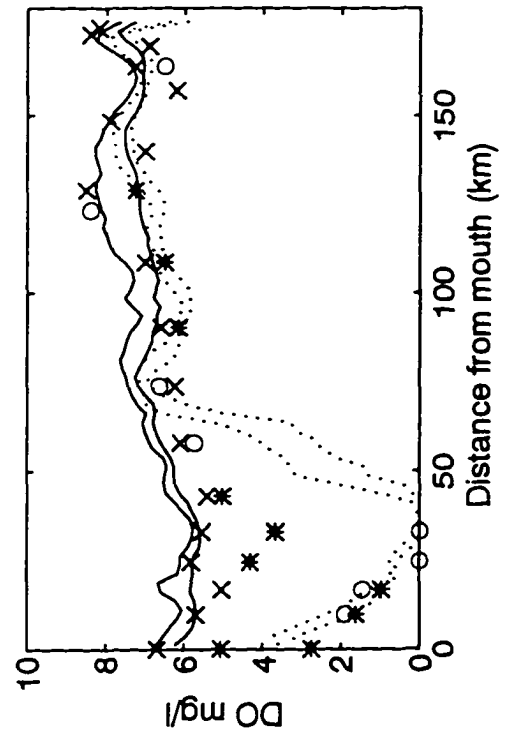
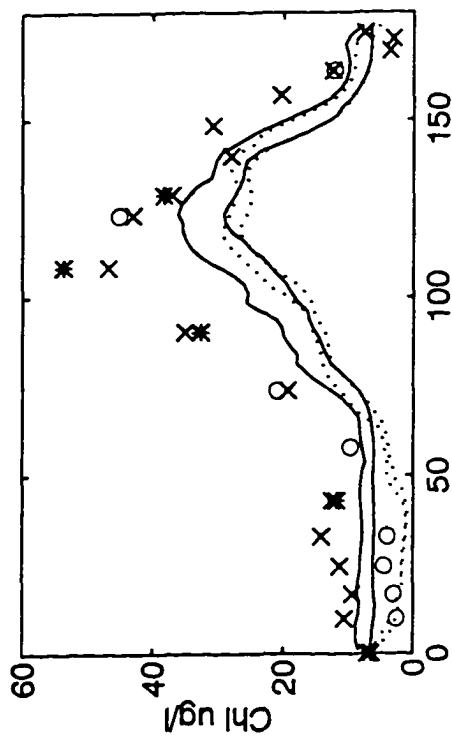
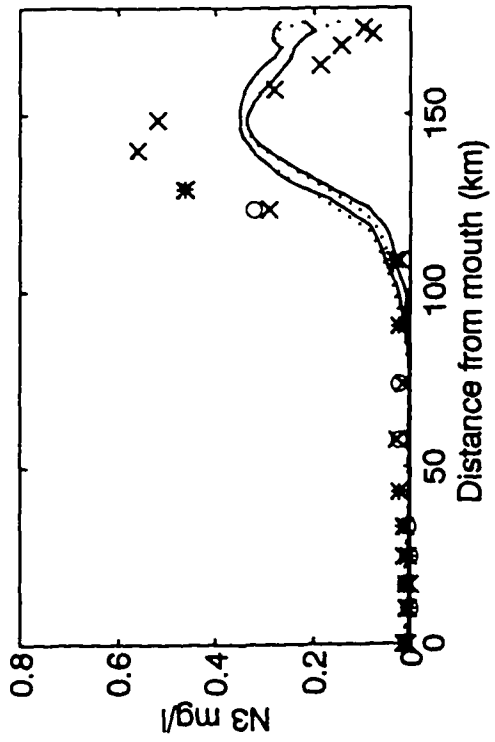
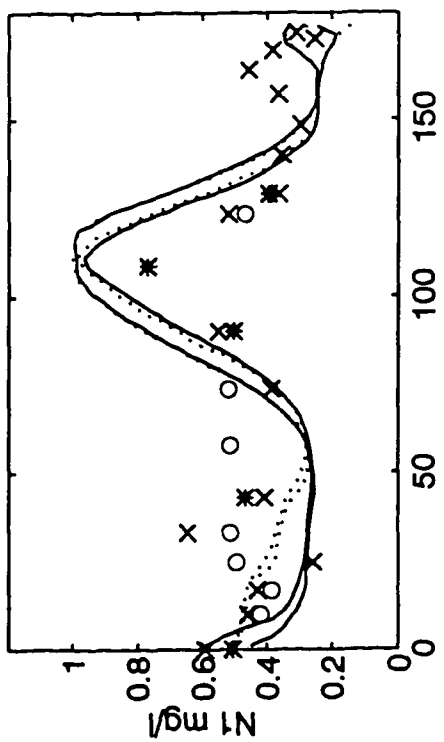
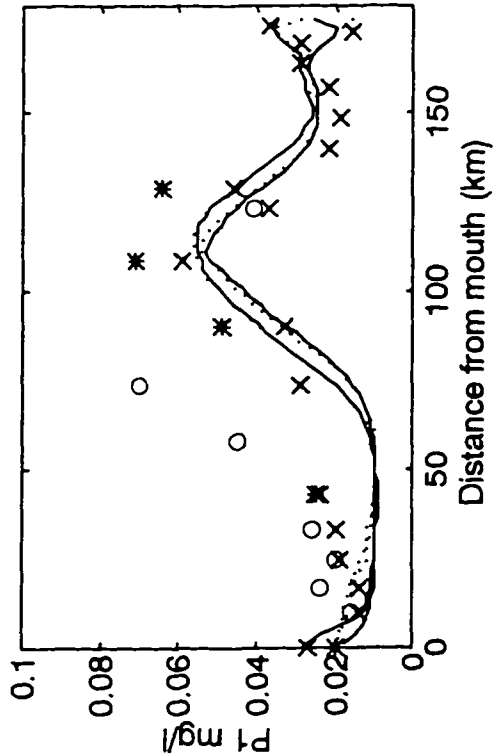
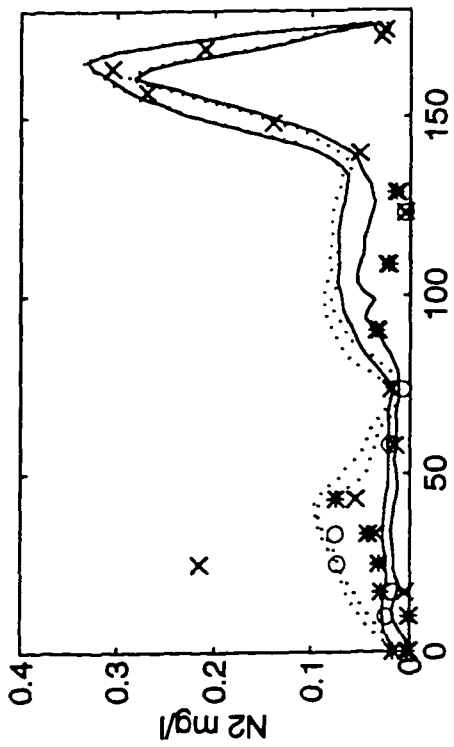
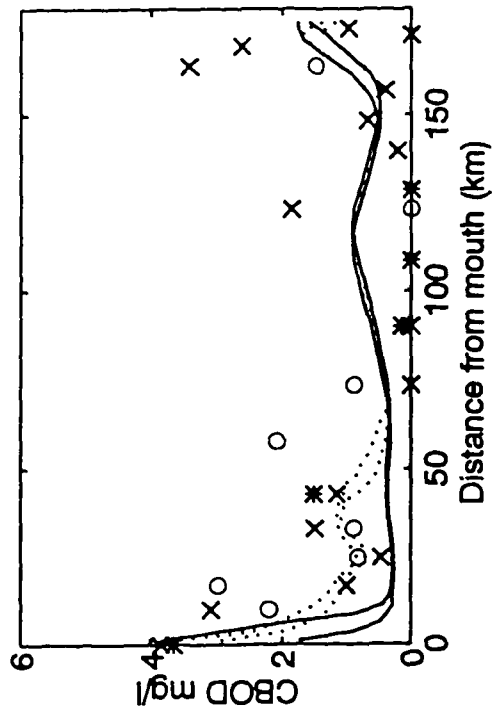
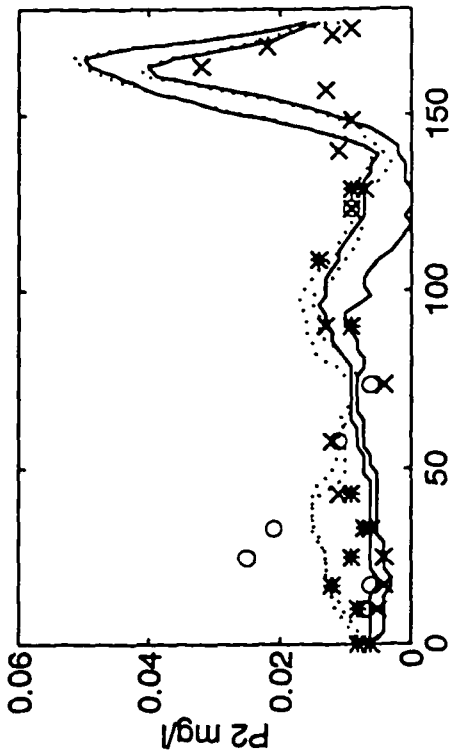
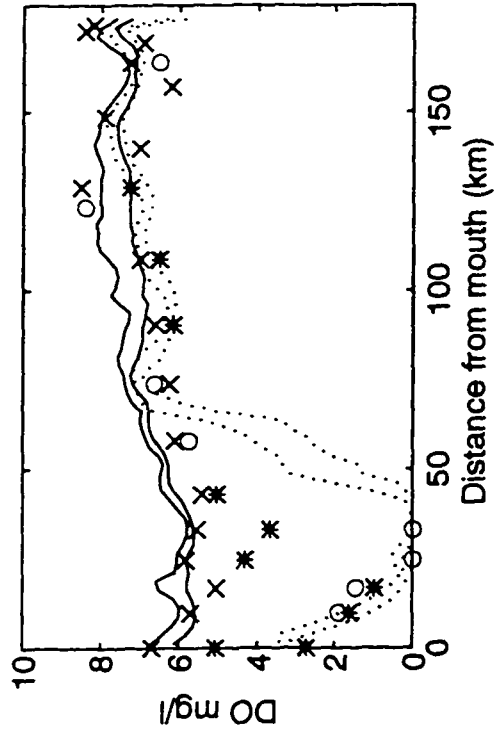
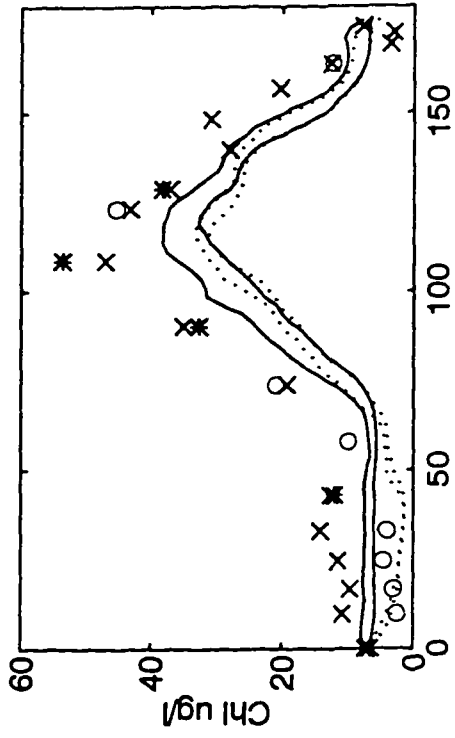


Figure 5-6 The inverse model (IMC-2) verification results on 8/7/90 (daily maximum and minimum at the surface and bottom, refer to Fig. 5-1 for line and symbol description).





VI. SUMMARY, CONCLUSIONS, AND RECOMMENDATIONS

6.1 Summary

An inverse mathematical estuarine eutrophication model with eight state variables has been developed. The model provides a framework to estimate unknown parameter values of the eutrophication model by assimilation of the concentration data of those state variables. The inverse model developed is a laterally integrated, two-dimensional, real-time model that consists of a hydrodynamic model, an eutrophication model (forward model) and an adjoint model (backward model). The hydrodynamic model simulates tide, current, salinity, and dispersion to supply the dynamic fields for the transport portion of both the eutrophication model and the adjoint model. The eutrophication model simulates eight water quality state variables which are phytoplankton, organic nitrogen, ammonium nitrogen, nitrite-nitrate nitrogen, organic phosphorus, inorganic (ortho) phosphorus, carbonaceous biochemical oxygen demand and dissolved oxygen. The adjoint model is used during the processes of the parameter estimation (model calibration) to provide intermediate results to calculate the gradients of the cost function, data misfit, with respect to the parameters to be estimated. The process of parameter estimation is an iteration process. The parameter values are improved during each iteration until the total data misfit is small. The inverse model is

solved by using a two time level, finite difference scheme. To increase the computation efficiency and reduce the computer storage space, a decoupling scheme is implemented in the model, in which the kinetic processes are decoupled from the physical transport processes for the purpose of numerical computation. An efficient preconditioning technique is introduced in the inverse model to speed up the convergence rate of the inverse model. Several numerical experiments with hypothetical data sets were conducted to study the identifiability of the kinetic parameters and data requirement for the model calibration. The inverse model was applied to aid calibration of the eutrophication model of the tidal Rappahannock River, Virginia.

6.1.1 The inverse model formulation

In this study, the variational technique is used to develop the inverse model. The basic idea of the inverse modeling is that the model parameter values are varied until a cost function, which measures the data misfit between the model results and observation data, is minimized while the model dynamics and kinetics are treated as strong constraints. The best fit is determined by a system of equations consisting of the eutrophication model equations and their corresponding adjoint model equations forced by the model data misfit. The adjoint equations provide the intermediate results to calculate gradients of the cost function with respect to the parameters those values are to be determined. These gradients are used with the conjugate gradient algorithm to search out the optimal estimations of the model parameter values. An outline procedure of the parameter estimation is given in section 2.4.1.

The detailed mathematical derivation of the inverse model is presented in chapter 2, section 2.1 to section 2.3. The main effort is to derive the adjoint model that is given in Eq. 2-14. In this study, only thirteen parameters were selected to be estimated so that only the gradients of the cost function with respect to these parameters are given (Eq. 2-17 - 2-29). However, it is easy to extend the method to estimate more parameters following the general derivation given in section 2.3. Because the conservative control volume scheme is used to solve the eutrophication model equations, the computation scheme of the adjoint model will be different from the forward model equations if it is derived from the continuity form of the adjoint model equations. The scheme used to solve the adjoint model equations is derived directly from the finite difference equations of the forward model and given in section 2.4.3 and Appendix C.

Since the time step used for calculating physical transport processes is on the order of a few minutes, the kinetic processes should be updated on the same time interval if they are solved simultaneously. Concentrations of all the state variables need to be stored for each time step at every cell because these values are required when integrating the adjoint model backward. For a long period model simulation, both computation speed for calculation and computer storage space should be considered. In the present model, the kinetic processes (or data misfit) are decoupled from the physical transport processes when integrating both the forward model and the adjoint model for the purpose of numerical computation. This permits the use of larger time step for computation of kinetic processes than that for the physical transport. The decoupling scheme used in the inverse model is presented in section 2.4.4 and an

example of test results is shown in Fig. 2-4. The decoupling treatment makes it possible to use the inverse model to calibrate the eutrophication model when long period model simulation is required.

The convergence of the inverse model is dependent on the condition of the Hessian matrix, the second derivative of the cost function with respect to the parameters. Convergence properties of the minimization are determined by the eigenvalue spectrum of the Hessian matrix and speed of convergence is related to the Hessian condition number, the ratio between its maximum and minimum eigenvalues. If the Hessian matrix is ill-conditioned, calculated descent direction is almost quasi-orthogonal to the optimal direction resulting in slow convergence or no convergence. In this study, the parameter transformation method is used to construct a preconditioner to relax the ill-conditioning of the Hessian. Because the true Hessian is hard to be estimated accurately, the empirical preconditioner is used. The theory and the method used in this study are discussed in section 2.6. A comparison of the convergence speed with different methods is presented in section 3.1.2.

6.1.2 The inverse model experiments

Several numerical inverse model experiments were conducted to study the parameter identifiability. Thirteen parameters were selected to be estimated in the present inverse model studies. They are phytoplankton optimum growth rate (K_{gr}) at 20 °C, respiration rate (R_{20}) at 20 °C, mortality rate (P_{20}) at 20 °C, ammonification rate (K_{n12}) of N1 to N2, nitrification rate (K_{n23}) of N2 to N3, denitrification rate (K_{n33}) at 20 °C, organic phosphorus mineralization rate (K_{p12}) at 20 °C, settling rate (K_{chl}) of

phytoplankton, settling rate (K_{n11}) of N1, settling rate (K_{p11}) of P1, settling rate (K_{p22}) of P2, first-order decay rate (K_c) of CBOD at 20 °C, and settling rate (K_{bod}) of CBOD. These parameters are assumed to be spatially and temporally invariant for the present study. In order to conduct the experiments to simulate better real environment, the geometry of the tidal Rappahannock River is used for the model experiments. The field measurements in the summer of 1990 were used as the model boundary conditions and the initial conditions as well as point sources and non-point source loads. The results of the model experiments with constant boundary conditions and time-varying boundary conditions are presented in section 3.1 and 3.2, respectively.

The experiments were designed to verify the convergence of the inverse model under different conditions. The conditions investigated by the model experiments are:

- (1) Convergence with different initial guess parameter values, Run C1 versus Run C2 and Run T1 versus Run T2;
- (2) Convergence under constant and time-varying boundary conditions, Run C1 versus Run T1;
- (3) Convergence for different environmental conditions, Run C1 versus Run C3;
- (4) Data requirement for the convergence, Run C1 versus Run C6;
- (5) Convergence with noisy data under different boundary conditions, Run 4 versus Run T2; and
- (6) Convergence with data sets of different errors, Run C4 versus Run C5.

The sample prototype data required for the inverse model experiments were generated by running the forward model with the "true" parameter values, which are the parameter values obtained from Park and Kuo's model calibration (1993b), except

that a constant settling velocity K_{p22} of 20 cm day^{-1} was used instead of using spatially varying parameter values. At particular times, based on the different model experiments, the forward model outputs were saved as "field" data sets. Each data set included concentrations of eight state variables at each cell vertically at seven locations along the estuary.

6.1.3 Inverse model application

The inverse model developed in this study was applied to calibrate the eutrophication model of the tidal Rappahannock River, Virginia. The field data collected on July 5, 1990 were used for the model calibration. The detailed procedures for the model calibration, including estimation of weights and selection of initial parameter values, are discussed in section 5.1. The calibration results with the inverse model are compared with the results obtained from conventional procedure. The model was further verified by the field data collected on August 7, 1990. The results of verification are presented in section 5.2.

6.2 Conclusions

The numerical experiments conducted in this study demonstrate the feasibility of using the inverse model to estimate unknown parameter values for an estuarine eutrophication model. The results of the experiments show that the parameter values can be accurately estimated for short period and long period model simulations under both constant and time-varying boundary conditions with hypothetical data sets. The

inverse model is convergent with different initial guess parameter values and under different environmental conditions. The results of long period experiments with limited data sets show that the inverse model is feasible in aiding real model calibration.

The inverse model was successfully applied to calibrate the eutrophication model of the tidal Rappahannock River. With the use of the inverse model, the results of model prediction are improved compared with the results obtained from conventional calibration. The results of the model calibration and verification show that the agreement between the model predictions and observations are very satisfactory. With the use of the inverse model, the eutrophication model can be calibrated more efficiently and systematically.

The studies also show that the inverse model is not only useful in aiding model calibration but also useful in addressing the important questions of whether the estimated parameter values are unique, and whether the sample data are sufficient to calibrate a model. Therefore, the inverse model may also serve as a tool in helping design a field program to collect data for model calibration.

The accuracy of parameter estimation is dependant on the quantity and quality of the field data. The experiments with noisy data show that the errors in estimated parameter increase when the random errors in the data sets increase. Caution must be exercised when using data with random errors and sampling errors to calibrate a model. The unique results cannot be guaranteed for those parameters to which the model is not sensitive. However, the model can provide satisfactory predictions of the state variables. For those insensitive parameters, the error in some estimated parameters can be very large even though the model predictions match the field data

graphically.

The uniqueness of parameter estimation is related to parameter identifiability. For a system with parameters highly correlated with one another, the unique solution of the parameter cannot always be obtained while the model predictions are very satisfactory in a sense of minimum data misfit because the concentrations of the state variables are dependent on the combined net results of several parameters rather than on the individual parameter. The feasibility of parameter estimation not only depends on how many data sets are available but also on how sensitive the system is to a particular parameter. The sensitivity is related to the error criterion given in the model. For a given error criterion, the solution may not be unique for those parameters to which the model is not sensitive within the given error criterion.

The convergence speed of the inverse model is very critical for long period modeling. The rate of convergence depends on the condition of the Hessian and varies with different initial guess parameter values and different environmental conditions. Two major factors that degrade the speed of convergence are cross correlation and multiple scales among the parameter system. Multiple scales pose a difficult problem. If unsuitable scales are used to scale the parameters, some parameters may be over-corrected and some under corrected during each iteration. The over-correction, or under-correction, often requires more iterations to correct them. For the present eutrophication system, the inverse model is not convergent without proper preconditioning. The experiments show that a proper preconditioner can speed up convergence very significantly. Since it is difficult to estimate the Hessian accurately, some judgements are needed in selecting scales and possibly some experiments are

required to construct a proper preconditioner.

6.3 Recommendations

During this study, the following limitations have been noted. These need to be further investigated and to be improved for the inverse eutrophication modeling.

(1) One of the critical problems in the inverse modeling is the uniqueness of the parameter values. The uniqueness problem is related to the problem of parameter identifiability. For a system with parameters highly correlated with one another, large error in the estimated parameters can occur when using data with large random errors, such as sampling errors, model structure errors, and random variability of the real system. Because convergence of the inverse model is measured by the best fit, which depends on the given cost function and available field data, incorporating error information of the field data into the cost function and increasing the amount of field data can improve the result. However, what kind of cost function should be used and how much data are required to ensure that the errors in the estimated parameters are in the acceptable range is still an issue. It requires further study both theoretically and experimentally.

(2) The model calibration conducted in this study assumes that the benthic fluxes of the nutrients and other parameters are certain. The parameter values may differ from that obtained from this calibration if model calibration is conducted with different boundary conditions. The results of the inverse model calibration can be improved if the benthic fluxes can be treated as the parameters and estimated during calibration.

(3) At this study, only the identifiability of limited constant parameter is concerned. The inverse model can be applied to estimate more parameters and even to estimate spatially varying parameters (distributed parameters) if enough data are available. However, the data requirement should be considered when using the inverse model to estimate distributed parameters because the system can easily become under-determined for limited data sets. For an undetermined problem, the parameters are not identifiable individually. Grouping distributed parameters by spatial domain and estimating parameters with respect to each group seems to be a good approach. However, grouping distributed parameters is not a simple task because there is no knowledge of the distribution of the parameters. For practical application, possibly some experiments are required to group the parameters for different environments.

(4) One difficulty of using the adjoint model is the speed of convergence. The speed of convergence is very critical when long period simulation is required. The present study shows that degradation of the speed of convergence occurs during the inverse model experiments because multiple scales are involved in the eutrophication system. The experiments show that a proper preconditioner will speed up the convergence dramatically. However, it is very difficult to construct a optimal preconditioner without knowing the Hessian matrix. To increase the rate of the convergence, an efficient technique to estimate the Hessian matrix is required.

APPENDIX A. SOURCE AND SINK FUNCTIONS

The model formulation of source and sink functions S_i (Eq. 2-1) are listed as follows:

A. Phytoplankton (Chl)

$$S_1 = (G - R - P)Chl + K_{Chl} \frac{\partial Chl}{\partial z} + \frac{WChl}{V} \quad (A-1)$$

where

$$G = K_{gr} \theta_1^{T-20} I_L(I_u, I_s, k_e, Chl, \Delta z) \cdot N(N2, N3, P2) ;$$

$$N = \min\{L_{N23}, L_{P2}\}, \quad L_{N23} = \frac{N2 + N3}{K_{mn} + N2 + N3}, \quad L_{P2} = \frac{P2}{K_{mp} + P2} ;$$

$$I_L = \frac{2.718}{K_e \Delta z} (e^{\alpha_s} - e^{\alpha_T}), \quad \alpha_B = -\frac{I_t}{I_s} e^{-K_s(H_t + \Delta z)}, \quad \alpha_T = -\frac{I_t}{I_s} e^{-K_s H_t} ;$$

$$I_t = I_a \left(\frac{24}{t_d - t_u} \right) \frac{\pi}{2} \sin \left(\pi \frac{t - t_u}{t_d - t_u} \right) \quad \text{if } t_u < t < t_d$$

$$I_t = 0 \quad \text{if } t \leq t_u \text{ or } t \geq t_d ;$$

$$K_e = k_e + K_{eChl} Chl, \quad R = R_{20} \theta_2^{T-20}, \quad P = P_{20} \theta_3^{T-20} ;$$

G & R = growth and respiration rate of phytoplankton (day^{-1}), respectively;

P = mortality rate due to predation and other factors (day^{-1});

K_{Chl} = settling rate of phytoplankton (cm day^{-1});

Δz & V = layer thickness (cm) and layer volume (liter), respectively;

$WChl$ = external loading of Chl ($\mu\text{g day}^{-1}$) including nonpoint source;

K_{gr} = optimum growth rate at 20°C (day^{-1});

θ_1 = constant for temperature adjustment of growth rate;

T = temperature ($^\circ\text{C}$);

I_L = attenuation of growth due to suboptimal lighting;

N = attenuation of growth due to nutrient limitation;

- H_s = depth from the free surface to the top of the layer (cm);
 K_e = light extinction coefficient (cm^{-1}) corrected for self-shading of phytoplankton;
 k_e = light extinction coefficient (cm^{-1}) at zero chlorophyll concentration;
 K_{eChl} = light extinction due to self-shading of phytoplankton (cm^{-1} per $\mu\text{g l}^{-1}$);
 I_s = optimum solar radiation rate (langley day $^{-1}$);
 I_t = solar radiation at time t (langley day $^{-1}$);
 I_a = total daily solar radiation (langley day $^{-1}$);
t = time of day (in hours);
 t_u & t_d = times (in hour) of sunrise and sunset, respectively;
 K_{mn} & K_{mp} = half-saturation concentrations (mg l^{-1}) for uptake of inorganic nitrogen and inorganic phosphorus, respectively;
 R_{20} & P_{20} = respiration and mortality rate at 20 °C (day $^{-1}$), respectively;
 θ_2 = constant for temperature adjustment of respiration rate; and,
 θ_3 = constant for temperature adjustment of mortality rate.

B. Organic Nitrogen (N1)

$$S_2 = -\frac{K_{n12}NI}{K_{h12}+NI} + a_n(R+a_rP)F_nChl + K_{n11}\frac{\partial NI}{\partial z} + BenNI\frac{1}{B}\frac{\partial B}{\partial z} + \frac{WN1}{V} \quad (\text{A-2})$$

where

$$K_{n12} = K_{n12}(20)\theta_4^{T-20};$$

- K_{n12} = ammonification rate of N1 to N2 (mg l^{-1} day $^{-1}$);
 $K_{n12}(20)$ = ammonification rate of N1 to N2 at 20 °C;
 θ_4 = constant for temperature adjustment of ammonification rate;
 K_{h12} = half-saturation concentration for ammonification (mg l^{-1});
 a_n = ratio of nitrogen to chlorophyll in phytoplankton ($\text{mg N per } \mu\text{g Chl}$);
 a_r = fraction of consumed phytoplankton recycled by zooplankton;
 K_{n11} = settling rate of N1 (cm day^{-1});
 F_n = fraction of metabolically produced nitrogen recycled to the organic pool;
 $BenNI$ = benthic flux of N1 (g m^{-2} day $^{-1}$); and
 $WN1$ = external loading of N1 (mg day^{-1}) including point and nonpoint source.

C. Ammonium Nitrogen (N2)

$$S_3 = -\frac{K_{n23}N2}{K_{h23}+N2}\frac{DO}{K_{nit}+DO} + \frac{K_{n12}NI}{K_{h12}+NI} + a_n(R+a_rP)(1-F_n)Chl - a_nG\cdot PR\cdot Chl + \frac{BenN2}{B}\frac{\partial B}{\partial z} + \frac{WN2}{V} \quad (\text{A-3})$$

where

$$PR = \frac{N2 \cdot N3}{(K_{mn} + N2)(K_{mn} + N3)} + \frac{N2 \cdot K_{mn}}{(N2 + N3)(K_{mn} + N3)} ;$$

$$K_{n23} = K_{n23}(20) \theta_5^{T-20} ;$$

- K_{n23} = nitrification rate of N2 to N3 ($\text{mg l}^{-1} \text{ day}^{-1}$);
 $K_{n23}(20)$ = nitrification rate at 20 °C;
 θ_5 = constant for temperature adjustment of nitrification rate;
 K_{h23} = half-saturation concentration for nitrification (mg l^{-1});
 K_{nit} = half-saturation concentration for oxygen limitation of nitrification (mg l^{-1});
 PR = preference of phytoplankton for N2 uptake;
 BenN2 = benthic flux of N2 ($\text{g m}^{-2} \text{ day}^{-1}$); and
 WN2 = external loading of N2 (mg day^{-1}) including point and nonpoint sources.

D. Nitrite-Nitrate Nitrogen (N23)

$$S_4 = \frac{K_{n23} N2}{K_{h23} + n2} \frac{DO}{K_{nit} + DO} - a_n G(1 - PR) Chl - K_{n33} \frac{K_{h33} N3}{K_{h33} + DO} + \frac{BenN3}{B} \frac{\partial B}{\partial z} + \frac{WN3}{V} \quad (\text{A-4})$$

where

$$K_{n33} = K_{n33}(20) \theta_6^{T-20} ;$$

- K_{n33} = denitrification rate (day^{-1});
 $K_{n33}(20)$ = denitrification rate at 20 °C;
 θ_6 = constant for temperature adjustment of denitrification rate;
 K_{h33} = half-saturation concentration for denitrification (mg l^{-1});
 BenN3 = benthic flux of N3 ($\text{g m}^{-2} \text{ day}^{-1}$); and
 WN3 = external loading of N3 (mg day^{-1}) including point source and nonpoint sources.

E. Organic Phosphorus (P1)

$$S_5 = -\frac{K_{p12} P1}{K_{hp12} + P1} + a_p (R + a_r P) F_p Chl + K_{p11} \frac{\partial P1}{\partial z} + \frac{BenP1}{B} \frac{\partial B}{\partial z} + \frac{WP1}{V} \quad (\text{A-5})$$

where

$$K_{p12} = K_{p12}(20) \theta_7^{T-20} ;$$

- K_{p12} = mineralization rate of P1 to P2 ($\text{mg l}^{-1} \text{ day}^{-1}$);
 $K_{p12}(20)$ = mineralization rate at 20 °C;
 θ_7 = constant for temperature adjustment of mineralization rate;

- K_{hp12} = half-saturation concentration for mineralization (mg l⁻¹);
 a_p = ratio of phosphorus to chlorophyll in phytoplankton (mg P per µg Chl);
 K_{p11} = settling rate of P1 (cm day⁻¹);
 F_p = fraction of metabolically produced phosphorus recycled to the organic pool;
 BenP1 = benthic flux of P1 (g m⁻² day⁻¹); and
 WP1 = external loading of P1 (mg day⁻¹) including point and nonpoint sources.

F. Inorganic (or ortho) Phosphorus (P2)

$$S_6 = \frac{K_{p12} P1}{K_{hp12} + P1} + a_p (R + a_r P) (1 - F_p) Chl - a_p G \cdot Chl +$$

$$K_{p22} \frac{\partial P2}{\partial z} + \frac{BenP2}{B} \frac{\partial B}{\partial z} + \frac{Wp2}{V} \quad (A-6)$$

where

- P2 = concentration of inorganic phosphorus (mg l⁻¹);
 K_{p22} = settling rate of P2 (cm day⁻¹);
 BenP2 = benthic flux of P2 (g m⁻² day⁻¹); and
 WP2 = external loading of P2 (mg day⁻¹) including point and nonpoint sources.

G. Carbonaceous Biochemical Oxygen Demand (CBOD)

$$S_7 = -K_c CBOD + a_c a_{co} (a_r P) Chl + K_{BOD} \frac{\partial (CBOD)}{\partial z} + \frac{SOD}{B} \frac{K_{DO}}{K_{DO} + DO} \frac{\partial B}{\partial z} + \frac{WBOD}{V} \quad (A-7)$$

where

$$K_c = K_c(20) \theta_8^{T-20} ;$$

- K_c = first-order decay rate of CBOD (day⁻¹);
 $K_c(20)$ = CBOD decay rate at 20 °C;
 θ_8 = constant for temperature adjustment of CBOD decay rate;
 a_c = ratio of carbon to chlorophyll in phytoplankton (mg C per µg Chl);
 a_{co} = ratio of oxygen demand to organic carbon recycled = 2.67;
 K_{BOD} = settling rate of CBOD (cm day⁻¹);
 SOD = sediment oxygen demand (g m⁻² day⁻¹);
 K_{DO} = half-saturation concentration for benthic flux of CBOD; and
 WBOD = external loading of CBOD (mg day⁻¹) including point and nonpoint sources.

H. Dissolved Oxygen (DO)

$$S_8 = -K_c C B G D - a_{no} \frac{K_{n23} N_2}{K_{h23} + N_2} \frac{DO}{K_{nit} + DO} + a_c a_{co} \left(PQ \cdot G - \frac{R}{RQ} \right) Chl$$

$$+ (1 - \gamma_1) K_r (DO_s - DO) - \frac{SOD}{B} \frac{DO}{K_{DO} + DO} \frac{\partial B}{\partial z} + \frac{WDO}{V} \quad (A-8)$$

where

$$K_r = K_r(20) \theta_9^{T-20}, \quad K_r(20) = \left(K_{ro} \sqrt{\frac{u_{eq}}{h_{eq}} + W_{rea}} \right) \frac{1}{\Delta z};$$

$$W_{rea} = 72.8 U_w^{1/2} - 31.7 U_w + 3.72 U_w^2;$$

$$DO_s = 0.146244 \cdot 10^2 - 0.36713 T + 0.4497 \cdot 10^{-2} T^2 - (0.966 \cdot 10^{-1} - 0.205 \cdot 10^{-2} T - 0.2739 \cdot 10^{-3} S) S;$$

- a_{no} = ratio of oxygen consumed per unit of ammonium nitrogen nitrified = 4.57;
 PQ = photosynthesis quotient (moles O_2 per mole C);
 RQ = respiration quotient (moles CO_2 per mole O_2);
 K_r = reaeration rate (day^{-1});
 $K_r(20)$ = reaeration rate at 20 °C;
 DO_s = saturated DO concentration ($mg\ l^{-1}$);
 WDO = external loading of OD ($mg\ day^{-1}$) including point and nonpoint sources;
 K_{ro} = proportionality constant = 393.3 in CGS unit;
 u_{eq} = weighted velocity over cross-section = $\sum (u_k B_k h_k) / \sum (B_k h_k)$;
 h_{eq} = weighted depth over cross-section = $\sum (B_k h_k) / B_\eta$;
 B_η = width at the free surface;
 W_{rea} = wind-induced reaeration ($cm\ day^{-1}$);
 U_w = wind speed (in $m\ sec^{-1}$) at the height of 10 m above surface;
 θ_9 = constant for temperature adjustment of reaeration rate; and
 γ_1 = 0 for $k=1$ (at top layer) 1 for $2 \leq k \leq N$, and N is the number of layers at each segment.

APPENDIX B. SCALED SOURCE AND SINK FUNCTIONS

The scaled source and sink functions of Eq. 2-2 are as follows:

$$S_1' = (G-R-P)Chl' + K_{chl} \frac{\partial Chl'}{\partial z} + \frac{WChl'}{V} \quad (B-1)$$

$$S_2' = -\frac{K_{n12}NI'}{K_{h12}+NI'} + \gamma_{CN1}a_n(R+a_rP)F_nChl' + K_{n11} \frac{\partial NI'}{\partial z} + \frac{BenNI'}{B} \frac{\partial B}{\partial z} + \frac{WNI'}{V} \quad (B-2)$$

$$S_3' = -\frac{K_{n23}N2'}{K_{h23}+N2} \frac{DO}{K_{nit}+DO} + \gamma_{N12} \frac{K_{n12}NI'}{K_{h12}+NI'} + \gamma_{CN2}a_n(R+a_rP)(1-F_n)Chl' - \gamma_{CN2}a_n G \cdot PR \cdot Chl' + \frac{BenN2'}{B} \frac{\partial B}{\partial z} + \frac{WN2'}{V} \quad (B-3)$$

$$S_4' = \gamma_{N23} \frac{K_{n23}N2'}{K_{h23}+N2} \frac{DO}{K_{nit}+DO} - \gamma_{CN3}a_n G(1-PR)Chl' - K_{n33} \frac{K_{h33}N3'}{K_{h33}+DO} + \frac{BenN3'}{B} \frac{\partial B}{\partial z} + \frac{WN3'}{V} \quad (B-4)$$

$$S_5' = -\frac{K_{p12}PI'}{K_{hp12}+PI'} + \gamma_{CP1}a_p(R+a_rP)F_pChl' + K_{p11} \frac{\partial PI'}{\partial z} + \frac{BenPI'}{B} \frac{\partial B}{\partial z} + \frac{WPI'}{V} \quad (B-5)$$

$$S_6' = \gamma_{p12} \frac{K_{p12}PI'}{K_{hp12}+PI'} + \gamma_{CP2}a_p(R+a_rP)(1-F_p)Chl' - \gamma_{CP2}a_p G \cdot Chl' + K_{p22} \frac{\partial P2'}{\partial z} + \frac{BenP2'}{B} \frac{\partial B}{\partial z} + \frac{Wp2'}{V} \quad (B-6)$$

$$\begin{aligned}
S_7' = & -K_c CBOD' + \gamma_{CBOD} a_c a_{cn} (a_r P) Chl' + K_{BOD} \frac{\partial(CBOD')}{\partial z} \\
& + \gamma_{CBDO}^{-1} \frac{SOD'}{B} \frac{K_{DO}}{K_{DO} + DO} \frac{\partial B}{\partial z} + \frac{WBOD'}{V}
\end{aligned} \tag{B-7}$$

$$\begin{aligned}
S_8' = & -\gamma_{CBDO} K_c CBOD' - \gamma_{N_2DO} a_{no} \frac{K_{n_2} N_2'}{K_{h_23} + N_2} \frac{DO}{K_{nit} + DO} \\
& + \gamma_{CDO} a_c a_{cn} \left(PQ \cdot G - \frac{R}{RQ} \right) Chl' + (1 - \gamma_1) K_r (DO_s' - DO') \\
& - \frac{SOD'}{B} \frac{DO}{K_{DO} + DO} \frac{\partial B}{\partial z} + \frac{WDO'}{V}
\end{aligned} \tag{B-8}$$

Note that all the terms of benthic fluxes and external loads are scaled by maxim values of their corresponding state variables.

APPENDIX C. FINITE DIFFERENCE EQUATIONS OF THE ADJOINT MODEL

In this appendix, the finite difference formulations of the adjoint model (Eq. 2-14) are given. The grid system is shown in Figure 2-2. Since the transport portion of the adjoint model (Eq. 2-14) are same for all the state variables, the superscript "j" for state variables will be omitted in the following derivations. The variables with superscript "1" indicate at new time level at "n+1" and the variables without superscript indicate at old time level "n". \sum is a summation of the terms over the spatial and temporal domains, i.e, summation for all the index n , i , and k , where n , i , and k are time level, cell and layer index, respectively. The finite difference scheme for the adjoint model is obtained by taking derivative of Eq. 2-31 with respect to $C_{i,k}$.

C-1. Finite Difference Scheme of The Adjoint Model

A. Inertial term

The finite difference form of the inertial term of Eq. 2-31 can be written as

$$\sum \lambda_{i,k}^n \frac{B_{i,k}(h_k + \theta_1 \eta_i^1) C_{i,k}^1 - B_{i,k}(h_k + \theta_1 \eta_i) C_{i,k}}{\Delta t} \quad (C-1)$$

Taking derivative of Eq. C-1 with respect to $C_{i,k}$ and summing all terms together, the corresponding adjoint form can be obtained as follows

$$\frac{B_{i,k}(h_k + \theta_1 \eta_i)(\lambda_{i,k}^{n-1} - \lambda_{i,k}^n)}{\Delta t} \quad (\text{C-2})$$

where $\theta_1 = 1$ for $k = 1$ (at top layer), and $\theta_1 = 0$ for the other layers. Notice that Eq. C-1 is the summation for all n , i , and k . There are several terms containing $C_{i,k}$. The result of finite difference scheme of the adjoint model is obtained by summing those terms together. The same fashion is applied in the following derivations.

B. Horizontal advection term

Using quick scheme, the finite difference form of the horizontal advection can be written as

$$\sum \lambda_{i,k}^n (HAdv_{i,k} C_{i,k}^* - HAdv_{i-1,k} C_{i-1,k}^*) \quad (\text{C-3})$$

where

$$HAdv_{i,k} = (B_{i,k} + B_{i+1,k}) \frac{(h_k + \theta_1 \eta_i) + (h_k + \theta_1 \eta_{i+1})}{\Delta x} u_{i+1,k+1} \quad (\text{C-3a})$$

$$C_i^* = \frac{1}{2}(C_i + C_{i+1}) - \frac{Cn_i}{2}(C_{i+1} - C_i) + \frac{1}{6}(Cn_i^2 - 1)CURV_i \quad (\text{C-3b})$$

Notice that

C_i^* is defined at the right side wall of the "i" cell and

$$Cn_i = \frac{\Delta t}{\Delta x} u_{i+1,k}$$

$$CURV_i = C_{i+1,k} - 2C_{i,k} + C_{i-1,k} \quad \text{for } u_{i+1} \geq 0$$

$$CURV_i = C_{i+2,k} - 2C_{i+1,k} + C_{i,k} \quad \text{for } u_{i+1} < 0$$

After substituting Eqs. C-3a and C-3b into Eq. C-3, Eq. C-3 can be written as follows

$$HAD_1 - HAD_2 + HAD_3 \quad (C-4a)$$

where

$$HAD_1 = \sum \frac{\lambda_{i,k}^n}{2} \left(HAdv_{i,k}(C_{i,k} + C_{i+1,k}) - HAdv_{i-1,k}(C_{i-1,k} + C_{i,k}) \right) \quad (C-4b)$$

$$HAD_2 = \sum \frac{\lambda_{i,k}^n}{2} \left(Cn_i HAdv_{i,k}(C_{i+1,k} - C_{i,k}) - Cn_{i-1} HAdv_{i-1,k}(C_{i,k} - C_{i-1,k}) \right) \quad (C-4c)$$

$$HAD_3 = \sum \frac{\lambda_{i,k}^n}{6} \left(HAdv_{i,k}(Cn_i^2 - 1)CURV_i - HAdv_{i-1,k}(Cn_{i-1}^2 - 1)CURV_{i-1} \right) \quad (C-4d)$$

The finite difference schemes of the adjoint model correspond to Eqs. C-4a to C-4d are as follows

$$AHAdv_{i,k} = AHAdv1_{i,k} - AHAdv2_{i,k} + AHAdv3_{i,k} \quad (C-5)$$

where

$$AHAdv1_{i,j} = -\frac{1}{2} \left((HAdv_{i,k}\lambda_{i+1,k}^n + HAdv_{i-1,k}\lambda_{i,k}^n) - (HAdv_{i,k}\lambda_{i,k}^n + HAdv_{i-1,k}\lambda_{i-1,k}^n) \right) \quad (C-5a)$$

$$AHAdv2_{i,k} = \frac{1}{2} \left(Cn_i HAdv_{i,k}(\lambda_{i+1,k}^n - \lambda_{i,k}^n) - Cn_{i-1} HAdv_{i-1,k}(\lambda_{i,k}^n - \lambda_{i-1,k}^n) \right) \quad (C-5b)$$

and

$$AHAdv3_{i,k} = \quad (C-5c)$$

$$\frac{1}{6} \left[-(Cn_{i-2}^2 - 1)HAdv_{i-2,k}\lambda_{i-1,k}^n\delta_{i,i-2} + (Cn_{i-1}^2 - 1)HAdv_{i-1,k}(\lambda_{i-1,k}^n - \lambda_{i,k}^n)\delta_{i,i-1} + \right.$$

$$(Cn_i^2 - 1)HAdv_{i,k}(\lambda_{i,k}^n - \lambda_{i+1,k}^n)\delta_{i,i} + (Cn_{i+1}^2 - 1)HAdv_{i+1,k}\lambda_{i+1,k}^n\delta_{i,i+1}]$$

where

$$\delta_{i,i-1} = \begin{cases} 1 & u_i \geq 0 \\ -2 & u_i < 0 \end{cases}$$

$$\delta_{i,i} = \begin{cases} -2 & u_{i+1} \geq 0 \\ 1 & u_{i+1} < 0 \end{cases}$$

$$\delta_{i,i-2} = \begin{cases} 0 & u_{i-1} \geq 0 \\ 1 & u_{i-1} < 0 \end{cases}$$

$$\delta_{i,i+1} = \begin{cases} 1 & u_{i+2} \geq 0 \\ 0 & u_{i+2} < 0 \end{cases}$$

C. Vertical advection term

The finite difference form of the vertical advection term can be written as

$$\sum \lambda_{i,k}^n \left(\frac{1-\theta_1}{4} (B_{i,k-1} + B_{i,k}) w_{i,k-1} (C_{i,k-1} + C_{i,k}) - \frac{\theta_2}{4} (B_{i,k} + B_{i,k+1}) w_{i,k} (C_{i,k} + C_{i,k+1}) \right) \quad (C-6)$$

The adjoint scheme is

$$\frac{1}{4} (1-\theta_1) (B_{i,k-1} + B_{i,k}) w_{i,k-1} (\lambda_{i,k}^n - \lambda_{i,k-1}^n) + \frac{\theta_2}{4} (B_{i,k} + B_{i,k+1}) w_{i,k} (\lambda_{i,k+1}^n - \lambda_{i,k}^n) \quad (C-7)$$

where

$\theta_2 = 0$ for $k = K$ (at the bottom layer), and $\theta_2 = 1$ for the other layers.

D. Vertical diffusion term

The vertical diffusion terms are treated implicitly. They can be written as

$$\sum \lambda_{i,k}^n \left((1-\theta_1) BKZ_{i,k-1}^{n+1} (C_{i,k-1}^1 - C_{i,k}^1) - \theta_2 BKZ_{i,k}^{n+1} (C_{i,k}^1 - C_{i,k+1}^1) \right) \quad (C-8)$$

where

$$BKZ_{i,k}^{n+1} = \frac{B_{i,k} + B_{i,k+1}}{(h_k + \theta_1 \eta_i^{n+1}) + h_{k+1}} K_{z(i,k)}$$

The adjoint scheme is

$$(1 - \theta_1) BKZ_{i,k-1}^n (\lambda_{i,k-1}^{n-1} - \lambda_{i,k}^{n-1}) - \theta_2 BKZ_{i,k}^n (\lambda_{i,k}^{n-1} - \lambda_{i,k+1}^{n-1}) \quad (C-9)$$

E. Horizontal diffusion term

The horizontal diffusion terms can be written as

$$\sum \lambda_{i,k}^n \left(HDif_{i,k}(C_{i+1,k} - C_{i,k}) - HDif_{i-1,k}(C_{i,k} - C_{i-1,k}) \right) \quad (C-10)$$

where

$$HDif_{i,k} = (B_{i,k} + B_{i+1,k}) \frac{(h_k + \theta_1 \eta_i) + (h_k + \theta_1 \eta_{i+1})}{4\Delta x^2} K_{x(i+1,k)}$$

The adjoint scheme is

$$HDif_{i,k} (\lambda_{i+1,k}^n - \lambda_{i,k}^n) - HDif_{i-1,k} (\lambda_{i,k}^n - \lambda_{i-1,k}^n) \quad (C-11)$$

F. Source and sink functions

The source and sink (or error misfit) functions of the adjoint model are treated explicitly, i.e., all the terms are evaluated using the values of state variables at time $n+1$. The error source functions are calculate by substituting $C_{i,k}^{L,n}$ and $\lambda_{i,k}^{L,n}$ into

Eqs. 2-14b - 2-14k and substituting summation for integral. The error source due to

data misfit at a cell (i,k) is calculated by

$$(C_{i,k}^{L^n} - \hat{C}_{i,k}^{L^n})B_{i,k} \quad (C-12)$$

C-2. Finite Difference Equation of The Adjoint Model

The implicit treatment of the vertical diffusion term in Eq. C-8 results in the equations containing the $K \times K$ tri-diagonal matrix in the vertical direction. In matrix notation,

$$[A \lambda^j] = [F] \quad (C-12)$$

That is

$$\begin{pmatrix} D_1 & E_1 & 0 & \cdot & \cdot & \cdot & 0 \\ C_2 & D_2 & E_2 & 0 & \cdot & \cdot & 0 \\ 0 & \cdot & \cdot & \cdot & \cdot & \cdot & 0 \\ 0 & \cdot & C_k & D_k & E_k & \cdot & 0 \\ 0 & \cdot & \cdot & \cdot & \cdot & \cdot & 0 \\ 0 & \cdot & \cdot & \cdot & C_{K-1} & D_{K-1} & E_{K-1} \\ 0 & \cdot & \cdot & \cdot & \cdot & C_K & D_K \end{pmatrix} \begin{pmatrix} \lambda_{i,1}^{j,n-1} \\ \lambda_{i,2}^{j,n-1} \\ \cdot \\ \lambda_{i,k}^{j,n-1} \\ \cdot \\ \lambda_{i,K-1}^{j,n-1} \\ \lambda_{i,K}^{j,n-1} \end{pmatrix} = \begin{pmatrix} F_{i,1} \\ F_{i,2} \\ \cdot \\ F_{i,k} \\ \cdot \\ F_{i,K-1} \\ F_{i,K} \end{pmatrix} \quad (C-13)$$

and the non-zero elements, C_k , D_k , E_k and F_k , are given by,

$$E_k = -\theta_2 \frac{B_{i,k} + B_{i,k+1}}{(h_k + \theta_1 \eta_i) + h_{k+1}} K_{z(i,k)} \quad (C-14)$$

$$C_k = (1 - \theta_1) E_{k-1} \quad (C-15)$$

$$D_k = B_{i,k} \frac{h_k + \theta_1 \eta_i^n}{\Delta t} - C_k - E_k \quad (\text{C-16})$$

$$\begin{aligned}
F_k = & B_{i,k} \frac{h_k + \theta_1 \eta_i^n}{\Delta t} \lambda_{i,k}^{j,n} + SoSk^j \\
& - \frac{1}{4} (1 - \theta_1) (B_{i,k-1} + B_{i,k}) w_{i,k-1} (\lambda_{i,k}^{j,n} - \lambda_{i,k-1}^{j,n}) - \frac{\theta_2}{4} (B_{i,k} + B_{i,k+1}) w_{i,k} (\lambda_{i,k+1}^{j,n} - \lambda_{i,k}^{j,n}) \\
& - (AHAdv1_{i,k} - AHAdv2_{i,k} + AHAdv3_{i,k}) \\
& + (HDif_{i,k} (\lambda_{i+1,k}^{j,n} - \lambda_{i,k}^{j,n}) - HDif_{i-1,k} (\lambda_{i,k}^{j,n} - \lambda_{i-1,k}^{j,n})) \quad (\text{C-17})
\end{aligned}$$

where

$$HDif_{i,k} = (B_{i,k} + B_{i+1,k}) \frac{(h_k + \theta_1 \eta_i) + (h_{k+1} + \theta_1 \eta_{i+1})}{4\Delta x^2} K_{x(i+1,k)}$$

and the terms $AHAdv1_{i,k}$, $AHAdv2_{i,k}$ and $AHAdv3_{i,k}$ are listed in Eqs. C-5b, C-5c and C-5d, respectively. $SoSk^j$ is a source functions due to data misfit (Eq. C-12).

LITERATURE CITED

- Ambrose Jr, R. B., Wool T. A., Connolly, J. P. and Schanz, R. W. (1988) "WASP4, a hydrodynamic and water quality model: model theory, user's manual and programmer's guide." EPA/600/3-87/039, US EPA, Athens, GA, 297 pp.
- Axellsson, O., and Barker, V. A. (1984) "Finite element solution of boundary value problems, theory and Computation." Academic Press, 432 pp
- Bard, Y., (1974) "Nonlinear Parameter Estimation." John Wiley, New York.
- Beck, M. B. (1987) "Water quality modeling: A review of the analysis of uncertainty." *Water resource Res.*, 23(8), 1393-1442.
- Beck, M. B., and Young, P. C. (1976) "Systematic identification of DO-BOD model structure." Proc. ASCE, *J. Environ. Eng. Div.*, 102(EE5), 902-927.
- Beck, M. B. (1974) "Maximum likelihood identification applied to DO-BOD-Algae model for a freshwater stream." Report 7431, Lund Institute of Technology, Lund., Sweden
- Bennett, A. F. and McIntosh, P. C. (1982) "Open ocean modelling as an inverse problem: tidal theory." *J. Phys. Oceanogr.*, 12, 1004-1018.
- Carrera, J., and Neuman, S. P. (1986) "Estimation of aquifer parameters under transient and steady state conditions: II. Uniqueness, stability, and solution algorithms." *Water Resour. Res.*, 22(2), 211-227.
- Carter, R. D., Kemp, Jr, L. F., and Pierce, A. C. (1982) "Discussion of comparison of sensitivity coefficient calculation methods in automatic history matching." *Soc. Pet. Eng. J.*, 22(2), 205-208.
- Carter, R. D., Kemp, Jr., L. F., Pearce, A. C. and Williams, D. L. (1974) "Performance matching with constraints." *Soc. Pet. Eng. J.*, 14(2), 187-194
- Cerco, C. F. and Cole, T. M. (1994) "Three-dimensional eutrophication model of Chesapeake Bay: Volume 1, main report." Technical Report EL-94-4, US Army Engineer Waterways Experiment Station, Vicksburg, MS.

- Chavent, G., Dupuy, M. and Lemonnier, P. (1975) "History matching by use of optimal theory." *Soc. Petrol. Eng. J.*, 15(1), 74-86.
- Chavent, G. (1974) "Identification of parameters in partial differential equations." in *Identification of Parameters in Distributed Systems*, edited by Goodson, R.E. and M. Polis, pp. 31-48, American Society of Mechanical Engineers, New York.
- Chavent, G. (1983) "Local stability of the output least parameter estimation technique." *Math. Appl. Comp.*, 2(1), 3-22.
- Conn, A.R, Gould, N. I. M., and Toint, Ph. L (1992) "LANCELOT- A fortran package for large-scale nonlinear optimization (Release A)." Spring-Verlag, 330 pp.
- Cooley, R. L. (1977) "A method of estimating parameters and assessing reliability for models of steady state groundwater flow, 1. Theory and numerical properties." *Water Resource Res.*, 12(2), 318-324.
- Courtier, P., Thepaut, J. N., and Hollingsworth, A. (1994) "A strategy for operational implementation of 4D-Var, using an incremental approach." *Q. J. R. Meteorol. Soc.*, 120, 1367-1387
- Das, S. K. and Lardner, R. W. (1991) "On the estimation of parameters of hydraulic models by assimilation of periodic tidal data." *J. Geophys. Res. (Oceans)*, 96(15), 15,187-15,196.
- Di Toro, D. M., and van Straten, G. (1979) "Uncertainty in the parameters and predictions of phytoplankton models." WP-79-27, International Institute for Appl. Syst. Anal., Laxenburg, Austria.
- Environment and Hydraulics Laboratories, (1986) "CE-QUAL-W2: A numerical two dimensional, laterally averaged model of hydrodynamics and water quality: user's manual, Instruction Report E-86-5." US Army Engineer Waterways Experiment Station, Vicksburg.
- Gill, P. E., Murray, W., and Write, M. H. (1982) "Practical optimization." Academic Press. pp. 401.
- Jacquard, P., and Jain, C. (1965) "Permeability distribution from field pressure data." *Soc. Pet. Eng. J.*, 5(4), 281-294.
- Johnson, P., Chan, W. H., Gherini, S. A., and Chamberlin, C. E. (1985) "Rates, constants, and kinetics formulations in surface water quality modeling." (2nd edition), U. S. Environmental Protection Agency, EPA/600/3-85/040, Environmental Research Lab. Athens, GA.

- Jørgensen, S. E., Jørgensen, L. A., Nielsen, K. L., and Mejer, H. F. (1981) "Parameter estimation in eutrophication modelling." *Ecological Modelling*, 13 111-129.
- Koivo, A. J., and Phillips, G. R. (1976) "Optimal estimation of DO, BOD, and stream parameters using a dynamic discrete time model." *Water Resour. Res.*, 12(4), 705-711
- Koivo, A. J., and Phillips, G. R. (1971) "Identification of mathematical models for DO and BOD concentrations in polluted streams from noise corrupted measurements." *Water Resour. Res.*, 7(4), 853-862.
- Kuo, A. Y., and Park, K. (1995) "A PC-based tidal prism water quality model for small coastal basins and tidal creeks." in *Computation Modelling of Sea and Coastal Regions II*, C. A. Brebbia, L. Traversoni, and L. C. Wrobel (ed), Computational Mechanics Publications, Southampton Boston, UK, 371-378.
- Kuo, A. Y., Neilson, B. J., and Park, K. (1991a) "A modelling study of the water quality of the upper tidal Rappahannock River." Special Report in Applied Marine Science and Ocean. Eng., No. 314. Gloucester Point, VA.
- Kuo, A. Y., Park, K., and Moustafa, M. Z. (1991b) "Spatial and temporal variabilities of hypoxia in the Rappahannock River, Virginia." *Estuaries*, 14, 113-121
- Kuo, A. Y. and Neilson, B. J. (1988) "A modified tidal prism model for water quality in small coastal embyments." *Water Science Technology*, 20(6/7), 133-142
- Lal, A. M. W. (1995) "Calibration of riverbed roughness." *J. Hydraulic Eng.* 121(9),664-671.
- Lardner, R. W., and Das, S. K. (1994) "Optimal estimation of eddy viscosity for a quasi-three-dimensional numerical tidal and storm surge model." *International Journal for Numerical Methods in Fluids*, 18, 295-312.
- Le Dimet, F. X., and Talagrand, O. (1986) "Variational algorithms for analysis and assimilation of meteorological observations: theoretical aspects." *Tellus*, 38A, 97-110
- Lee, E. S. and Hwang, I. (1971) "Stream quality modelling by quasilinearization." *J. Water Pollut. Contr. Fed.*, 43(2), 306-317.
- Li, Y., Navon, I. M., Courtier, Yang, W., Zou, X., Bates, J. R., Moorthi, S., and Higgins, R. W. (1994) "Four-dimensional variational data assimilation experiments with a multilevel semi-Lagrangian semi-implicit GCM." *Mon. Wea. Rev.*, 122, 5, 966-983.

- Lorenc, A. C. (1986) "Analysis methods for numerical weather prediction." *Q. J. R. Meteorol. Soc.*, 112, 1177-1194.
- McLaughlin, D. (1978) "Parameter estimation problems in water resource modeling." in *Modeling, Identification and Control in Environment System*. Vansteenkiste, ed., IFIP, North-Holland Publishing Company, 137-151.
- Mejer, H. F., and Jørgensen, L. A. (1983) "Identification methods applied to two Danish lakes." in *Uncertainty and Forecasting of Water Quality*, edited by M. B. Beck and G. van Straten, Springer Verlag, New York, 173-182.
- Navon, I. M. (1986) "A review of variational and optimization methods in meteorology--a review." Res. Rep., Supercomputer Computations Research Institute, Florida State University, Tallahassee, FL.
- Navon, I. M., and Legler, D. M. (1987) "Conjugate-gradient methods for large-scale minimization in meteorology." *Monthly Weather Review*, 115,1479-1502.
- Neuman, S. P. (1973) "Calibration of distributed parameter groundwater flow models viewed as a multiple-objective decision process under uncertainty." *Water Resour. Res.*, 9(4), 1006-1021.
- Noble, B., and Daniel, J. (1975) "Applied linear algebra." Rrentice Hall Publishers, Englewood Cliffs, N. J.
- Nutbrown, D. A. (1975) "Identification of parameters in a linear equation of groundwater flow." *Water resource Res.*, 11(4), 581-588
- Panchang, V. G., and Richardson, J. E. (1992) "Inverse adjoint estimation of eddy viscosity for coastal flow models." *J. Hydraulic Engin.*, 119(4), 506-524
- Park, K., Kuo, A. Y., Shen, J. and Hamrick, J. M. (1995) "A three-dimensional hydrodynamic-eutrophication model (HEM-3D): description of water quality and sediment process submodels." Special Report in Applied Science and Ocean Eng. No. 327, Gloucester Point, VA."
- Park, K., and Kuo, A. Y. (1996) "A numerical model study of hypoxia in the tidal Rappahannock River of Chesapeake Bay." *Estuarine, Coastal and Shelf Science*, 42(5),563-381.
- Park, K., and Kuo, A.Y. (1993a) "A vertical two-dimensional model of estuarine hydrodynamics and water quality." Special Report in Applied Science and Ocean Eng. No.321, Gloucester Point, VA.
- Park, K., and Kuo, A. Y. (1993b) "A model study of hypoxia and eutrophication in

- the tidal Rappahannock River, Virginia." Special Report in Applied Science and Ocean Eng. No. 322, Gloucester Point, VA.
- Parker, R. A. (1972) "Estimation of aquatic ecosystem parameters." *Verh. Int. Ver. Limnol.*, 18, 257-263.
- Polak, E. and Ribiere, G. (1969) "Note sur la convergence de methodes de directions conjuguées." *Rev. Franc. Informat. Rech. Operationnelle*, 16, 35-43.
- Prevost, C., and Salmon, R. (1986) "A variational method for inverting hydrographic data." *J. Marine Sci.*, 44, 1-34.
- Rabier, F., and Courtier, P. (1992) "Four-dimensional assimilation in the presence of baroclinic instability." *Q. J. R. Meteorol. Soc.*, 118, 649-672.
- Richardson, J. E. and Panchang, V. G. (1992) "A modified adjoint method for inverse eddy viscosity estimation in coastal circulation models." in M. L. Spaulding et al. (eds), *Estuarine and Coastal Modeling*, Proc. 2nd Int. Conf., Amer. Soc. Civil Engrs. New York, 733-745.
- Rinaldi, S., Romano, P., and Sessa, R. S. (1979) "Parameter estimation of Streeter-Phelps models." *Proc. Am. Soc. Civ. Eng. J. Environ. Eng.* 105(EE1), 75-88.
- Rinaldi, S., Romano, P., and Sessa, R. S. (1976) "Parameter estimation of a Streeter-Phelps type water pollution model." 4th IFAC symposium on identification and system parameter estimation, Tbilisi, Union of Soviet Socialist Republic, Sept.
- Sagaret, B., Yakowitz, S. and Duckstein, L. (1975) "A direct method for the identification of the parameters of dynamic nonhomogeneous aquifers." *Water Res. Research*. 11(4), 563-570.
- Shastri, J. S., Fan, L. T., and Erickson, L. E. (1973) "Non-linear parameter estimation in water quality modelling." *Proc. ASCE, J. Environ. Eng. Div.*, 99(3) 315-331.
- Smedstad, O. M., and O'Brien, J. J. (1991) "Variational data assimilation and parameter estimation in an equatorial Pacific Ocean model." *Progress in Oceanography*, 26, 179-241.
- Sun, N. Z., and Yeh, W. W. G. (1985) "Identification of parameter structure in groundwater inverse problem." *Water Resource Res.*, 21(6), 869-883.
- Sun, N. Z., and Yeh, W. W. G. (1990) "Coupled inverse problems in groundwater modeling. 1. Sensitivity analysis and parameter identification." *Water Resource Res.*, 26(10), 2507-2525.

- Thomann, R. V., and Mueller, J. A. (1987) "Principles of surface water quality modeling and control." Harper and Row, Publishers, NY. 644 pp.
- Tziperman, E., and Thacker, W. C. (1989) "An optimal-control/adjoint-equations approach to studying the oceanic general circulation." *J. Phys. Oceanogr.*, 19,1471-1485.
- Uhrhammer, R. A. (1980) "Analysis of seismographic station networks." *Bull. Seismological Soc. of Am.*, 70(4), 1369-1379.
- USGS. 1991. Water resources data, Virginia-water year 1990, Vol I. surface water and surface-water-quality records. USGS Water-DATA Report VA-90-1. Water resources Division, USGS, Richmond, VA. 591 pp.
- van Straten, G. (1983) "Maximum likelihood estimation of parameters and uncertainty in phytoplankton models." in *Uncertainty and Forecasting of Water Quality*. M.B. Beck and G. van Straten (ed), Springer-Verlag, 157-171.
- Wiggins, R. A. (1972) "The general linear inverse problem: implications of surface waves and free oscillations for surface structures." *Rev. Geophysics and Space Physics* 10,251-285.
- Yeh, W. W. G and Sun, N. Z. (1990) "Variational sensitivity analysis, data requirement, and parameter identification in a leaky aquifer system." *Water Resource Res.* 26(9), 1927-1938.
- Yeh, W. W. G. (1986) "Review of parameter identification procedures in ground hydrology: The inverse problem." *Water resource Res.* 22(2), 95-108.
- Yeh, W. W.-G and Sun, N. Z. (1984) "An extended identifiability in aquifer parameter identification and optimal pumping test design." *Water Resour. Res.*, 20(12), 1837-1847.
- Yeh, W. W. G., Yoon, Y.S. and Lee, K. S. (1983) "Aquifer parameter identification with kriging and optimum parameterization." *Water Resour. Res.*, 19(1), 225-233.
- Yu, L., and O' Brien, J. J. (1991) "Variational estimation of the wind stress drag coefficient and the oceanic eddy viscosity profile." *J. Physical Oceanography*, 21, 709-719.

VITA

JIAN SHEN

Born in Shanghai, People's Republic of China, on October 14, 1958. Received B.S. in mathematics from Shanghai Teacher's University, Shanghai, P. R. C. Was a teacher assistant and a lecturer of the Institute of Estuarine and Coastal Research, East China Normal University for six years. Received M.A. from Virginia Institute of Marine Science/School of Marine Science, The College of William and Mary in August, 1993. Entered Ph.D. program in the Virginia Institute of Marine Science/School of Marine Science, The College of William and Mary in August, 1993